PREDICTIVE MAPPING FOR OROGENIC GOLD PROSPECTIVITY IN UGANDA

SARAH HERBERT
February, 2012

SUPERVISORS:
Dr. T. Woldai
Dr. E. J. M. Carranza

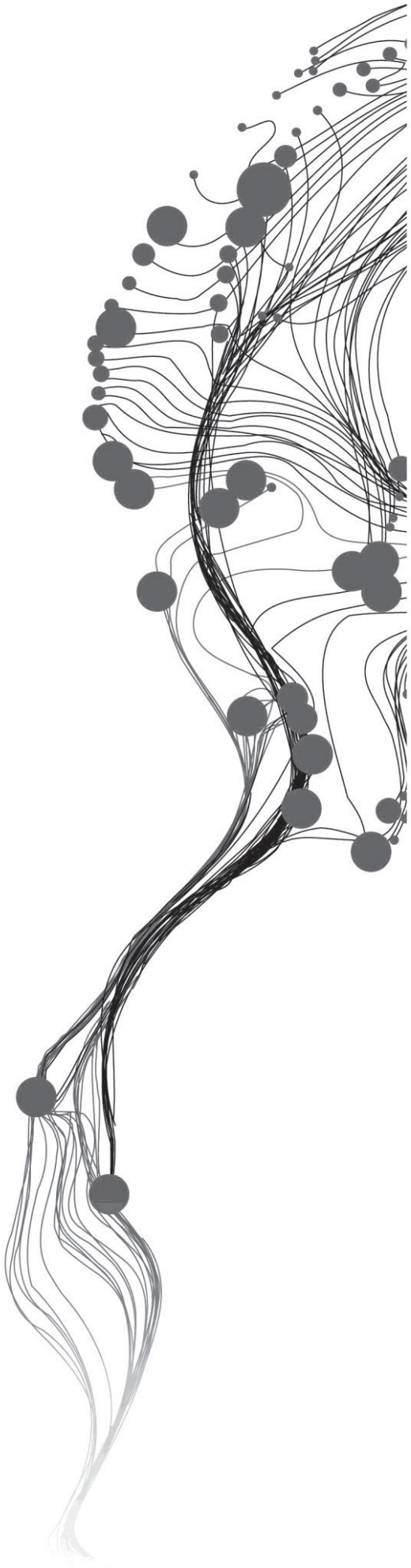

PREDICTIVE MAPPING FOR OROGENIC GOLD PROSPECTIVITY IN UGANDA

SARAH HERBERT
Enschede, The Netherlands, February, 2012

Thesis submitted to the Faculty of Geo-Information Science and Earth Observation of the University of Twente in partial fulfilment of the requirements for the degree of Master of Science in Geo-information Science and Earth Observation.
Specialization: Applied Earth Sciences

SUPERVISORS:
Dr. T. Woldai
Dr. E.J.M. Carranza

THESIS ASSESSMENT BOARD:
Prof. Dr. F.D. van der Meer (Chair)
Dr. M. Buxton (External Examiner, University of Delft - Department of Geotechnology - Civil Engineering & Geosciences)

ABSTRACT

Integration of visually enhanced regional geo datasets has facilitated a new geological interpretation, (covering 55 000 km^2) and prospectivity model for orogenic gold in south-west Uganda. The datasets include historical geological maps, geological field data, digital terrain models, Landsat TM data and airborne geophysical data.

The study area, bordered by the western branch of the East African Rift, covers a range of different aged terranes including the Archaean basement gneisses, Palaeoproterozoic volcano-sedimentary Buganda Toro Belt, Mesoproterozoic clastic sedimentary Karagwe Ankolean Belt and several outliers of undeformed Neoproterozoic sediments.

The Archaean aged basement gneisses are found in the north and centre of the study area. South-east of Kamwenge, repetition of the gneiss and schist units imply a stacked geometry typical of fold and thrust belts. Undifferentiated gneisses are exposed in the south of the study area (Rukungiri) by erosion of the younger Proterozoic rocks.

The S-shaped volcano-sedimentary Palaeoproterozoic Buganda Toro Belt has a WNW-ESE orientation in the east of the study area where south dipping thrusts and tight north verging folds indicate northward tectonic transport onto the basement gneiss. West of the Mubende granite the belt trends NE and is marked by NE trending fold axes and sinistral shears. A pull-apart basin coupled with roof-uplift is proposed to account for the intrusion of the Mubende granite. Palaeoproterozoic schists are exposed beneath the Mesoproterozoic rocks in the Buhweju area and to the south.

In the south of the study area, the Karagwe Ankolean Belt comprising weakly deformed conglomerate sandstone, quartzite and argillitic sediments is folded into a series of NW trending asymmetrical anticlines and synclines and intruded by post and syn-tectonic granites.

Three major orogenies have been mapped in the study area. The oldest being the Ubendian Orogeny (D1 and D2), marking the collision of the Tanzanian and Congo cratons. This was followed by a global orogenic event at 1000 Ma (D3) which gave rise to the tin metallogenic province and led to the formation of the Rodinia supercontinent. The youngest orogeny is the Pan African (D4) which marks the collision between East and West Gondwana.

The mineral system understanding was used to address the critical processes of orogenic gold formation at the district-scale. These processes are translated into mappable mineral proxies using the available regional datasets. Tectono-stratigraphic domains, mantle indicators and gold occurrences represent the "source of gold" as a critical process. Hydrothermal alteration, extracted from radiometric data, structures involved in the orogenies and terrane contacts were extracted to represent the active pathway as a critical process and finally the physical throttle is represented by rheological contrasts and geological complexity.
Knowledge-driven multi-class index overlay method is used to model the orogenic gold prospectivity. Weighting of the predictor layers occurs at the level of the critical process and takes in to account the relative importance of the critical process mineralisation, the representativeness of a proxy and the accuracy of the proxy. The resultant prospectivity model shows that 83% of all gold occurrences were predicted within 30 % of the study area. Eight areas, covering 2500 km^2, have been recommended for follow-up exploration.

ACKNOWLEDGEMENTS

First and foremost I would like to thank Randgold Resources Ltd for granting me the opportunity to pursue my studies in The Netherlands.

I am grateful to Mr Lucien Mitima and his team in Entebbe for providing logistical support during fieldwork in Uganda. My gratitude also goes to Mr John Odida at the Geological Society of Uganda for granting access to the visited field localities and to Saka Zziwa our driver, for opportunity to see such a beautiful country.

The cooperation and collaboration of the Geological Society of Finland (GTK), particularly Mr Tapio Lehto, is highly appreciated.

Thanks also go to Mr Chris Hecker for his willingness to help with processing the TIR ASTER imagery.

Finally to my supervisors, Dr Tsehaie Woldai and Dr John Carranza, your wisdom, guidance and experience have been invaluable. I have enjoyed our insightful discussions and I've learnt an incredible amount this year.

TABLE OF CONTENTS

LIST OF FIGURES

LIST OF TABLES

LIST OF APPENDICES

1. INTRODUCTION

In the last 15 years the concept of mineral systems approach to understanding orogenic gold systems has been developed. The orogenic gold model, as defined by *Groves et al. (1998)* argues for gold to be deposited during compressional deformation in accretionary orogens, from hydrothermal fluids derived from the metamorphism of greenstones. These deposits are typically found in late Archaean or in Palaeoproterozoic greenstone belts *(Groves et al., 2007)* and include the world class gold provinces of Yilgarn Craton, Superior Province, the Birimian of West Africa and the Tanzania Craton. Archaean and Palaeoproterozoic gold-forming events correlate with the growth of juvenile continental crust and resulting ores have been protected for billions of years within large, stable cratons.

Uganda overlies the African plate, formed by the accretion of smaller Archaean Cratons welded together by mobile belts *(Begg et al., 2009)* of Archaean – Proterozoic age. Much of the northern and central Uganda is underlain by Archaean basement gneisses, forming approximately two-thirds of the country. Archaean rocks of the Nyanzian-Kavirondian system are exposed in the south-east and form part of the extensive granite-greenstone terrane of the Tanzanian Craton. Three major Proterozoic belts underlie central and west Uganda: the Palaeoproterozoic Ubendian belt (2100-1860 Ma) comprises the Buganda Toro metasediments, the Mesoproterozoic Kibaran belt (1375 Ma) comprising the Karagwe Ankolean metasediments and Neoproterozoic Pan African rocks (~500 Ma).

According to *Trauth et al. (2008)* gold mineral occurrences have been found at Busia in the south-east, hosted within the Nyanzian-Kavirondian Archaean greenstone belt, whilst in the south-west at Kiboga and Kigezi, gold in quartz veins is hosted in the Palaeoproterozoic metasediments of the Buganda Toro Supergroup. Karamoja, in the north-east, is of particular interest since favourable gold potential is known to exist in the intrusive and volcano-sedimentary rocks of Proterozoic and possibly Archaean age. The potential significance of north-west Uganda is poorly understood, however the Kibalian mobile belt known host to the Kilo-Moto gold mines of the Democratic Republic of Congo (DRC) is believed to extend into Uganda.

Despite the known gold occurrences (artisanal mining) in Uganda, modern exploration has rarely been applied and as a result very little is known about the controlling factors of mineralisation. Understanding the orogenic gold mineral system of Uganda is of fundamental importance to the government of Uganda, international investors and exploration companies.

Conventional geological field mapping *(Hepworth et al., 1966)* provides excellent fact information, however it is costly, time consuming and an inefficient method of understanding the regional framework. Previous studies have been isolated in their discipline; *Buchwaldt et al. (2008)* and *Tack et al. (2010)* studied isotope data to unravel the relative ages of cratons, mobile belts and intrusives, while *Leggo (1973)*, *Schenk et al. (2007)* and *Cahen (1982)* focused on the metamorphic events affecting the Archaean crust. Most structural oriented studies have concentrated on the evolution of the East African Rift in Uganda *(Aanyu et al., 2011*); however there has never been an attempt to unravel the deformational history in the context of orogenic gold mineralisation.

The focus of this research is thus to synthesize the evolution of the cratons and surrounding mobile belts in south-west Uganda and assess the implications for orogenic gold mineralisation using the mineral systems approach outlined by *McCuaig et al. (2010)*. This approach is used to encapsulate the critical processes of orogenic gold which are then translated into mappable units and combined in weights-of-evidence model to predict the potential orogenic gold deposits.

1.1. Literature review

1.1.1. Orogenic gold

As the name suggests, orogenic gold deposits, are related to convergent margin tectonics *(Kerrich, 1993)* where several allochtonous terranes are accreted along major faults. Subsequent transpressive tectonics related to either a shift in plate motion or a flip in the principal minimum stress direction (σ3) from a vertical to horizontal position (due to the build of lithostatic pressure) accounts for the efficient fluid migration along major fault networks *(Goldfarb et al., 2001)*. As a result orogenic deposits are structurally controlled and usually located within the second or higher order splays off major terrane bounding structures, where fluid accumulation is highest. Deposits are usually located at the brittle-ductile transition associated with hydrothermal breccias and discreet shears. Orogenic deposits tend to form post peak deformation where mineralised veins and fabrics often crosscut the host rock geometry.

As well has having an inherent spatial distribution, orogenic gold deposits also have a heterogeneous temporal distribution *(Goldfarb, et al., 2001)*, strongly correlated to major peaks in crustal growth as shown in Figure 1. Two major Precambrian peaks exist; the first during the late Archaean (2800-2550 Ma) and the second during the Palaeoproterozoic (2100-1860 Ma) believed to be influenced by plume induced mantle overturns. Continuous crustal growth from 600-50 Ma correlates to the widely accepted decrease in global heat flow during the Phanerozoic.

The complete absence of deposits during 1800-900 Ma (a time of global extension) has been inferred by *Groves et al. (2000)*, *Goldfarb et al.(2001)* and *Kerrich (1993)* to be the result of erosion during the onset of modern tectonics. Although orogenies did exist (Rodina at 1300-1000 Ma), deposits have since been eroded down to the higher metamorphic grade roots.

The preservation of Precambrian deposits is attributed to a hotter mantle and smaller more numerous buoyant plates during the Archaean. The higher buoyancy reduces stress and viscosity at the subduction zone and as a result the Archaean sub-continental lithosphere could not have been delaminated by gravitational processes alone. In summary the early Precambrian deposits were protected from uplift and erosion in the centre of buoyant cratons. As the earth moved away from plume dominated tectonics, slower plate motion and decreased buoyancy, increases the chances of sub-continental delamination and hence uplift and erosion all decreasing the chances of preserving a deposit *(Bierlein et al., 2009)*. The presence of deposits 900-50 Ma is the approximate threshold for preservation. The complete absence of deposits in the last 50 Ma reflects the amount of time needed to uproot to levels of the crust where orogenic gold deposits occur.

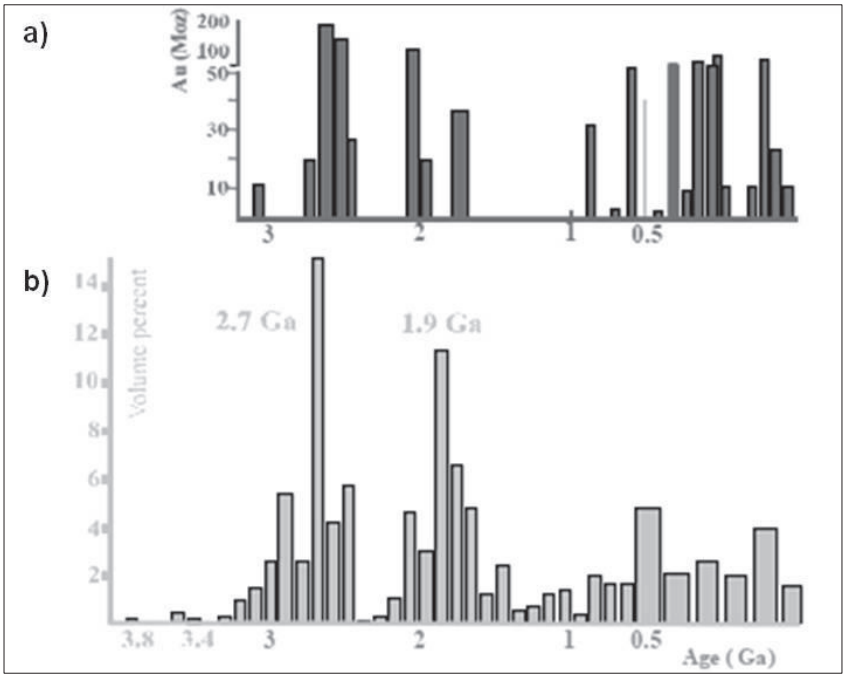

Figure 1: Positive correlation between a) Global orogenic gold production with time b) Volume percent increase in crustal growth with time (after *Goldfarb et al. 2001).*

Most orogenic gold deposits are typically found in greenschist facies rocks indicating moderate temperature and low pressure, due to higher solubility of gold, however few orogenic gold deposits are known to occur in higher metamorphic terranes extending into the amphibolite facies *(Groves, et al., 1998)* where the sheer volume of fluid released at these temperatures can account for the amount of gold deposited. Orogenic deposits have also been referred to as mesothermal *(Kerrich, 1993)* and mesothermal hydrothermal deposits *(Robb, 2005)* implying depths of 1500-4500 m and temperatures between 200-400 °C, contradicting with the understanding that orogenic gold can only occur in greenschist-amphibolite facies conditions (depths of 2-15 km and temperatures of 180-700 °C).

The accepted classification of orogenic gold deposits, *(Groves, et al., 1998)*, takes into account that these deposits are formed at convergent plate margins as well as the wide range in depth and temperatures of formation associated with different metal association as shown in Figure 2.

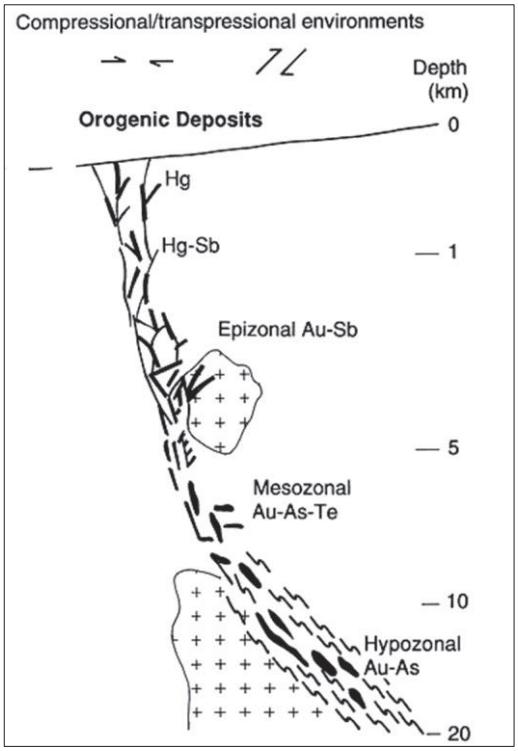

Figure 2: Schematic representation of the range orogenic gold deposits, their metal associations related to the depth of formation (after *Groves et al. 1998*).

1.1.2. Regional geology and tectonic setting in Uganda

1.1.2.1. Archaean

Unravelling the evolutionary structural history was initiated in 1966 where *Hepworth, et al.(1966)* used conventional field mapping methods map the Archaean basement rocks of the gneissic granulite complex which they termed "Ugandan Basement Complex" (BC) considered by subsequent authors *(Link et al., 2010)* and *(Leggo, 1973)* to represent the eastern extension of the Congo Craton. The BC consists of four subunits defined on the basis of their structural and metamorphic characteristics:

- Watian event dated at 2900 Ma *(Leggo, 1973),* displays E-W fold axes, representing a NS compressional event and granulite-facies metamorphism.
- Aruan event dated at 2600 Ma *(Leggo, 1973)* displays NNE plunging fold axes and steep axial planes. The onset of this event is marked mafic dykes.
- Mirian event, (2550 Ma) represents a major tectonothermal event *(Gabert, 1990)* and displays NE trending recumbent isoclinal folds that are overturned towards the NW.
- Chuan or Aswa is characterised by a NW trend grading locally into mylonites.

1.1.2.2. Palaeoproterozoic

The Buganda Toro belt also known as the Ruwenzori fold belt *(Hepworth, et al., 1966)* unconformably overlies the BC and was affected by the Ubendian Orogeny between 2100-1860 Ma *(Cahen, 1982)*. The Ubendian Orogeny represents a high grade metamorphic event through two deformational phases. The early (more regional) deformational phase (2100–2025 Ma) marked by an E–W to WNW–ESE foliation and granulite-facies metamorphism, interpreted as a product of a collisional orogeny along the south-western margin of the Tanzania, and possibly Congo cratons *(Aanyu, et al., 2011)*. The second phase (1950–1850 Ma) according to *Theunissen (1989)* is restricted to the Ubendian belt, south of the Tanzanian Craton and is characterised by large NW–SE trending dextral shear zones. According to *Lenoir et al. (1994)*

this event also caused the northwards thrusting of the Usagaran belt and the intrusion of post tectonic granitic calc-alkaline batholiths at 1860 Ma, marking the upper time limit of this event.

1.1.2.3. Mesoproterozoic

Historical literature describes the Mesoproterozoic events (1.4-0.9 Ga) of central Africa as the Kibaran Orogeny. This 'prolongued' event was based on the Rb-Sr age dating *(Cahen, 1982)* of S-type granitoids and scarce regional geological data. Subsequently any other orogenic event falling within this time span adopted the term "Kibaran" leading to much confusion. Early theories for the Kibaran Orogeny include intra-cratonic deformation with a prolongued period of extension, *(Klerkx, 1987)*, collision and subduction *(Rumvegeri, 1991)*, delamination of sub-continental lithospheric mantle *(Tack et al., 1994)* and an intracratonic extensional detachment model modified by strike slip reactivation of the Palaeoproterozoic basement *(Theunissen, 1989)*. As a result, *Tack et al. (2010)* used U-Pb dating to constrain the time span for the Kibaran event to 1375 Ma an proposed that the term "Kibaran event" be restricted to the 'tectonomagmatic event corresponding to prominent emplacement of the bimodal magmatism under intra-cratonic regional scale extension stress regime'.

North-east of the Ubendian Rusizian basement, the Karagwe Ankolean sediments, now defined by *Tack et al.,(2010)* as the Karagwe Ankolean Belt (KAB), unconformably overlie the Palaeoproterozoic Buganda Toro Supergroup. The metasedimentary sequence consists of pelitic rocks with quartzite intercalations and minor conglomerates. The KAB characterised by NW-SE trending regional fold axes and NE-SW cross folds *(Aanyu, et al., 2011)* are intruded by S-type granites differentiated by their ages. The G1 granites (1330 Ma) predate the Lomamian Orogeny (1000 Ma) where as the G2 granites are syntectonic formed under extensional stress regime between 1280-1260 Ma *(Klerkx, 1987)*. The Kibaran event, defined as a short lived extensional event precludes the younger granites which intruded during later compressional deformation. This post Kibaran event or Lomamian Event is defined by the local emplacement of syntectonic S-type granites (G3), under compressional stress *(Tack, et al., 2010)* and syntectonic A-type granites (G4), which formed under transpression *(Klerkx, 1987)* at 1205 Ma *(Tack, et al., 2010)*. This was followed by the Lomamian Orogeny linked to a global orogenic event at 1000 Ma which gave rise to the tin metallogenic province and led to the Rodinia amalgamation *(De Waele et al., 2008)*. Generally the regional metamorphism in the KAB is of low grade while higher metamorphic grades are confined to the contacts of intrusions.

1.1.2.4. Neoproterozoic

The Pan African Orogeny which occurred between 725 and 500 Ma was comprised of two phases. The early phase (725 Ma) describes the oblique collision between East and West Gondwana, resulting in mostly sinistral NS trending shear zones. *(Westerhof, pers. comm.)* The second phase is correlated with the thermal effect dated at 500 Ma *(Lenoir, et al., 1994)* and *(Cahen, 1982)*.

1.1.2.5. Pleistocene

The Western branch of the East African Rift System (EARS) runs along the western side of the study area, comprising a series of grabens bordered by high angle normal faults. Volcanism commenced in the North at Virunga Province at ~12 Ma and propagating southwards, reached Rungwe in the Tanganyika Rift at ~7 Ma *(Ebinger, 1989)*. The western branch is characterized by the abundance of potassic alkaline rocks that consists of basalts, carbonatites, ultrapotassic mafic rocks and potassic mafic-felsic lava.

1.1.3. Tectonic setting and implications for gold mineralisation

1.1.3.1. The Mesoproterozoic Kibaran belt (KAB) in south-west Uganda

The Kibaran mobile belt is well known for its metallogenic endowment, particularly in Sb, Nb/Ta W and Au mineralisation where the more important deposits have been discovered in eastern DRC and Rwanda. The model of intra-plate regional scale stress regime proposed by *Tack et al. (2010)* to explain the voluminous bimodal magmatism at 1375 Ma redefines the tectonic evolution of the KAB and has significant implications for the orogenic gold mineralisation. This major extensional event established mantle–crust connectivity where the mantle derived magmas exploited the zone of weakness between the Archaean Tanzanian Craton (East) and the Palaeoproterozoic Buganda Toro Belt (West). Additionally these mantle derived magmas initiated large scale crustal melting of the Palaeoproterozoic basement characterised by a thin lithosphere in contrast to the thick Tanzanian Craton. Studies of orogenic systems around the world have indicated that regions of thin continental crust are most prospective for gold mineralisation *(Bierlein, et al., 2009; Groves, et al., 2007)*. Crustal reworking and remobilisation of gold rich fluids during this phase, prior to the Lomamian Orogeny, implies that certain areas of the crust more enriched in gold (Western Domain, overlying Palaeoproterozoic basement) compared to others (Eastern domain, overlying the Tanzanian Craton).

Following the Kibaran thermal event, compressional deformation associated with the intrusion of syntectonic S-type granites at 1000 Ma facilitated efficient fluid mixing via pre-existing lines of weakness. These events were followed by strike-slip deformation and tensional tectonics *(Pohl, 1987)* associated with A-type granites *(Klerkx, 1987)*. The resultant local stress heterogeneities focussed fluids into zones of structural complexity. Between 1000-900 Ma numerous granites and pegmatites associated with the Sn-W mineralisation intruded the Kibaran sequence.

According to *Pohl, (1994)* the discovered gold-rich quartz veins in south-west Uganda, are found at the contact between in clastic Kibaran metasediments (specifically the conglomerate unit) and the older Palaeoproterozoic schists and are associated with pyrite, arsenopyrite ± magnetite and specularite. Gold present in the Palaeoproterozoic units would have been remobilised during the Lomamian Orogeny (1 Ga) and the Pan African Orogeny (~650 Ma) and concentrated in the basal conglomerate unit. Structurally the tectonic setting indicates that these veins are linked to a brittle-ductile regime associated with tight upright NW-SE trending folds and thrusts located away from the tin granite domes *(Pohl, 1994)*. Fluid inclusion studies *(Pohl et al., 1991)* have shown that these auriferous quartz veins and breccias formed at temperatures of 450 °C and pressures of 2 kbar (7.5 km burial depth) suggesting a hypothermal environment, not typical of normal orogenic gold which forms at 200 – 400 °C, and 1.5 - 4.5 km depth *(Groves, et al., 1998)*. The fluid salinity attained (NaCl – 8 wt % eq) is the upper limit for orogenic gold and may reflect fluid mixing with a mafic or mantle derived source. Fluids rich in CO_2 are normal for orogenic gold where the CO_2 is derived from metamorphic reactions. The major solute phases (Na, K, Ca) indicate a strong interaction with the country rocks and the absence CH_4 and N_2 in the CO_2 rich fluids precludes any derivation of the Sn-W fluids associated with the 985 Ma 'tin-granites'.

In neighbouring NW Burundi, *Brinckmann et al. (1994)* argue for a two stage genetic model of formation for gold mineralisation. Gold bearing hydrothermal veins spatially overlap with rare metal G4 granite related-pegmatite systems and radiometric ages for both pegmatites and gold rich quartz veins suggest synchronous formation. The second stage of gold formation is associated with breccia bodies containing hydrothermal quartz, indicating low pressure and temperature conditions (T= 140-190°C, P= 200bar) and a U-Pb age date of 535 ± 2 Ma *(Brinckmann, et al., 1994)*. Although not genetically linked to the tin

granites, the auriferous breccias formed contemporaneously in a similar tectonic setting and may be remobilised by epithermal fluids during the Pan African event

1.1.3.2. The Palaeoproterozoic Buganda Toro Belt

Very little research has been undertaken to understand the gold potential of the Buganda Toro belt, despite known gold occurrences at Kisita. According to a press release *(Griffis, 2010)* current mining operations have excavated a 200 x 50m wide trench across a sheared zone of quartz vein stockwork associated with hydrothermal quartz sericite alteration thought to extend for 1 km. The mineralisation is hosted in schist.

Field observations in the Buganda Toro Belt summarised in *Link et al. (2010)* describe a thrust-stacking geometry and location reactivation along steeply dipping shear zones. This setting implies thick-skinned tectonics providing the framework for a deep crustal event and hence a source of gold.

1.1.4. Previous work in the region

In an unpublished study, in an area to the south, *Msechu, (2011)*, attempted to establish the geological controls of gold mineralisation and delineate favourable zones of undiscovered gold mineralisation. Although this work did identify the importance of NW-SE trending faults/shears and NE-SW faults/shears and fold hinges it failed to demonstrate whether these structures were active during mineralisation or whether they post-dated mineralisation. Assuming these structures were active during mineralisation simply identifying fluid conduits is insufficient evidence for the formation ore deposits, which are expressions of a geologically complex environment. In addition the study intentionally ruled out the Palaeoproterozoic and Archaean rocks as being prospective but did little to differentiate between the metasediments of the KAB rocks in which exist important rheological contrasts.

The geological features (predictor layers) extracted during this study (structures and host lithology were then integrated in the wildcat modelling technique proposed by *Carranza (2010)*. In this knowledge-guided, data driven method, *Msechu, (2011)* assumes that all the quartz vein gold deposits in the study area are related to orogenic-gold mineralisation which is unlikely given the fluid inclusion results *(Pohl, et al., 1991)* described in Chapter 1.1.3.1.

This work identified a prospective host terrane and potential fluid conduits however, it failed to predict where and how the gold rich fluid might be trapped in sufficient quantities for the formation of a gold deposit. Such studies would involve the identification of a physical throttle (see Chapter 4).

1.2. Research problem statement

In Uganda gold is known to occur in Archaean-Proterozoic aged rocks where the tectonic setting implies that several deformation events have resulted in the metamorphic reworking of the ancient crust, and ultimately the remobilisation and concentration of gold enriched fluids, consistent with the current understanding of orogenic gold *(Groves, et al., 1998)*. Traditional field mapping culminated in the first published geological map of Uganda *(Hepworth, et al., 1966)*. Since then attempts at understanding the geological evolution have only been studied in broad outline and much remains to be understood about the structural controls on mineralisation. In previous studies *Pohl (1994, 1991)* have shown that gold mineralisation in the Karagwe Ankolean Belt is associated with successive periods of extension and compression spanning the time period 1400-900 Ma and termed the Kibaran event. Recent work by *Tack et al. (2010)* has shown that the Kibaran event is a short-lived tectonomagmatic event at 1375 Ma concluding that the gold mineralisation post-dates this tectonomagmatic event and most likely to be

associated with the Lomamian Orogeny dated 1000-950 Ma *(Pohl, et al., 1991)* or the Pan African Orogeny at ~500 Ma *(Dewaele et al., 2011)*.

With this new understanding and the recent acquisition of high quality geophysical data, the challenge is now to improve our understanding of the regional structural architecture thus improving our knowledge of the source and causes of gold deposition and hence mineral potential in the area.

1.3. Aims and objectives

The general aim of this project is to develop a district-scale mineral systems understanding of south-west Uganda and use this knowledge to identify gold exploration opportunities.

Exploration success is often inhibited by the explorer who selects a specific model at the expense of others and often misses different styles of mineralisation. In recognition of this limitation, this district-scale study has adopted the concept of a 'mineral system' which is independent on the type of deposit but which is constrained by the scale of the data. The mineral system approach was first developed for the petroleum industry by *Magoon et al. (1991)* and then later modified by *Wyborn et al. (1994)* to accommodate large energy and fluid systems typical of hydrothermal deposits. Mineral systems at this scale are complex and at best poorly understood, requiring a process-based conceptual approach using the "Five question paradigm" outlined by *Walshe et al. (2005)*. The five question scheme which takes into account the spatial and temporal evolution of the system at all scales. The five questions are:

1. *What is the architecture and size of the system?*
2. *What is pressure, temperature and geodynamic history of the system?*
3. *What is the nature of the fluids and fluid reservoirs in the system?*
4. *What are the fluid pathways and drivers of the fluid flux?*
5. *What are the transport and depositional mechanisms?*

Specific aims include:

- The aim of this study is to effect a complete geological reassessment of the south-west Uganda, integrating historical geological maps, geological field data, and remotely sensed optical and airborne geophysical data into a new geological interpretation.

- Identify and delineate favourable regional scale controls (proxies) of gold mineralisation within the geodynamic history that are related to critical orogenic gold forming processes.

- These proxies are then weighted according to their role in the mineralisation processes, translated into predictor maps and finally integrated into a gold prospectivity map for south-west Uganda. Details of the specific critical processes and process proxies are defined in methology section (Chapter 2).

1.4. Research questions

Of the five questions paradigm, outlined in section 1.3, questions 3-5 can be immediately ruled out of this study as they are primarily concerned with economic and ore geological studies involving fluid inclusions work, isotope studies and petrographic analyses which for which the available dataset is inappropriate and such studies are beyond the scope of research at this time. In addition spectral data, which would normally

provide information on the key alteration mineral assemblages and hence proxies to answer to questions 3 and 4, is impractical in this densely forested region of Uganda. Multielement geochemical datasets are also not available at this early stage of Uganda's modern exploration history.

Given the available data, and the scale of investigation, questions 1 and 2 of the 'Five Question Paradigm' can be answered following the methodology outlined in Chapter 2.

What is the architecture of the system?
What is the geodynamic history of the system?

1.5. Available regional datasets

In an attempt to revamp the mineral sector and attract new investment, the Ugandan government, funded by the Wold Bank, Nordic development fund and the African development bank has acquired regional scale high quality geophysical datasets covering nearly 80% of the country. These datasets include:-

- High resolution airborne aeromagnetic data (50 m resolution) and
- Gamma-ray spectrometric data (50 m resolution).
-

The magnetic and gamma-ray spectrometric data was acquired by Fugro at a flying height of 80 m along NE-SW trending flight lines separated by 200 m and at a sampling interval of 0.1s and 1s respectively. Additional datasets include:

- SRTM DEM (90 m resolution).
- ASTER DEM (15 m resolution).
- Digitised geological map sheets at 1:100 000 and 1:150 000 supplied by the Ugandan Geological survey which partially cover the area.
- Six scenes of Landsat TM bands 1, 2, 3, 4, 5 and 7 (30 m resolution) acquired from different dates varying between July 1999 and December 2001.
- Fact structural data extracted from various map sources and additional data was made available by the geological survey of Finland (GTK) from the ongoing geological mapping project in Uganda.
- Isotopic age data *(Mänttäri, 2011).*
- Known gold occurrences from the mineral database.

Further data collected in the field, aimed to understand the controls of gold mineralisation on a local scale at artisanal mining sites and on structural kinematic indicators to validate the geological interpretation. Figure 3 illustrates the study area and the available datasets.

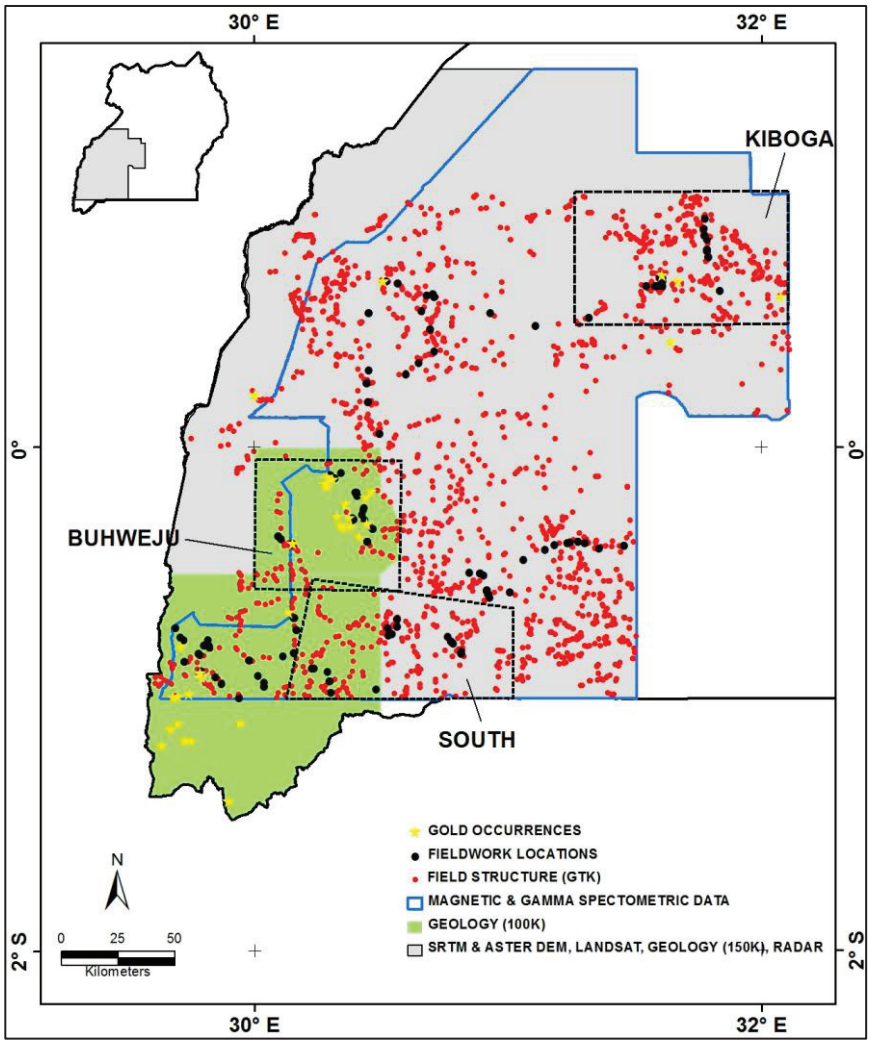

Figure 3: Location of the study area in south-west Uganda, illustrating the coverage of the available datasets.

1.6. Organisation of the thesis

This thesis aims to integrate the available geological datasets and map the gold potential of the south-west Uganda.

The first chapter defines the research problem in relation to the available datasets. The literature review provides critical background information from which the conceptual model was formulated, leading to the research objectives and research questions.

Chapter 2 outlines the methodology of first two phases of the research, the geological interpretation and the fieldwork. It also includes a brief description of the methodology used in prospectivity modelling phase, however since this largely depends on the results of the geological interpretation (Chapter 3), they are discussed in more detail in Chapter 4.

Chapter 5 is a discussion of the results from all phases and Chapter 6 presents answers to the research questions, concluding with recommendations for future work.

2. METHODOLOGY

2.1. Introduction

Translating the mineral systems approach to practical exploration targeting requires a framework to link conceptual models with the available data. The conceptual model requires a good understanding of the key processes and their timing within the geodynamic history of the area. The challenge is that processes cannot be mapped, only their results. The processes must then be translated into to mappable units from the available datasets. *McCuaig, et al.(2010)* have proposed a four step process (Figure 4) linking a conceptual mineral system with the available datasets thus illustrating the need to define (1) the critical processes of the mineral system – without which the mineral deposit cannot form, (2) constituent processes of the mineral system are specific to an orogenic gold mineral system (3) targeting elements, reflected in the geology, are features that provide evidence that the processes have occurred, (4) targeting criteria used to detect the targeting elements directly or by proxy. These are the predictor maps, queried by GIS-based prospectivity analyses.

The significance of the targeting elements and their mappable criteria is defined on the basis of scale and available datasets. In this study, a district-scale (1:100 000) investigation is considered appropriate given the scarcity in geological information and absence of existing world-renowned deposits. At this scale of orogenic gold mineral systems understanding, evidence for the source of gold, active pathways and the physical traps are considered to be critical and is less concerned with the chemical depositional mechanisms. Figure *5* illustrates a conceptual model modified from *McCuaig et al. (2010)* highlighting how the critical and constituent processes of orogenic gold can be identified through mapping the fundamental boundaries, magmatic history and structural deformation using the available datasets in Uganda and Figure 6 illustrates how all the datasets are integrated to ultimately provide answers to the research questions.

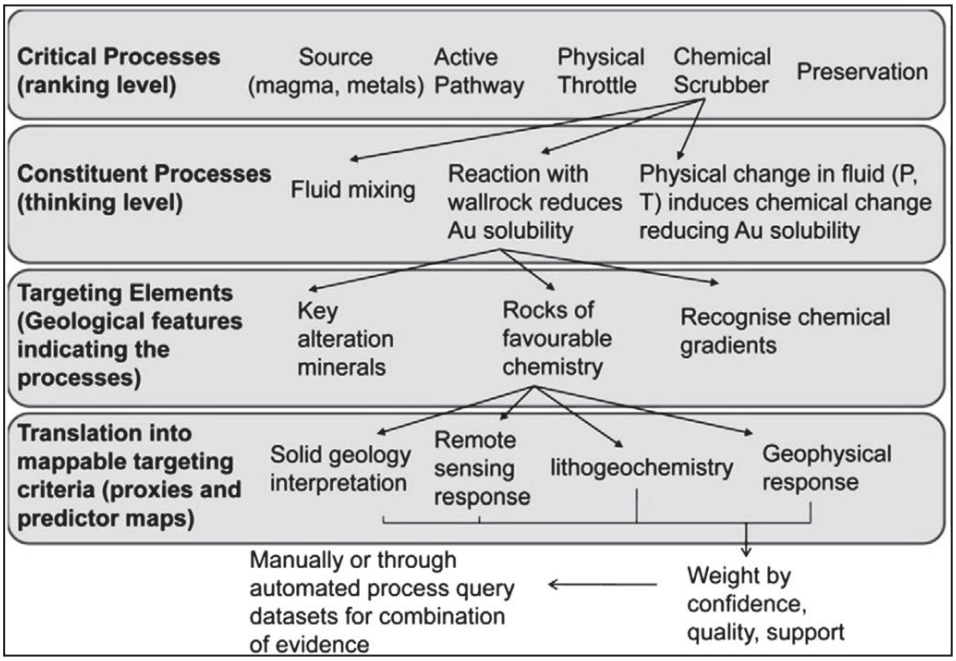

Figure 4: Critical processes of an orogenic gold mineral system and the related mappable targeting criteria, using a chemical scrubber as an example (after *McCuaig et al., 2010*).

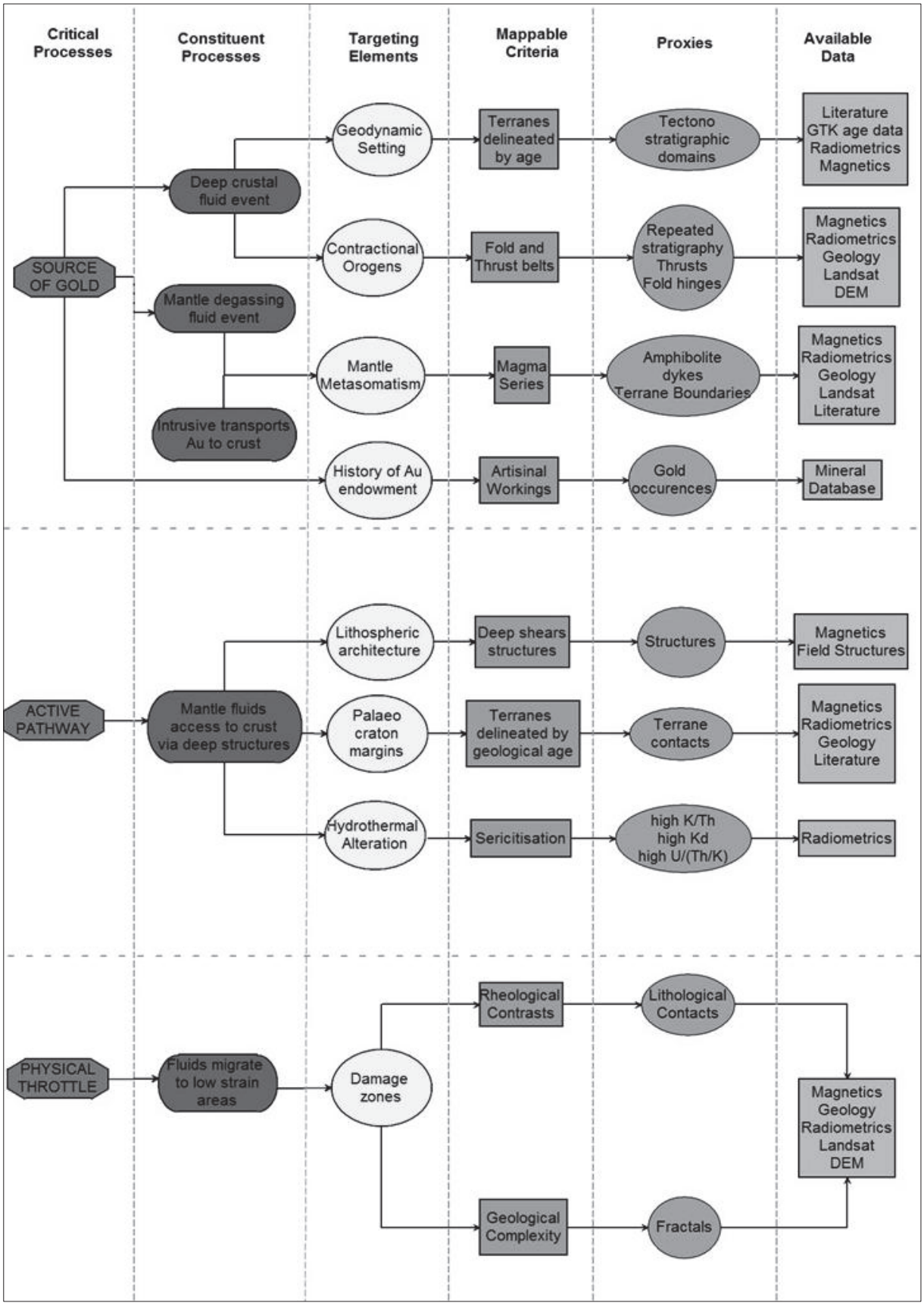

Figure 5: Conceptual framework illustrating how the critical processes (source, active pathways and physical throttle) of orogenic gold formation are related to the mappable mineral proxies at a district-scale given the available dataset in Uganda. (Modified after *McCuaig et al., 2010*)

The research has been divided into four main phases as summarised in Figure 6 below:

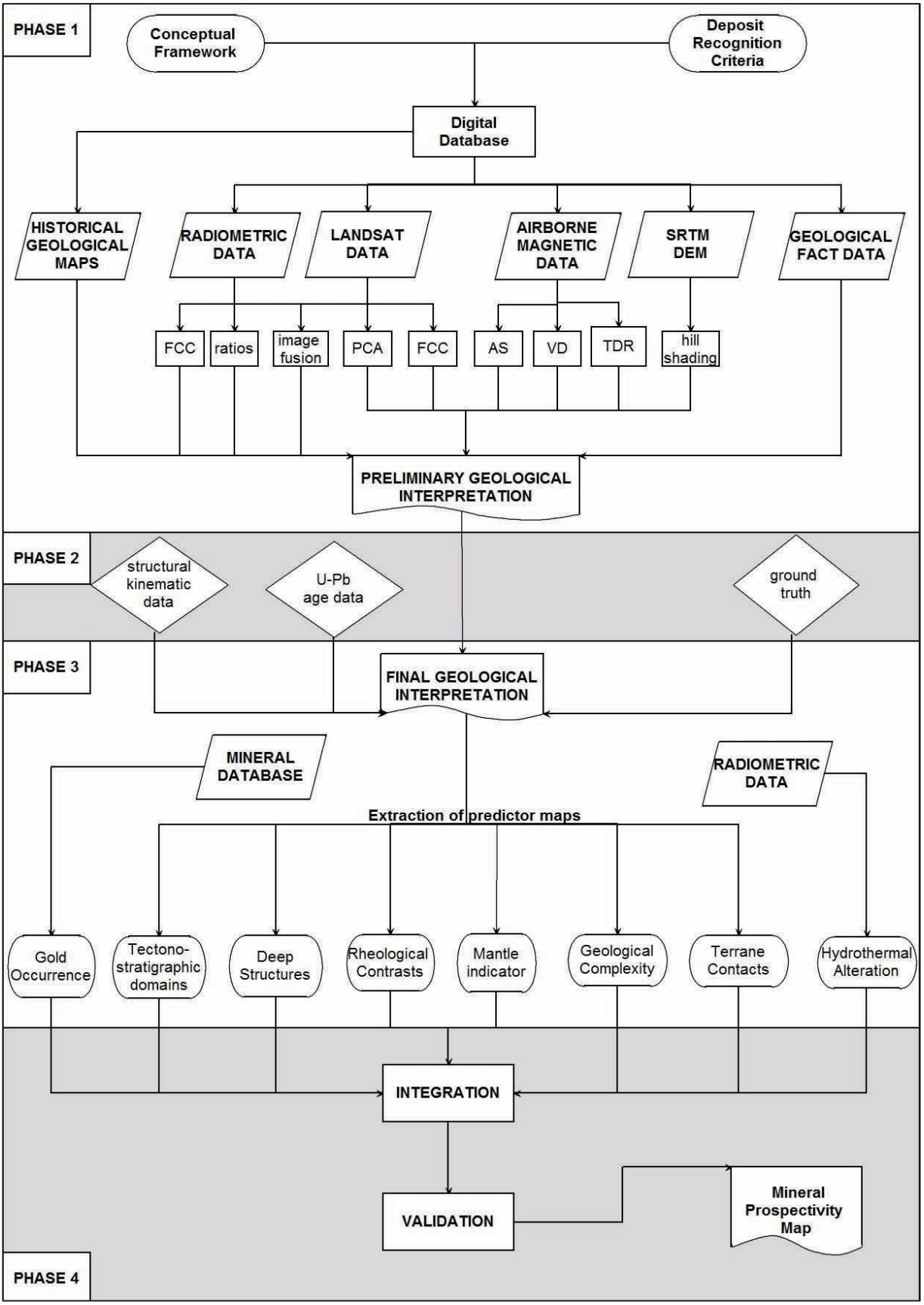

Figure 6: Research framework

2.2. Phase 1 - Preliminary geological interpretation

The geological interpretation (lithological and structural) is principally based on remote sensing data from a regional perspective, outlining the mobile greenstone belts, lithological formations in geochronological order and the related deformation events, towards a detailed interpretation of individual units and structures. This first stage of the project is divided into five main steps; data evaluation, image processing, data integration, digitizing, geological interpretation and map visualization.

During data evaluation, all datasets were inspected and georeferenced into UTM WGS 1984 coordinate system, zone 36N and clipped into study area.

2.2.1. Landsat TM

Image enhancement techniques of Landsat TM data includes linear and contrast stretching of single bands, band ratios, and False Colour Composites (FCC) and Principal Component Analyses (PCA).

Landsat TM B5 and B7 provided the best single bands for the extraction of different textures from which lithological information was derived. Texturally smooth prominent ridges were used to delineate quartzite, whereas the parallel drainage patterns help to delineate less competent sediments such as phyllite and shale. Band ratios 3/1, 5/4 and 5/7 are applied to enhance areas rich in Fe-Oxide, Fe Oxide-hydroxide and OH-phyllosilicate which were regarded as laterite and hence unimportant for this study. False colour composites were created into order to delineate lithological units. The correlation coefficient calculated for Landsat TM data in the Kiboga and South areas (Table 1) reveals that Bands 4, 5 and 7 shows the least correlation with the other bands. RGB band combinations 457 and 731 and 732 were thus chosen as they provide the best colour composites for visual interpretation over the drier and mountainous regions (Figure 7).

The diagnostic spectral properties of the rocks and minerals are disturbed by the prolific vegetation in the area and so were not employed. The location of the subset areas is illustrated in Figure 3.

Table 1: Correlation coefficients of Landsat TM data in the Kiboga and South Regions

Correlation coefficient matrix for the Kiboga Area						
	B 1	**B 2**	**B 3**	**B 4**	**B 5**	**B 7**
B 1	1.00					
B 2	0.89	1.00				
B 3	0.89	0.93	1.00			
B 4	0.10	0.16	-0.04	1.00		
B 5	0.66	0.79	0.79	0.23	1.00	
B 7	0.74	0.80	0.87	-0.01	0.90	1.00

Correlation coefficient matrix for the South Area						
	B 1	**B 2**	**B 3**	**B 4**	**B 5**	**B 7**
B 1	1.00					
B 2	0.92	1.00				
B 3	0.78	0.91	1.00			
B 4	0.45	0.54	0.30	1.00		
B 5	0.70	0.85	0.91	0.47	1.00	
B 7	0.63	0.76	0.90	0.16	0.90	1.00

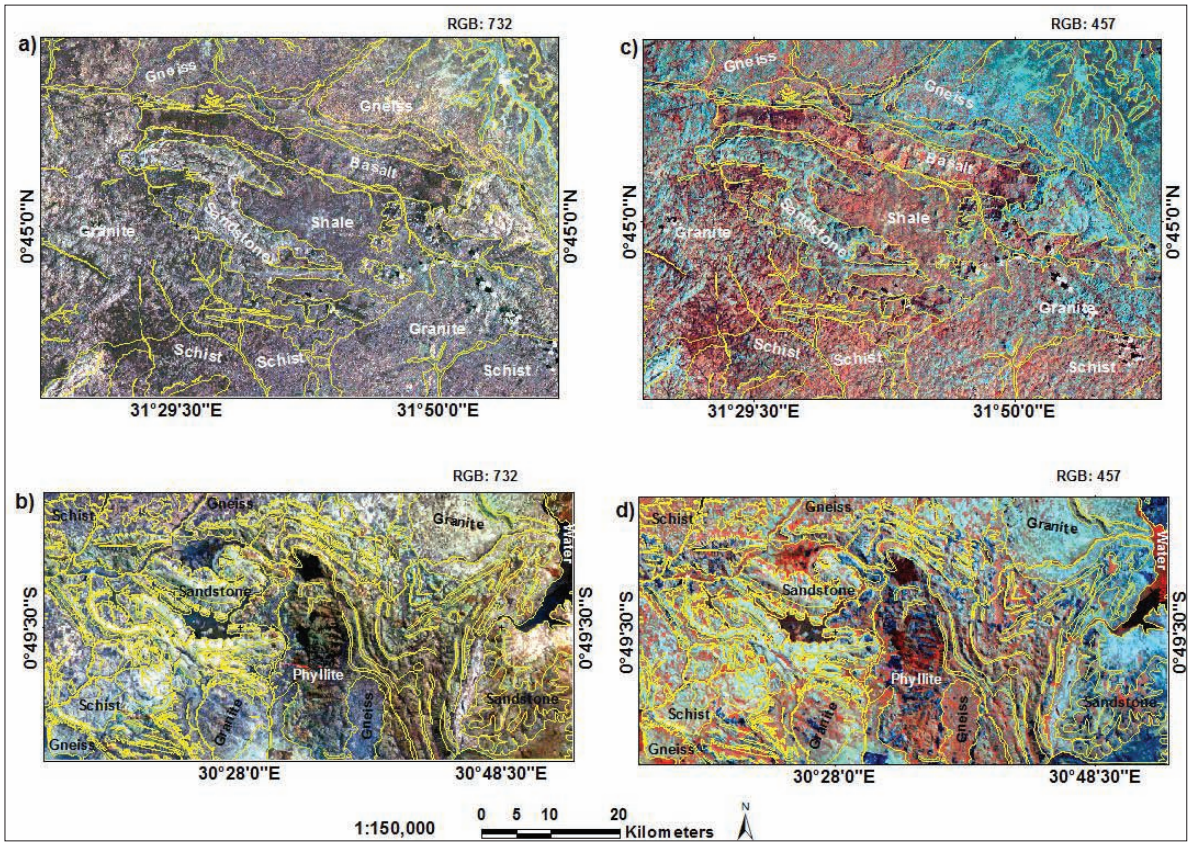

Figure 7: LANDSAT TM false colour composites of selected regions in the study area a) Kiboga Area: RGB: 732 b) South Area RGB: 732 c) Kiboga Area RGB: 457 d) South Area RGB: 457

A principal component analysis was used to effectively minimize the redundant information within highly correlated bands. The PCA processes the original input band values into a new set of orthogonal coordinate axes. The first principal component (PC1) is in the direction of the greatest variance of the data. The second principal component is perpendicular to the first and has the next largest variance. Since the study area is covered by six LANDSAT scenes of variable cloud, water and vegetation cover, and the coefficients used in the principal component analysis are derived from a statistical analysis, certain areas were manually subset in order to minimise the variance in the data. PC1 was used to enhance subtle linear features from which structural information was extracted in grey scale. In addition, because it provides optimal enhancement of geomorphological features, PC1 was also useful in extraction of lithological features based on differing textural relief. Figure 8 illustrates the RGB FCC of PCA results of two areas where a) bands PC 1;2;3 b) PC band 2;3;4 in RGB order provided the best combination to extract lithological information illustrated by their eigenvalues (Table 2).

Table 2: Eigenvalues and their relative percentages from the PCA in a) the South region and b) the Kiboga region

a)			
Axis	**Eigenvalues**	**%**	**Cumulative %**
PC1	1081.13	73.72	73.72
PC2	234.89	16.02	89.74
PC3	100.81	6.87	96.61
PC4	31.26	2.13	98.74
PC5	11.10	0.76	99.50
PC7	0.91	0.06	100.00

b)			
Axis	**Eigenvalues**	**%**	**Cumulative %**
PC1	164.41	54.39	54.39
PC2	113.90	37.68	92.07
PC3	16.19	5.36	97.42
PC4	3.32	1.10	98.52
PC5	2.51	0.83	99.35
PC7	0.56	0.18	100.00

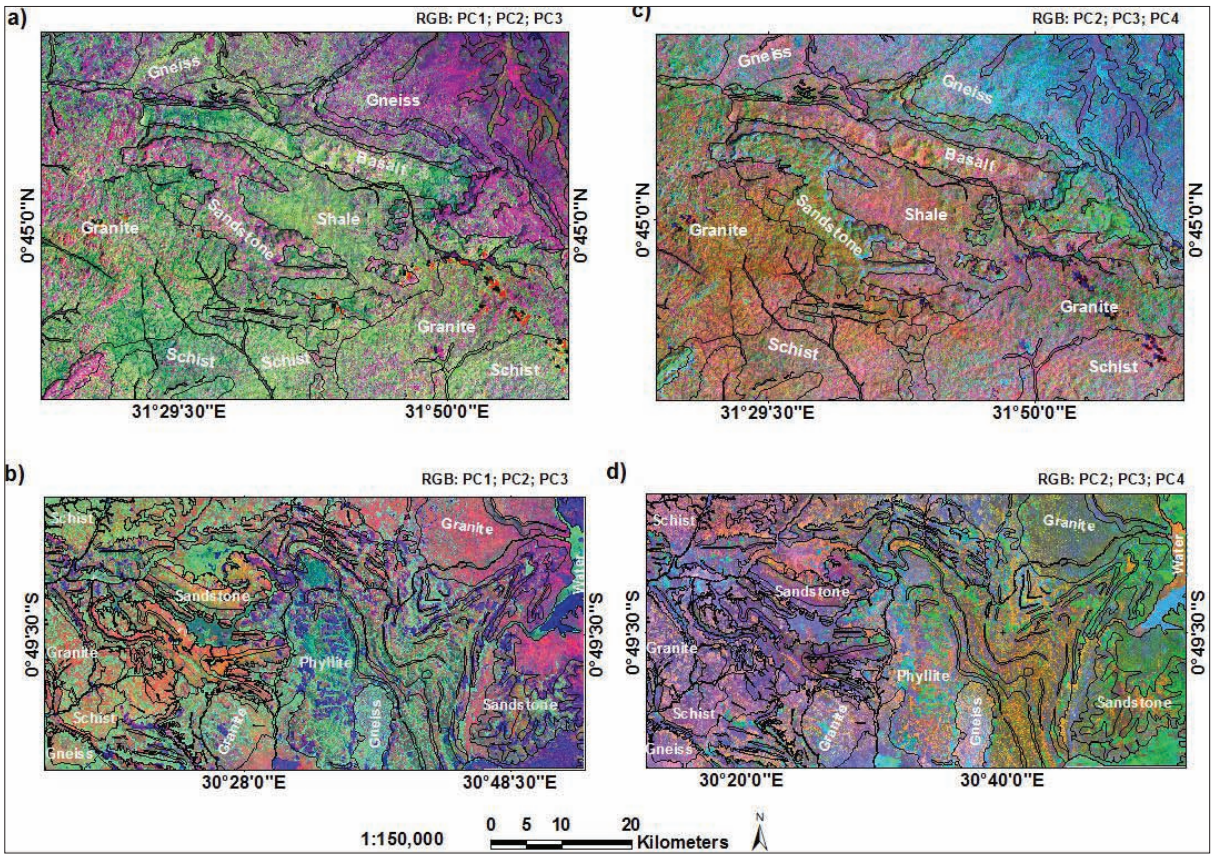

Figure 8: LANDSAT TM PC false colour composites of selected regions in the study area a) Kiboga: RGB: PC123 b) South RGB: PC123 c) Kiboga RGB: PC234 d) South RGB: PC234

2.2.2. Gamma-ray spectrometric Data

The gamma-ray spectrometric data enhancement techniques include ternary radioelement maps in RGB colour space (Figure 9), band ratios and interactive contrast stretching of single bands during the interpretation.

Integration of gamma-ray spectrometric data with higher resolution satellite imagery was used to enhance the geochemical information contained in the lithological units (provided in the gamma-ray spectrometric data) and textural features (provided in the satellite imagery). The integration process requires the registration of all datasets to a common grid call size (30m) before they are 'fused' in colour composite images to the pixels according to the following algorithm *(Chavez et al., 1991).*

$$\text{Red} = 1/c\ (a*K + b*TM5)$$
$$\text{Green} = 1/c\ (a*eTh + b*TM5)$$
$$\text{Blue} = 1/c\ (a*eU + b*TM5)$$
$$c = a+b$$

Where a = 2, b = 3 and c = (a+b) = 5 which are factors used to weigh the hue and saturation with the intensity contrast from Landsat TM band 5.

Figure 10 illustrates the effectiveness of this image fusion technique in highlighting geological information. Additionally, the ternary imaged was pan-sharpened with both the DEM (Figure 9) and the magnetic tilt derivative (TDR) (Chapter 2.2.5) to enhance structural information.

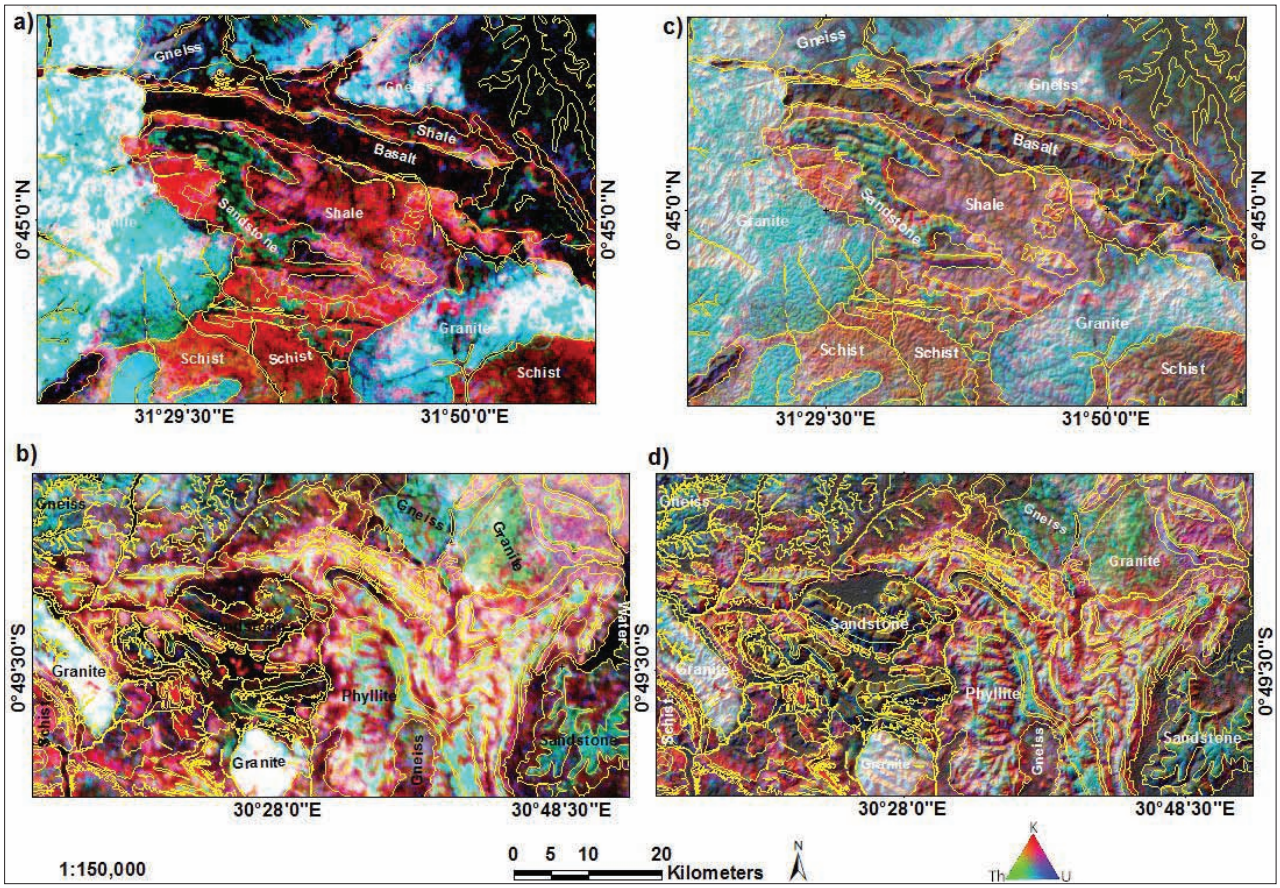

Figure 9: Gamma ray spectrometric data of selected regions in the study area a) Kiboga: RGB: K eTh eU b) South RGB: K eTh eU c) Kiboga RGB: K eTh eU pan sharpened with hill shaded ASTER DEM d) South RGB: K eTh eU pan sharpened with hill shaded ASTER DEM

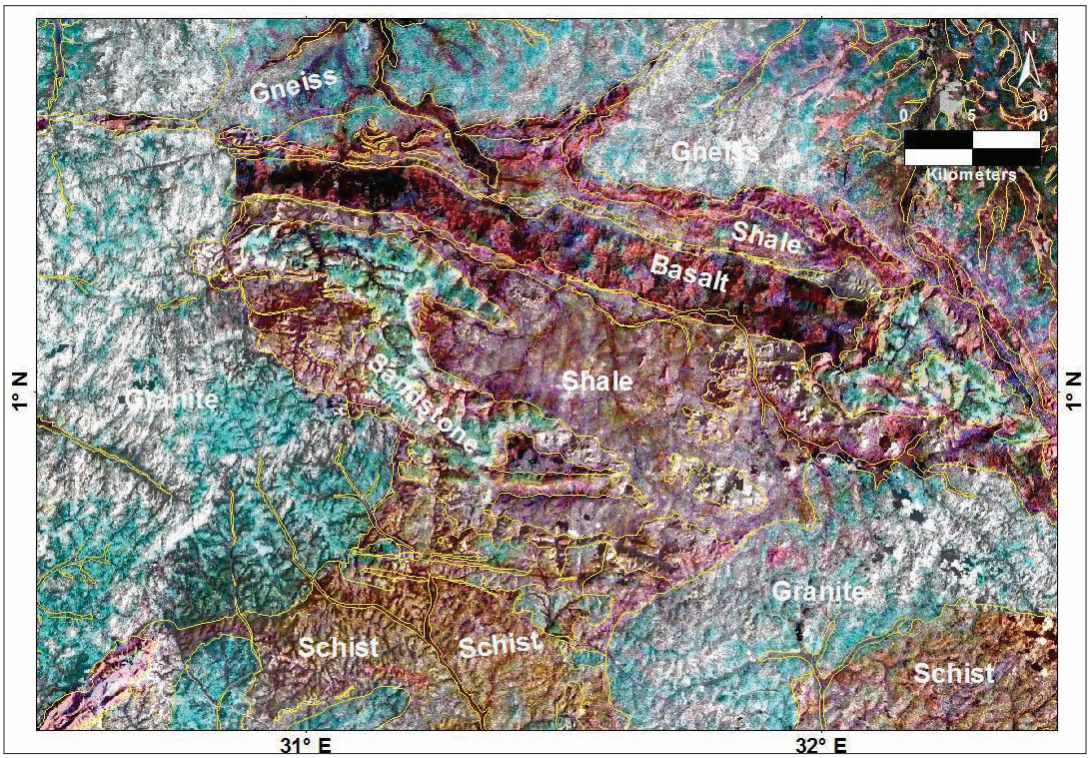

Figure 10: Image fusion of gamma-ray spectrometric data and Landsat TM B5 in the Kiboga Region (RGB= K eTh eU)

2.2.3. SRTM DEM Data

A hill-shaded DEM from both SRTM and ASTER DEM data was created using tri-directional illumination (270°, 315°, and 360°) and 30° sun inclination. Figure 11 a and b are subsets of the hill-shaded aster DEM. Additionally the hill-shaded SRTM DEM was fused with LANDSAT TM band 7 in order to create stereo anaglyphs (Figure 11 c and d).

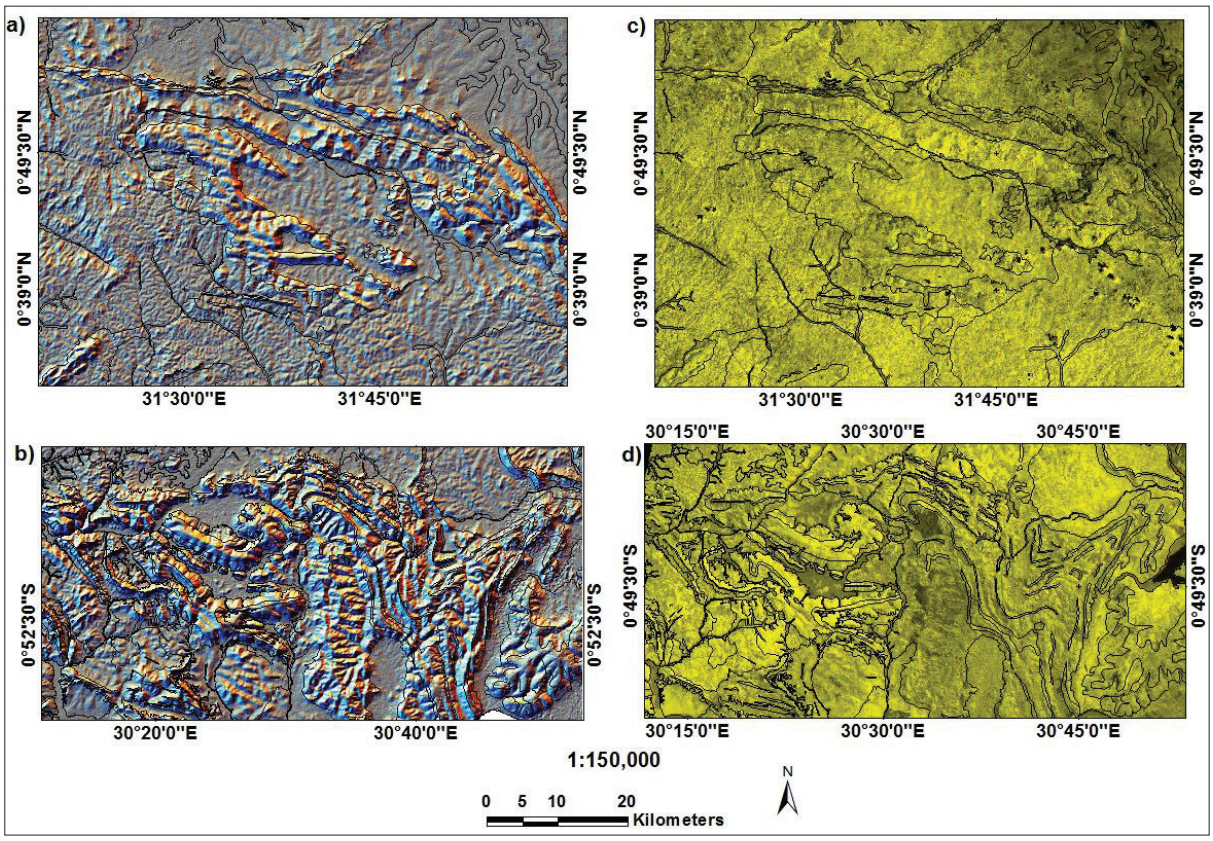

Figure 11: Processed DEM data of selected regions in the study area a) Kiboga: hill shaded ASTER DEM b) South: hill shaded ASTER DEM c) Kiboga: Stereo anaglyph d) South: Stereo anaglyph

2.2.4. RADAR Data

The ScanSAR is a large scale dataset covering 400 km x 400 km with a spatial resolution of 100 km. The ability this radar data to penetrate through clouds and vegetation to give a surface roughness makes it especially useful for geological mapping in densely forested tropical regions of Uganda. The scanSAR data was geometrically corrected and used to extract lithological boundaries based on differences in surface roughness.

2.2.5. Aeromagnetic Data

The aeromagnetic data was supplied in grid format as Total Magnetic Intensity (TMI) format, where data spikes (undesired high amplitude short wavelength features) were removed by non linear filtering.
Enhancement filters of the airborne total magnetic intensity (TMI) data includes extraction of the analytical signal (AS) and first vertical derivative (VD) and magnetic tilt (TDR) derivatives using Oasis Montaj displayed in Figure 12 .

The AS is the magnitude of the total derivative, and therefore has the effect of broadening the magnetic anomalies. The AS is particularly useful in determining major terrane boundaries based on differing

magnetic properties and lithological boundaries marked by large changes in the intensity of the AS for example the Bujangali basalt in Kiboga region and the dolerite dyke swarms.

The VD enhances the higher frequency shallow features, and has the effect of removing the regional trends. The VD is useful in identifying closely spaced magnetic bodies (dolerite dyke swarms) by providing better resolution. Similarly the TDR, which represents the direction of the total derivative highlights the narrow linear features and provides an excellent base for the structural interpretation.

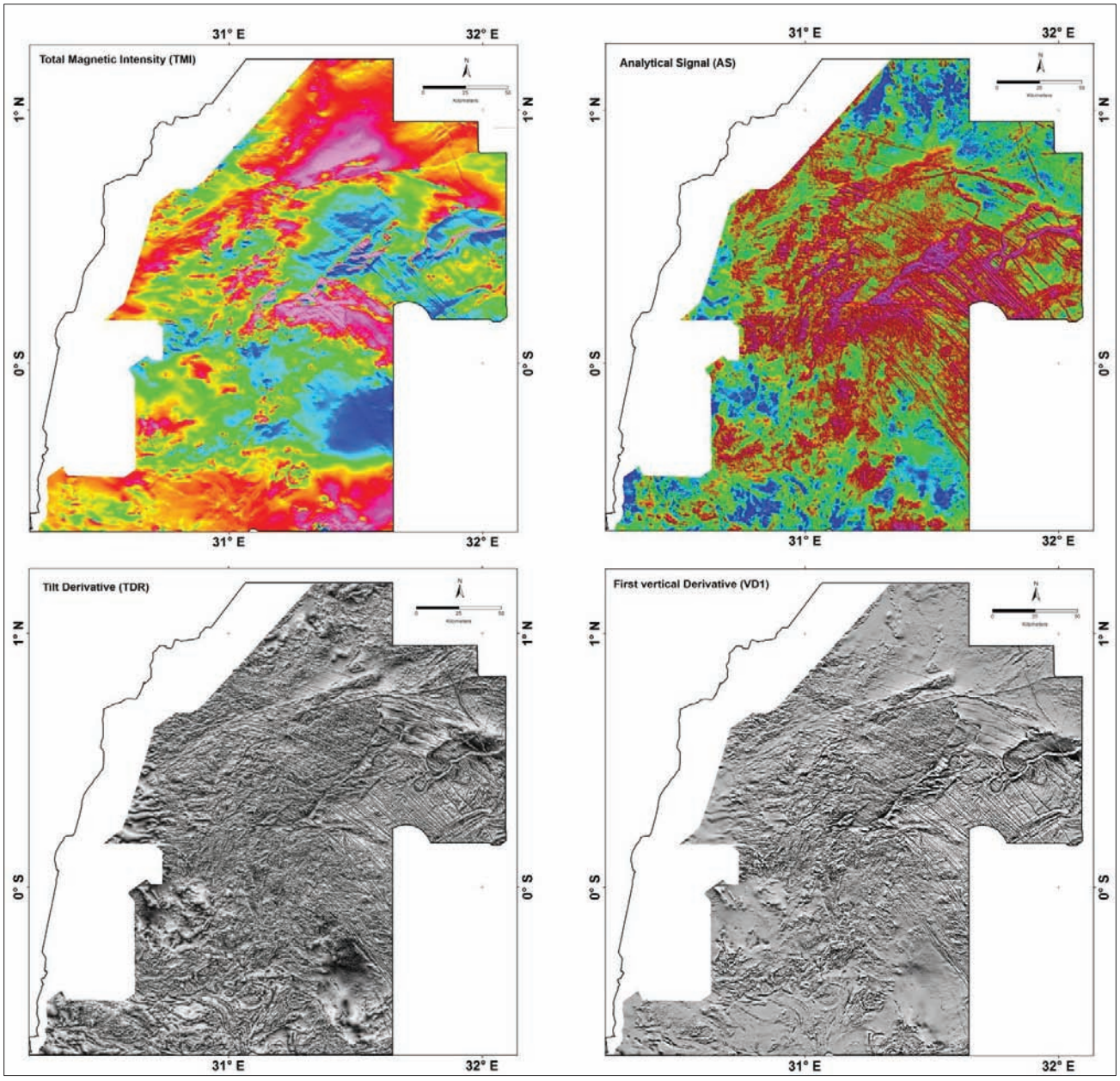

Figure 12: Derivatives of the magnetic data a) Total magnetic intensity b) Analytical signal c) Tilt derivative d) First vertical derivative.

2.3. Phase 2 - Field work in Uganda

The fieldwork phase involved the validation of the interpreted geology along selected cross sections and the collection of structural data.

Figure 13 below illustrates the areas visited (red) combined with the distribution of available structural data structural data (green). In areas where structural data was little or missing, complementary data from the Ugandan Geological Mapping Project conducted by GTK was used. Field work also reviewed several areas of artisanal gold mining in order to understand the local scale geological controls of mineralisation. Structural measurements are detailed in (Appendix 2).

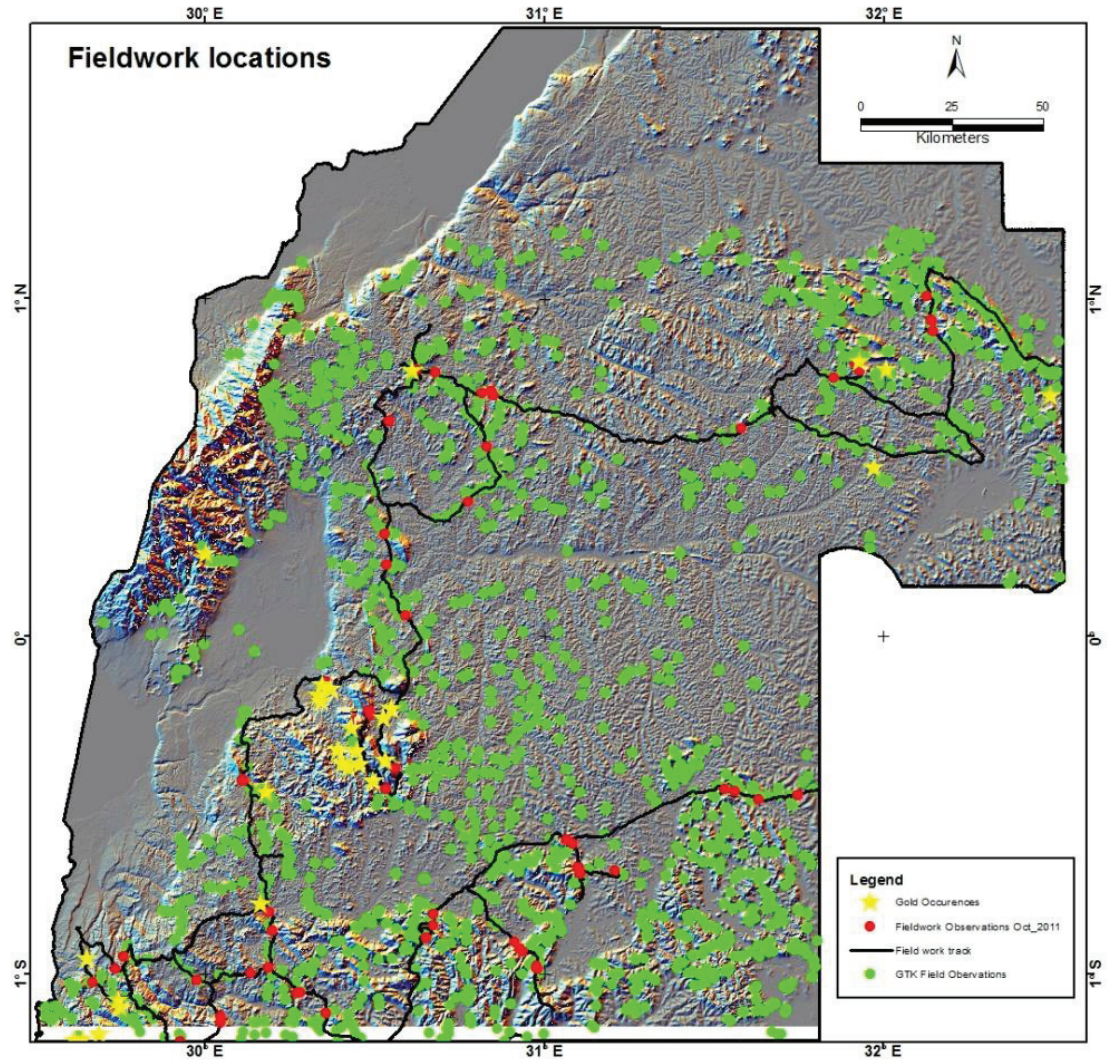

Figure 13: Map showing the area covered by fieldwork in October 2011. Field observations in current study =red dots, GTK =green dots

2.4. Phase 3 - Prospectivity modelling

The ultimate aim of this phase of research is to construct a 'prospectivity' map, that has a predictive capability in assessing the likelihood that the given study area could host an orogenic gold deposit.

Using the conceptual approach to prospectivity mapping, the genetic concepts of orogenic gold formation (Figure 5) are translated into mappable criteria at a district-scale, and integrated into a single prospectivity

map. There are several different integration techniques available, ranging from very simple Boolean techniques to more complex index overlay, Bayesian, algebraic and fuzzy logic methods.
Multi-class index overlay method will be used to model the prospectivity in the study area. Each class of evidence (j) in a predictor map (i) is given a score S_{ij} (0-10) depending on its importance in mineral prospectivity and each predictor map is assigned a numerical weight (W_i) based on 'expert' judgement of its role in the critical processes of orogenic gold. Finally each of the predictor maps will be combined according to the following equation from *Carranza (2009)*:

$$\overline{S} = \frac{\sum_{i}^{n} S_{ij} W_i}{\sum_{i}^{n} W_i}$$

Multi-class index overly method used to model the prospectivity in the study area. Where the output $\overline{S}$ for each location is the sum of the products of S_{ij} and W_i in each evidential map divided by W_i for each evidential map.

The predictor layers are summarised in Figure 5 as proxies.

3. GEOLOGICAL INTERPRETATION RESULTS

The interactive display of enhanced imagery provided a solid framework for the interpretation of lithological units based of subtle differences in tone, texture, shape, pattern height and association. The relationships between lithological units, structures and intrusives was initially established based on contrasting hues of the ternary radioelement image and textural differences in the SRTM DEM, then later refined using the higher resolution Landsat and anaglyph imagery. All new recognizable lithological units were assigned codes, descriptive characteristics and a source of information. The preliminary codes were later replaced by more comprehensible lithostratigraphic units and geological formations which have been chronologically ordered where possible.

The following section outlines a summary of the geological image interpretation (Appendix 1) of the study area. The descriptions of the image diagnostics for the lithostratigraphic units are ordered from oldest to youngest (Archaean-Quaternary).

3.1. The Archaen basement complex

Rocks of the Archaean aged Basement Complex (BC) are exposed in the north-east, centre and interleaved with Palaeoproterozoic rocks in west of the study area. The BC was broadly identified by lighter hues in the ternary radioelement image reflecting higher concentrations of K eTh and eU and low lying areas with smooth undulating topography and dendritic drainage patterns in the hill shaded SRTM DEM.

Several subunits of the BC exist based on different geochemical signature in the gamma-ray spectrometric data as well as textural differences evident from the SRTM DEM. The variation in geochemistry is evident in the NE of the study area where gneiss subunit shows elevated potassium that can be traced around the folded Buganda Toro Supergroup.

The central portion of the study area displays textural variation within the BC identified by differences in the drainage patterns, where field evidence in the east confirms the presence of finer grained biotite gneiss and in the west the biotite gneiss is porphyritic in texture (Figure 14). The subunits and geochemical variation within the BC were not differentiated in the interpretation.

Figure 14: Photograph of biotite gneiss (Observation point WP020 looking south)

3.2. The Palaeoproterozoic schists

The Toro schists occupy the east of the study area (Kiboga Region) in an EW orientation and are identified by low lying topography and prominent dense dendritic drainage pattern from the Landsat TM and SRTM DEM, and shows characteristically high K values in the gamma-ray spectrometric data. The schists were formed by metamorphosed sandstone and semi-pelitic rocks which mainly consist of quartz, muscovite, cordierite, biotite and chlorite with a flow cleavage or schistosity sub-parallel to the bedding *(Johnson et al., 1960)*. The Toro schist belt adopts a NE orientation west of the Mubende granite, where it is stacked against the BC along NE trending SE dipping thrusts.

Around the Buhweju area (Figure 3) the schists are known as the Igara schist series with varying degrees intercalated quartzite. Field characteristics of the schist appear grey-green in fresh outcrop and red purple (Figure 15) when weathered. Within the schist the more micaceous bands are deformed around the competent quartzite bands. The micaceous flakes measure up to 3mm in diameter.

Figure 15: Photograph of weathered micaceous schist (Igara series) at Mashonga, Buhweju. Photo courtesy of Dr T. Woldai (Observation point WP066 looking down).

The Palaeoproterozoic schists outcrop in the south of the study area beneath the KAB, where cross cutting quartz veins contain tourmaline.

3.3. The Palaeoproterozoic Buganda Toro Supergroup

The Buganda Toro Supergroup unconformably overlies the BC in the Kiboga area and comprises (from oldest to youngest), the Victoria (ortho) quartzite, the Nile shale formation and the Bujangali basalt formation. These units trend WNW-ESE and have been isoclinally folded where main antiformal fold axis plunges steeply to the ESE. These units can be recognized on Landsat TM colour composites by their linear appearance since these units correspond to alternating linear valleys and topographic ridges. The Victoria (ortho) quartzite, Bujangali basalt and Kitumbi metasandstone formations tend to form elevated ridges, with sparse drainage whereas the Nile shale formation occurs in areas of lower elevation. The Victoria (ortho) quartzite is characteristically lighter in tone, and higher in elevation, forming narrow linear ridges. The Nile shale is the least competent of the Buganda Toro Supergroup and tends to pinch out along strike as a result of the intense folding. It is recognized by its dark tone, smooth texture, its position areas of lower elevation and its contact with both the Bujangali basalt above the Victoria ortho quartzite below in the hinge of a syncline. The Bujangali basalt occupies the hinge of the major anticline, forming a competent unit, easily recognizable in Landsat 457 and the analytical signal of the aeromagnetic data. Within this unit, the analytical signal of the TMI reveals WNW-ESE trending nonmagnetic material, possibly indicating hydrothermal alteration along thrusts.

The tight isoclinal folding is accompanied by thrust faults trending subparallel to the main fold axes and extensional faults oriented perpendicular to the fold belt (Figure 16) A major thrust separates the isoclinally folded units of the Victoria ortho quartzite, the Nile shale formation and the Bujangali basalt formation from the unit to the south comprising shale, siltstone, chert and ironstone, of possible Archaean age. This unit is competent and forms elevated areas with sparse drainage and was recognized by bedding/foliation traces in Landsat false colour composite 457.

This fold and thrust belt is thought to be the first deformational event in the area (D1) coincident with the Ubendian Orogeny.

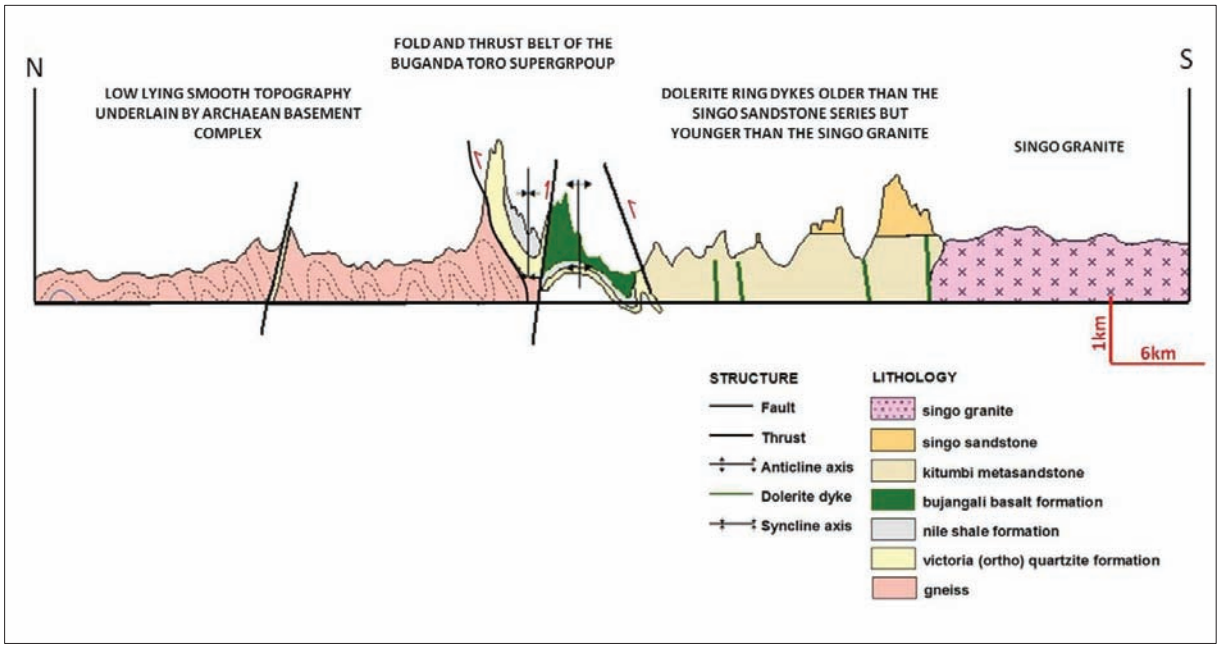

Figure 16: Geological cross section (A-A') through the Buganda Toro Supergroup in the Kiboga area (See Appendix 1).

West of the Mubende granite, the Buganda Toro Supergroup, identified from historical 150k geological map and supported by field evidence, has been divided into subunits based on the differences in geochemical signature from the gamma-ray spectrometric data and texture from the radar imagery. In this region the Buganda Toro has a predominantly NE-SW orientation and is separated from the Archaean basement gneisses by sharp NE trending SE dipping thrusts identified as linear zones of demagnetisation on the TMI, AS and TDR imagery. NE trending fold axes have been truncated by NE trending sinistral shear zones. The shear zones were recognised on the basis of their anastomosing geometry on the TDR. In this area the NE trending fold and thrust belt indicates a possible second deformation event (D2) and a change from a compressional to transpressional tectonic regime.

In the west of the study area the Buganda Toro Supergroup is cut by the western rift of the EARS and is commonly known as the Ruwenzori Mountains, thought to represent an uplifted horst *(Bauer, 2010)*.

3.4. The Mesoproterozoic Karagwe Ankolean Belt

The KAB has been subdivided into an Eastern domain (ED) and a western Domain (WD) *(Tack, et al., 1994)*. The ED domain unconformably overlies the Tanzanian Craton in the SE of the study area, where as the WD unconformably overlies the Palaeoproterozoic Buganda Toro Supergroup and forms the northern limits Kibaran belt.

The ED of the KAB comprises a metasedimentary sequence reflecting a quiet deltaic-marine environment consisting of dark laminated carbonaceous shale (east of Mbarara town) and pelitic sedimentary rocks intercalated with quartzites, sandstone and siltstones. Localised tuffaceous bands interbedded with the fine grained sediments mapped in the hinge of the NE trending syncline, south-east of Mbarara, suggesting it forms part of the Lower Group of the KAB *(Pohl, 1994)*. Regional metamorphism in the sediments is very low grade and syn sedimentary structures are clearly visible as shown in (Figure 17).

Figure 17: Cross bedding in pink quartzite unit. Photograph courtesy of Dr T. Woldai (Observation point WP082 looking NW).

The folded sequence of fine grained sediments is identified from the Landsat TM band 5 by the characteristic parallel drainage patterns (Figure 18). Quartzites within this sequence are useful marker beds, identified by texturally smooth ridges and lighter tone from the Landsat TM B5 and PC1.

Figure 18: Photograph illustrating the parallel drainage pattern characteristic of the fine grained sediments (Phyllite and pelite) of the KAB (Observation point WP021 looking NW).

Folding in the ED has been attributed to the Lomamian Orogeny (1000 Ma) characterized by NE-SW compression. However fold axes in the ED domain trend NE and verge slightly to the SE (onto the Tanzanian craton). Previous authors have described this as cross folds *(Aanyu, et al., 2011),* however early granitic intrusives which are evident in the TDR and AS as round competent bodies are believed to predate the main compressional event and cause strain partitioning.

The WD is differentiated from the ED by its higher metamorphic grade commonly greenschist-amphibolite facies (Figure 19). The metasediments of the western domain reflect a similar depositional environment to the ED, comprising fine grained argillitic sediments and intercalated quartzite.

Figure 19: Amphibolite schist indicative the high metamorphic grade in the WD of the KAB. Kinematic indicators reveal dextral reverse movement. (Observation point WP 040, looking east).

The underlying basement rocks composed of schists and gneisses are recognised in the ternary gamma-ray spectrometric data (RGB: K eTh eU) as cyan – magenta corresponding to high eTh and eU (gneiss) and high K and eTh in the schists. This was differentiated from the younger intrusions in the sedimentary sequences which bear a bright white colour reflecting high concentrations of all ternary elements.

Several S-type granites have intruded the metasedimentary sequence and are easily identified on the ternary gamma-ray spectrometric images in possessing a bright light colour. The TDR highlights several round intrusions which are overlain by swamps and hence not easily visible in the gamma-ray spectrometric data. Field observations reveal that these S-type granites are composed of biotite, muscovite, quartz, K-feldspar and plagioclase and posses a weak-moderate foliation at the contacts (Figure 20). The intrusions appear to have exploited the hinges of the major folds in the metasediments.

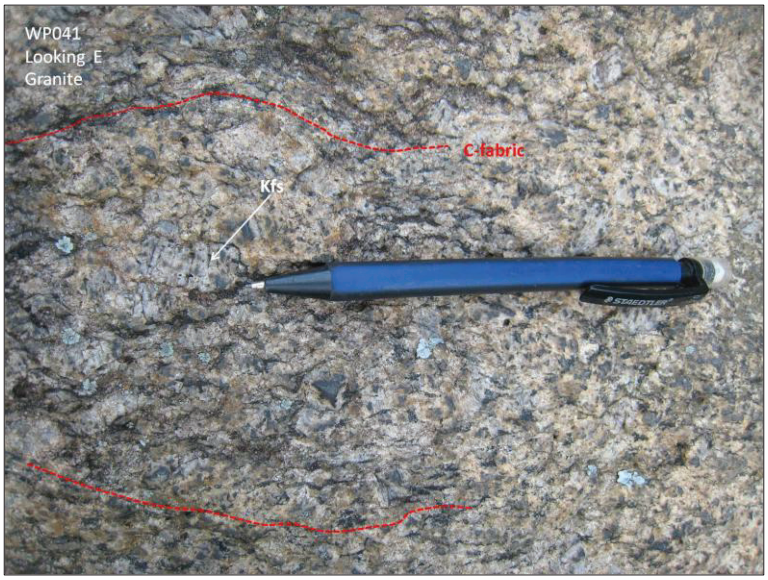

Figure 20: Photograph of weakly sheared Ntungamo granite containing porphyritic potassium feldspar (Kfs) aligned parallel to the shear direction. (Observation point WP041, looking east).

Mafic intrusions comprising hornblende and biotite crosscut the KAB sediments as well as the underlying basement rocks and are undeformed and often associated with contact metamorphic aureoles, indicating intrusion to be relatively late in the evolution of the KAB. These are differentiated from the amphibolite schist based on their sharp contacts.

NE-SW compression created the Karagwe Ankolean fold belt (Lomamian Orogeny , 1 Ga) in the south of the study area. South-west verging folds mapped in the WD of the KAB (Figure 21 and Figure 22) indicate the dominant force came from the NE.

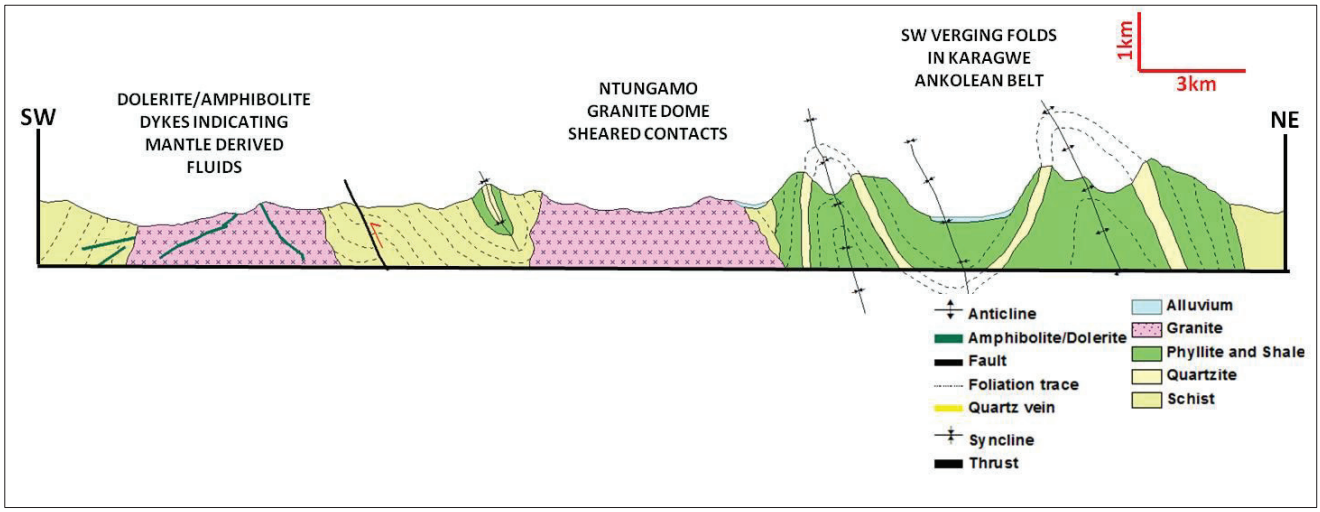

Figure 21: Geological cross section (B-B') through the western domain (WD) of the KAB (see Appendix 1).

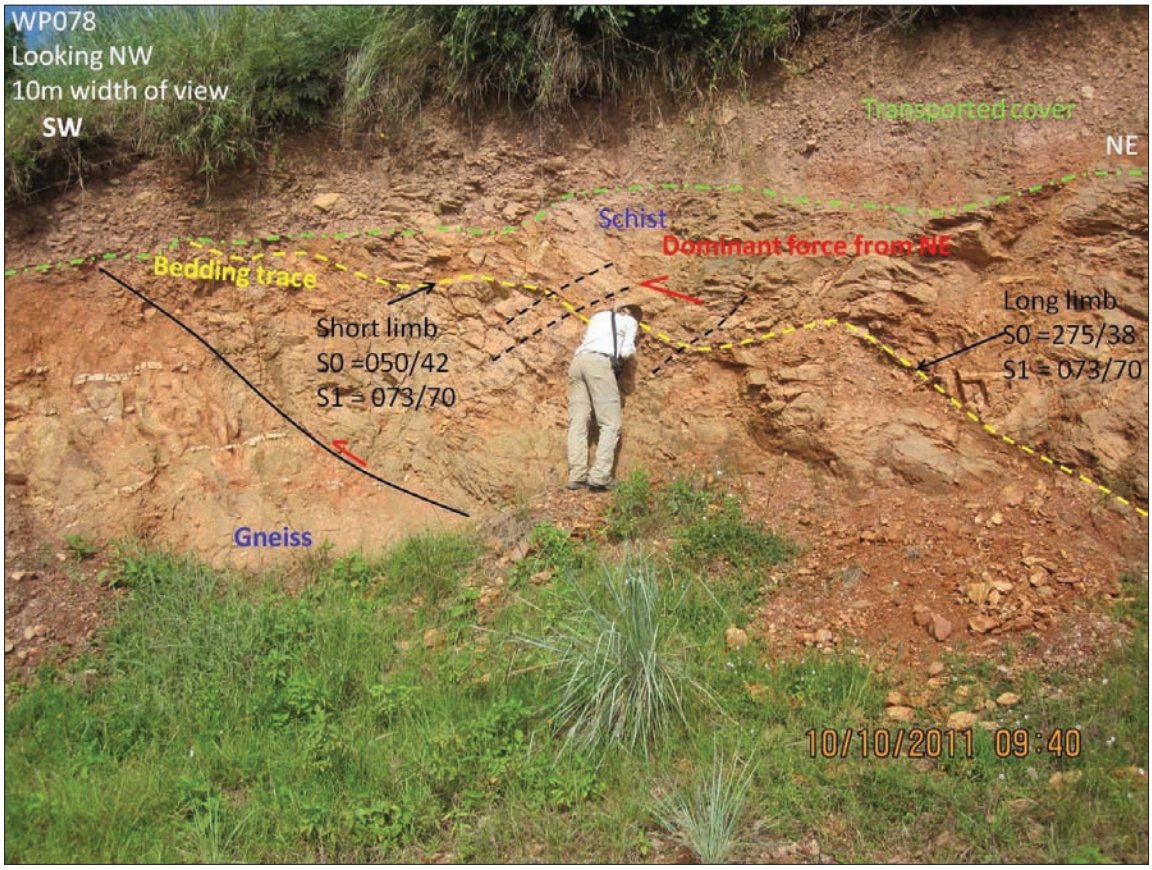

Figure 22: Photograph illustrating the SW directed thrusting in the western domain of the KAB, courtesy of Dr T. Woldai. (Observation point WP078 looking NW).

In the Buhweju area fluvial conglomerates with well rounded quartzitic pebbles (Figure 23) are mapped locally overlying the schistose basement rocks. The conglomerate, reddish quartzite and fine grained pelitic sediments are folded in an open syncline (Figure 24), which according to *Pohl (1994)* forms part of the Upper Group. The basal conglomerate forms elevated topography and coincides with high potassium concentrations from the ternary image.

Figure 23: Poorly sorted, well rounded, matrix-supported conglomerate, Buhweju (Observation point WP071 looking NE)

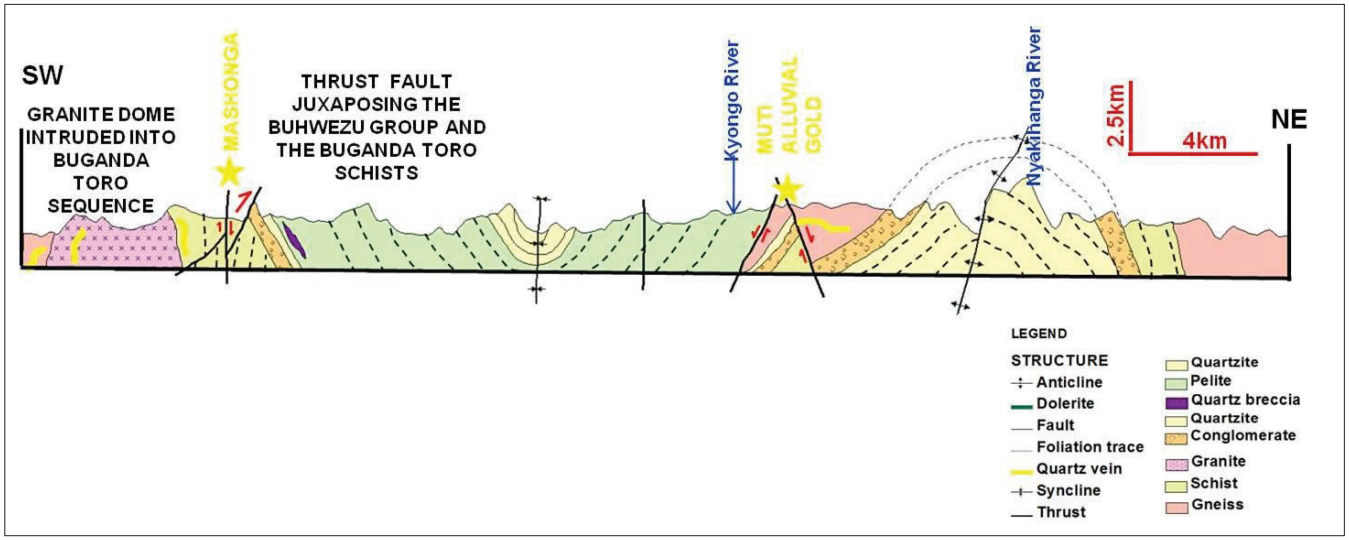

Figure 24: Geological cross section (C-C') through the Buhweju area of the KAB (see Appendix 1).

3.5. The Neoproterozoic sediments

The Neoproterozoic-aged formations within the study area include, Bunyoro, Bukoban and Mityana Series The Bunyoro series appears as an oval-shaped area in the north-west of the study area and comprises a sequence of shale and tillite. Although this area was not visited, *Cahen (1982)* reported that this unit is flat lying and relatively undeformed. Additionally, tillite forms the lower part of the Bunyoro sequence and contains pebbles of up to 50cm in diameter which are dominated by quartzite.

Mityana series occurs in the east of the study area and comprises flat lying undeformed sandstones and conglomerates. The Singo series unconformably overlies the units of the Buganda Toro Supergroup and forms slightly warped plateau dipping gently towards the centre of the study area. This unit consists of conglomerates and sandstones and can easily be detected from the stereo anaglyph image on the basis of its flat geometry, elevated topography and sparse drainage and confirmed during field work. The

sandstone forms the basal unit and conglomerates occupy the upper unit. It is unclear whether it is a separate formation or whether it forms part of the Singo series.

3.6. Cretaceous

Several carbonatites recognized in the NE of the study area have characteristically high eTh and low K and was recognized on the basis of its radioelement concentrations, rounded shape and enhanced elevation.

3.7. The Pleistocene - Recent

Alluvial sediment occupies the river valleys and is composed of unconsolidated alluvial sediments interpreted from Landsat TM imagery. The western branch of the East African Rift System identified using the SRTM DEM and confirmed during field work. Figure 25 below shows unconsolidated rift conglomerates.

Figure 25: Photograph illustrating the unconsolidated rift conglomerates and sediments (Observation point WP046 looking NW).

3.8. Structure

The structural framework was built up from field data and the cross cutting relationships seen in the hill-shaded SRTM DEM, PC1 of the Landsat TM data and various derivatives of the magnetic data including the TDR, VD and AS. The structures have been classified according to type, age and sense of movement in an attempt to place the study area in the context of regional deformation. Figure 26 below summarises the main deformation event using rose diagrams created from field data (bedding, foliation and fold axes). The interpreted structures, extracted by tectono-stratigraphic domain, display a similar clockwise rotation of the principal compressive stress field as shown in Figure 27.

The oldest structures, D1, comprise north verging folds and south-east dipping thrusts in the Buganda Toro Supergroup, suggesting north directed thrusting across an S-shaped basement. The D1 event corresponds to NS compression of the Ubendian Orogeny (2100-1860 Ma) outlined by *Cahen (1982)* (Figure 26 and Figure 27). Post peak deformation and related subsidence coincides with the intrusion of the Mubende granite at 1848 ± 6 Ma *(Mänttäri, 2011)* and the deposition of the Singo series at maximum

sedimentation age of < 1970 Ma *(Mänttäri, 2011)*. NE trending thrusts and fold axes ('D2 structures', Appendix 1) west of the Mubende granite are considered to be part of the same D1 event in the and difference in the orientation is due to the S-shaped ramp-flat basement. In the west of the study area the trend of the structures in the Buganda Toro belt adopts a more ENE orientation coinciding with the Ruwenzori Mountains. The change in orientation is marked by a major NW trending fault believed to be part of the Lomamian Orogeny. The D1 and D2 structures cross cut the basement complex and the Buganda Toro Supergroup but not the Karagwe Ankolean Supergroup.

Later sinistral reactivation of the D1 and D2 structures occurred during the Lomamian Orogeny at 1000 Ma, *(De Waele, et al., 2008)* where NE-SW compression (Figure 27) created the Karagwe Ankolean fold belt in the south of the study area. South-west verging folds mapped in the WD of the KAB (Figure 21) indicate the dominant force came from the NE, whereas in the ED, early granitic intrusives appear to predate the main compressional event and cause strain partitioning. Fold axes in the ED thus trend NE trending and verge to the SE. Within the KAB the two domains (ED and WD) have therefore evolved differently.

Oblique collision between east and west Gondwana during the Pan African event (650 Ma) resulted in the dextral reactivation of the EW trending D1 structures (reactivated D1 = RD1 see Appendix 1) and formation of NS sinistral shear zones.

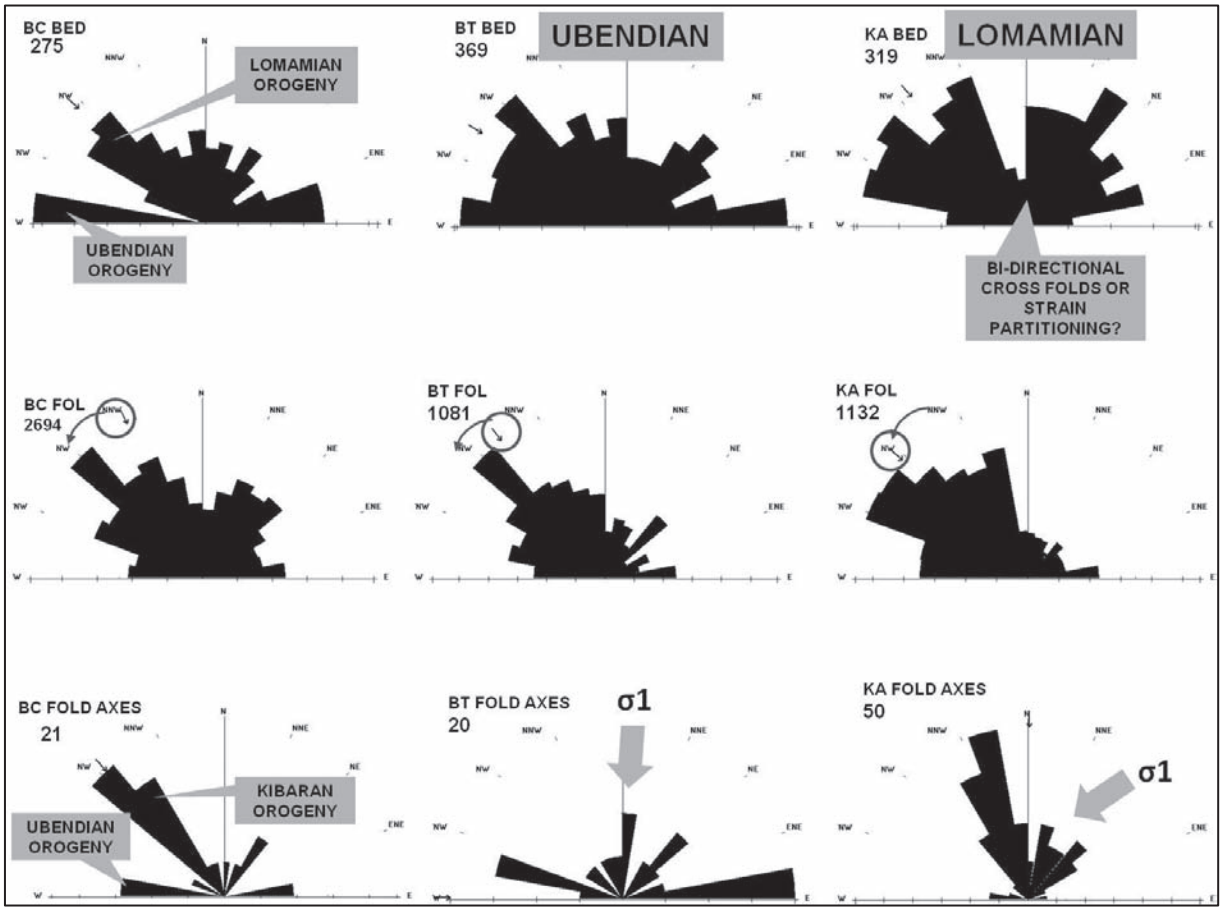

Figure 26: Rose diagrams created from field structural measurements illustrating the major deformation events from oldest (Left) to youngest (Right). (BED = bedding, FOL = foliation, FOLD AXES = fold axes). The foliation mean resultant vector (arrow) rotates anticlockwise indicating that the principal stress field rotates clockwise with time. BC = undifferentiated basement complex, BT = Buganda Toro Supergroup, KA = Karagwe Ankolean Belt, Western Domain

The youngest structures (D5) are related to the Western Rift (Figure 28), and are dominated by NE and NS trending brittle normal faults accompanied by NW and EW transfer faults. These faults cross cut all earlier faults and lithologies.

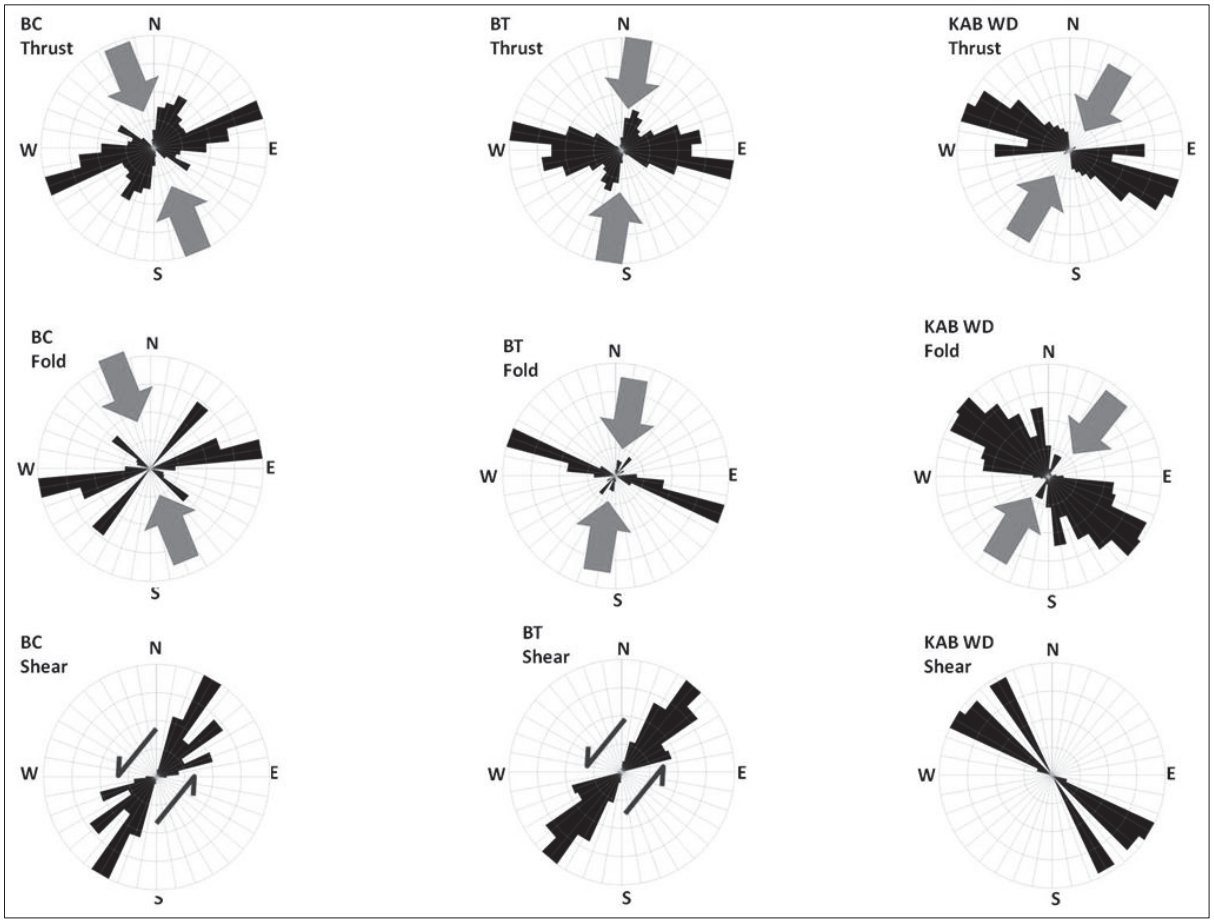

Figure 27: Directional analysis of interpreted structures by tectono stratigraphic domain. BC = undifferentiated basement complex, BT = Buganda Toro Supergroup, KAB WD=Karagwe Ankolean Belt (Western Domain)

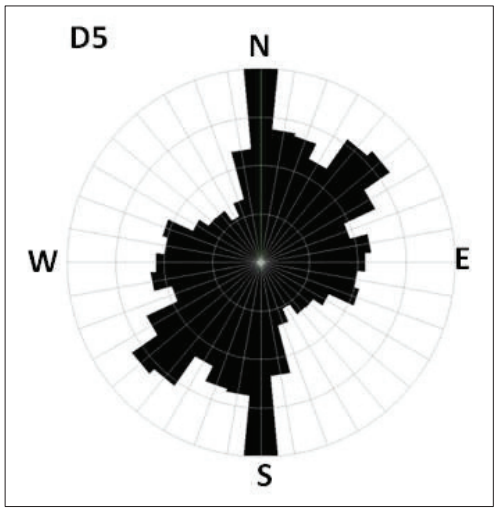

Figure 28: Directional analysis of structures which post-date the main orogenies (D5) related to the western branch of the East African Rift.

4. PROSPECTIVITY MODELLING

In this chapter the reader is referred to the conceptual model described in Chapter 2 and summarised in Figure 5. The lithological interpretation (Appendix 1) was converted into a solid geology map, removing the alluvium that was not attributed to major lakes.

The following sections describe the extraction of proxies derived from mappable criteria, reflecting the critical processes for orogenic gold formation as outlined in Figure 5. Sections describing the tectono-stratigraphic domains (4.1), mantle indicators (4.2), gold occurrences (4.3) reflect the 'source of gold' as a critical process. The 'active pathway' is reflected in the sections about structures (4.4), terrane contacts (4.5) and hydrothermal alteration (4.6) and finally the 'physical throttle' is explained by the sections about geological complexity (4.7) and rheological contrasts (4.8).

4.1. Tectono-stratigraphic domains (Source of Gold)

Our global understanding of the spatial and temporal distribution of world class orogenic gold deposits in the last 15 years has greatly benefitted from the advances in geochronology and global palaeo-reconstructions. *Goldfarb et al. (2001)* have recognised that orogenic gold is linked to thermal events associated with crustal growth and less affected by the immediate lithology, for example the gold occurs in the greenstone belts of the Yilgarn Craton, Western Australia and/or within the clastic metasedimentary belts of the Birimian in West Africa. Figure 1 demonstrates the inherent temporal link between crustal growth and global orogenic gold production.

Taking these advances in research into account and using recent geochronological data from the ongoing mapping project conducted by GTK and referenced in *Mänttäri (2011)* the geological interpretation was broken down into separate tectono-stratigraphic domains as summarised in Table 3 and the weighting is illustrated in Figure 29.

Table 3: Summary of the weights assigned to the tectono-stratigraphic domains

Domain	Unit	Age (approx in Ga)	Weight	Comment
Basement complex	undifferentiated gneisses	>2.5 *(Leggo, 1973)*	1	Low weighting due to less favourable lithology (i.e. not greenstones or clastic sediments). Gneisses represent granulite facies metamorphism which is unfavourable for orogenic gold mineralisation.
Buganda Toro	volcano-sedimentary	2.1-1.8 *(Cahen, 1982)*	8	High weighting due to age and favourable lithology (greenstones represent processes favourable to orogenic gold mineralisation).
Singo	Sandstone	2.1-1.8 *(Mänttäri, 2011)*	6	Recently dated by GTK, however the unit is undeformed and does not appear to have been involved in deformation hence lower weighting.
Mobilised intrusives	granites and quartz vein dykes	~1.8 *(Mänttäri, 2011)*	5	Correct age range however granites post date peak deformation and are less favourable to orogenic gold mineralisation.
KAB ED	metasedimentary	1.4-1.0 *(Tack, et al., 2010)*	3	Underlain by Tanzanian Craton where the chances of gold remobilisation are limited (less prospective).
KAB WD	metasedimentary + amphibolites	1.4-1.0 *(Tack, et al., 2010)*	7	Underlain by Palaeoproterozoic Buganda Toro with a good chance of gold remobilisation. Mafic intrusives indicate a mantle derived fluid source.
Mobilised intrusives	granites and quartz vein dykes	~900 *(Tack, et al., 2010)* & *(Mänttäri, 2011)*	3	Mostly associated with tin mineralisation and narrow discreet quartz veins.
Mityana	sandstone and conglomerate	~500	1	undeformed Neoproterozoic sediments.
Bunyoro	Shale	~500	1	undeformed Neoproterozoic sediments.
Pan-African	Carbonatite	~500	0	Post dates all deformation phases and therefore irrelevant.
Rift	recent sediments and volcanics	~0.001	0	Post dates all deformation phases and therefore irrelevant.
Lakes	Alluvium	0	0	Post dates all deformation phases and therefore irrelevant.

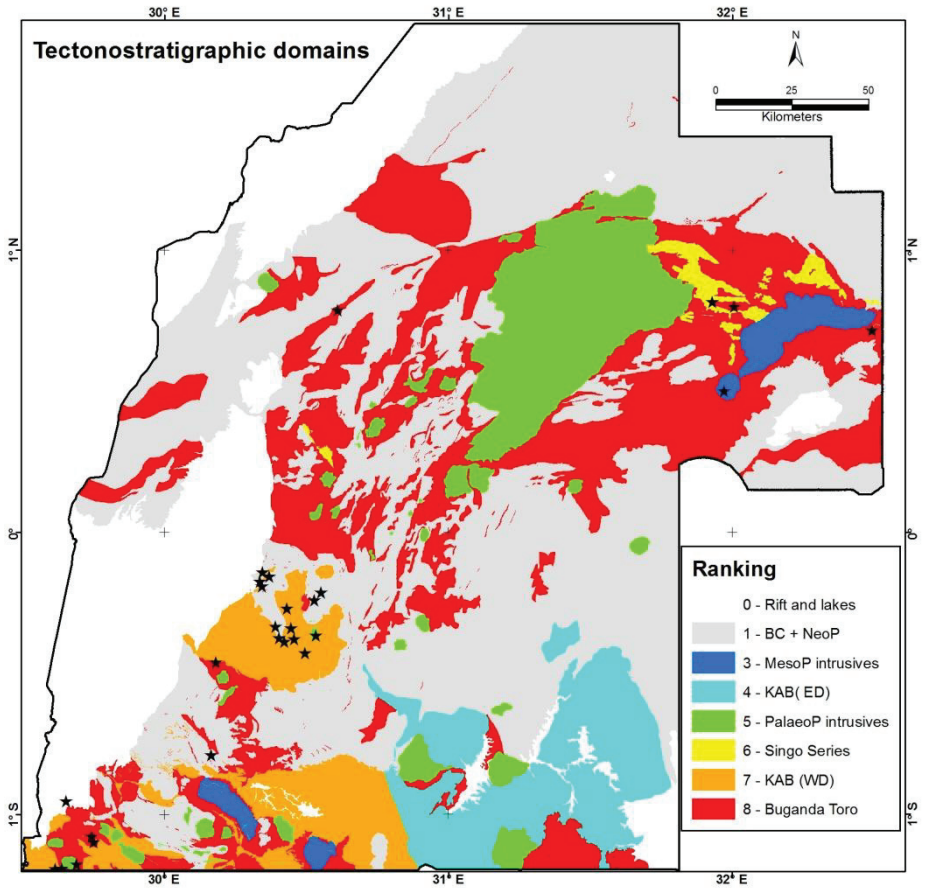

Figure 29: Tectono-stratigraphic domains weighted according to age. Black stars indicate gold occurrences

4.2. Mantle indicators (Source of Gold)

Mantle-crust connectivity is considered to be a critical process in the formation of orogenic gold deposits as it implies a source of gold. However, direct detection of mantle-tapping structures would employ the use of magnetotelluric or seismic methods to image the crust and upper mantle and great expense and cost in resolution. In this case translithospheric structures can only be inferred and are mapped as terrane bounding structures. The presence of mafic rocks such as amphibolites (WD of the KAB) and the occurrence of the Kabanga-Musongati mafic-ultramafic layered complex (marking the boundary between the WD and ED of the KAB) strengthen this inference. *Duchesne et al. (2004)* believe that the Kabanga-Musongati layered intrusion was derived from two magma types originating from the same enriched mantle source, indicative of an old sub-continental lithospheric mantle. In addition Chapter 1.1.3.1 summarises the results of *Pohl et al. (1991)*, concluding that the fluid salinity (8 wt% NaCl eq.), temperature (450°C) and pressure (2 kbars) were atypical for orogenic gold and must reflect fluid mixing with mantle derived sources.

All mapped amphibolites were extracted from the geological interpretation, buffered to 500m and weighted 5 as an indicator of mantle metasomatism. The boundary separating the ED and the WD *(Tack, et al., 1994)* was buffered according to the minimum width of the Kabanga-Musongatic mafic- ultramafic layered complex in Burundi (7-24 km) and weighted 6 as a translithospheric structure. The margin of the Tanzania Craton is inferred based on the existence of several +95 km long discontinuities. This was extracted as a mantle tapping structure and weighted 7. The terrane boundary separating the northern gneiss complex from the volcano-sedimentary Buganda Toro belt was extracted and buffered to 5 km and

weighted 8. Figure 30 illustrates the spatial distribution of the amphibolite intrusions and the major terrane boundaries.

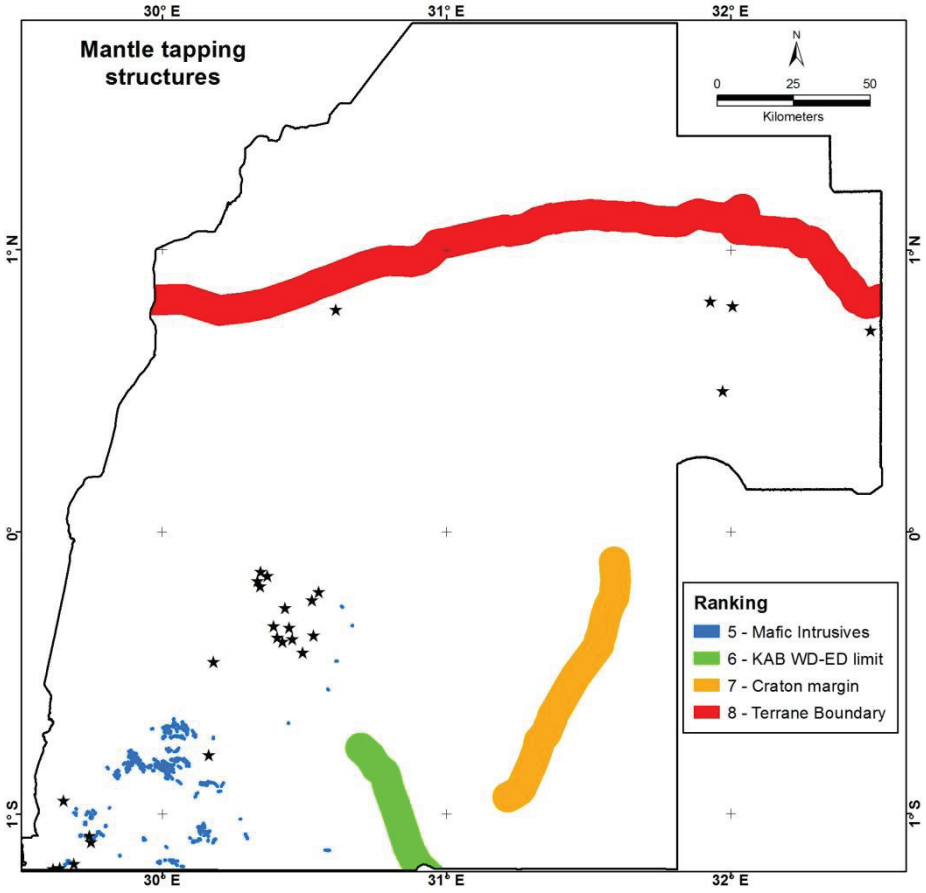

Figure 30: Major terrane boundaries as indicators of mantle tapping structures. Black stars indicate gold occurrences

4.3. Gold occurrences (Source of Gold)

The distributions and genesis of the gold occurrences within the study area is at best poorly understood, with the majority being alluvial gold extracted by artisanal miners. All of the gold occurrences were extracted from the database, buffered to 1.5 km and weighted according to the criteria summarised in Table 4 and illustrated in Figure 32.

Of the 27 gold occurrences, 18 are alluvial with scarce reliable information on the source of gold or production statistics. Although not *in situ*, gold recovered from these workings is typically coarse and angular (Figure 31) indicating a proximal source and are weighted 5.

Figure 31: Photographs from Muti alluvial gold workings. a) Lateritized fluvial pebble layer (palaeoplacer) b) Coarse angular gold derived from panning in the Muti River. c) Artisanal miners working the Muti River.

Anderson's Reef, Buckley's reef and Mashonga all classified as alluvial, were weighted slightly higher (weight=6) as previous authors *(Barnes, 1961)* have noted that the alluvial gold is probably derived from quartz veins hosted within the Palaeoproterozoic schists. Mashonga is located at a thrusted contact between the Palaeoproterozoic schists and the basal conglomerate of the Buhweju Group. This additional structural control weights Mashonga higher (weight =7) than Anderson's or Buckley's Reefs'.

Gold, tin, tungsten and bismuth mineral association spatially related to granitic intrusions are found at Kamalenge, Muramba, Rwanzu and Kitahulira and weighted 6. Typically gold of this type occurs in narrow discreet veins lacking large hydrothermal systems.

Gold occurrences associated with iron, molybdenum and tungsten (Kyerima-Mugoyi and Kyasampawo) occur in the WD of the KAB (south-west of the study area) and are spatially associated with granites, but possibly indicated an iron oxide copper gold (IOCG) system. Worldwide, most of the IOCG deposits are within the 1.6-0.85 Ga range *(Williams, 2005)*, related to a major regional thermal event *(Williams, 2005)* and associated with mafic intrusions under low-medium grade metamorphism. The KAB (1.4-0.9 Ga) has been subjected to the 1375 Ma Kibaran tectonomagmatic event *(Tack, et al., 2010)* and is host to numerous amphibolite dykes suggesting amphibolite facies metamorphism. This geological knowledge provides good evidence for the probability of finding IOCG deposits in the south-west of the study area. Hence gold occurrences of this type are weighted 7.

At Kitaka, alluvial gold associated with a predominantly lead-zinc deposit, is believed to have originated from sheared diorite intrusions hosted within the Igara schists *(Barnes, 1961)*. The gold mineralisation is associated with scheelite (sch), chalcopyrite (cpy), pyrrhotite (po), pyrite (py), galena (gal) and sphalerite (sphal). Coarse crystalline gold occurs within the quartz vein vugs. The presence of structure (shearing) alteration (silica) and mineralisation (cpy, py, po, sphal, gal, sch) and rheologically contrasting lithologies weights Kitaka as 8.

Current mining operations at Kisita Gold Mine have excavated two 10 m x 2 m wide trenches across a NS trending quartz vein hosted at the contact between NE trending sandstone and shale. The quartz vein is associated with gold nuggets and disseminated magnetite, reporting average gold values of 10 g/t gold. The presence of favourable lithological contacts, intersecting structures and magnetite alteration weight this gold occurrence as 8.

Table 4: Summary and weighting of the gold occurrences in the study area

Type	Names	Comment	Weight
Alluvial	Kashenyi, Kanungu, Nyamwegabira, Kitagata, Rwengwe, Bisisa, Katenga R, Katonga R, Bisya, Muti R, Chonyo R, Kyangwahanda R, Nyamunyobwa R, Kitomi R, Butiti, Kampono	Unknown source of gold. No production records.	**5**
Alluvial & quartz vein stockwork	Buckley's Reef, Anderson's Reef	Quartz veins stockwork in schist.	**6**
Alluvial & quartz vein stockwork	Mashonga	Quartz veins stockwork in schist, adjacent to granitic intrusion. Proximal to thrusted contact of Mesoproterozoic conglomerate.	**7**
Granite related	Kamalenge, Muramba, Rwanzu and Kitahulira	Gold, tin, tungsten and bismuth mineral association in narrow discreet veins lacking large hydrothermal systems.	**6**
IOGC	Kyerima-Mugoyi and Kyasampawo	Mesoproterozoic host, affected by tectonomagmatic event (Kibaran) associated with amphibolite dykes.	**7**
Intrusive control	Kitaka	Sheared diorite contacts, silica alteration, sulphide mineralisation (cpy, py, po, sphal, gal, sch).	**8**
Structure control	Kisita	Intersecting NS and NE structure, sandstone-shale contact magnetite-silica alteration.	**8**

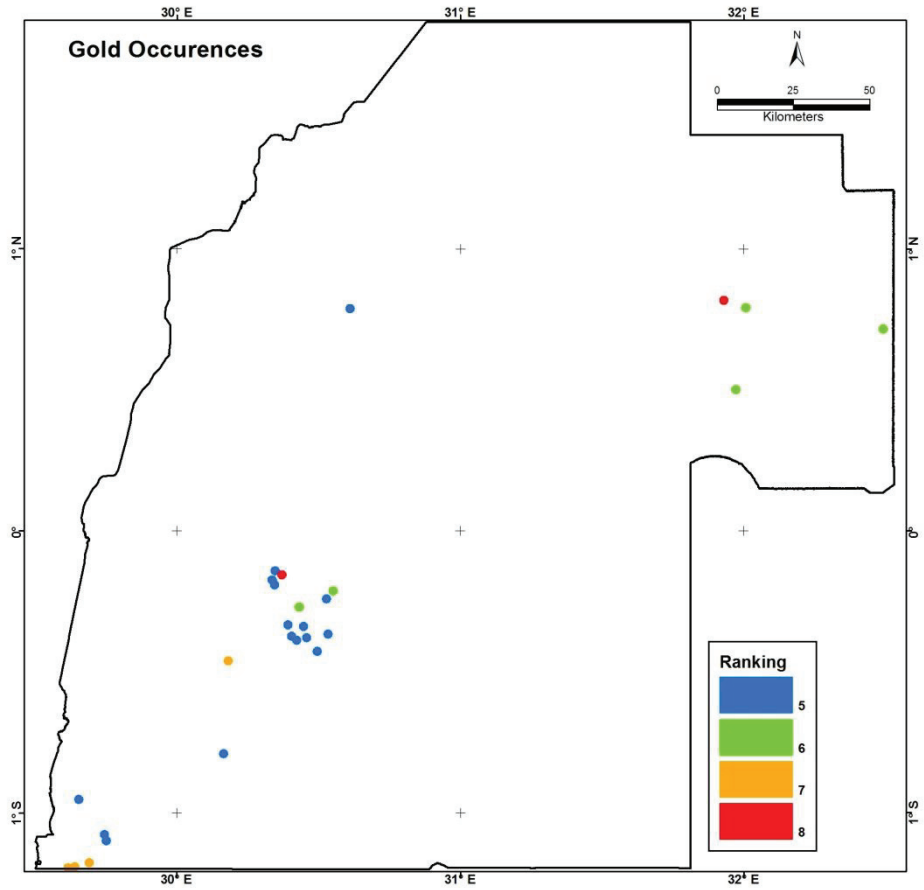

Figure 32: Weighting of the gold occurrences in the study area

4.4. Structures (Active Pathway)

The single most dominant control on orogenic gold mineralisation is extensively believed to be structure. Given the late kinematic timing of mineralisation, deposits occur in dilational jogs, at inflections along strike or down-dip and along linking faults between first order structures. In addition gold deposits occur in reactivated fold hinges and thrust ramps and failure occurs when the fluid pressure exceeds the minimum principal stress (σ3) *(Sibson, 1988).*

Thrusts, shears, fold axes and non-differentiated faults believed to be active during the mineralisation events of the Ubendian Orogeny (D1 and D2) and the Lomamian Orogeny (D3) and Pan African Orogeny (D4) were extracted and buffered at distances of 1 km, 3 km and 5.0 km. The distances to these structures were then weighted according to the following criteria, summarised in Table 5 and displayed in Figure 33.

- Deposits are normally sited in second or higher order structures adjacent to large scale crustal scale structures (major faults).
- Gold occurrences tend to occur on or close to major structures where larger deposits are typically found proximal to the fault where fluid accumulation is greatest.
- 3 out of 5 *in situ* gold occurrences in the south-west of the study area; occur within 3-5 km of a fold axis.

Table 5: Summary of fault proximity and weights

Structure Type	Buffer distance (km)			Weighting (out of 10)			
				1 km	3 km	5 km	>5 km
THRUST	1	3	5	8	6	5	1
SHEAR	1	3	5	8	7	6	1
MAJOR FAULTS	1	3	5	6	8	7	1
FAULTS	1	3	5	8	7	5	1
FOLD AXES	1	3	5	4	6	8	1

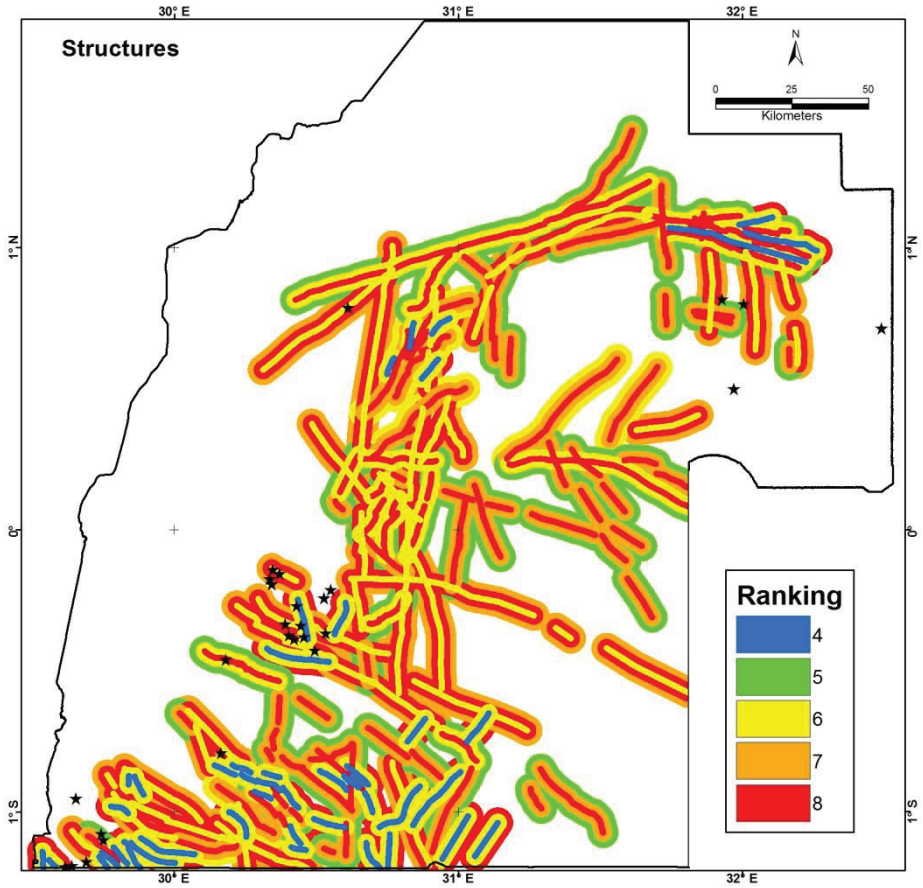

Figure 33: Structures involved in Ubendian, Lomamian and Pan African orogenies. Weighted according to the size and type of structure. Black stars indicate gold occurrences

4.5. Terrane contacts (Active Pathway)

Pekkala et al. (1994) stated that the gold at Mashonga (South of Buhweju) and Kitaka was derived from small quartz vein stringers associated with pyrite within the Palaeoproterozoic schists and gneisses, that gold was also contained within the basal conglomerate unit of the Karagwe Ankolean sediments at Buhweju, and that the Buhweju sediments are not considered an important source of gold. The basal conglomerate unit is considered to be an important host of remobilised gold during the Lomamian Orogeny.

Taking this field evidence into account the Palaeoproterozoic schists and Archaean gneiss units were extracted from the lithological interpretation and buffered to 1 km. Similarly the Mesoproterozoic KAB metasediments were also buffered to 1 km. The contacts were then extracted and weighted as shown in Figure 34. Palaeoproterozoic - Mesoproterozoic contact = 7, Archaean – Mesoproterozoic contact = 6, Archaean-Palaeoproterozoic-Mesoproterozoic = 8

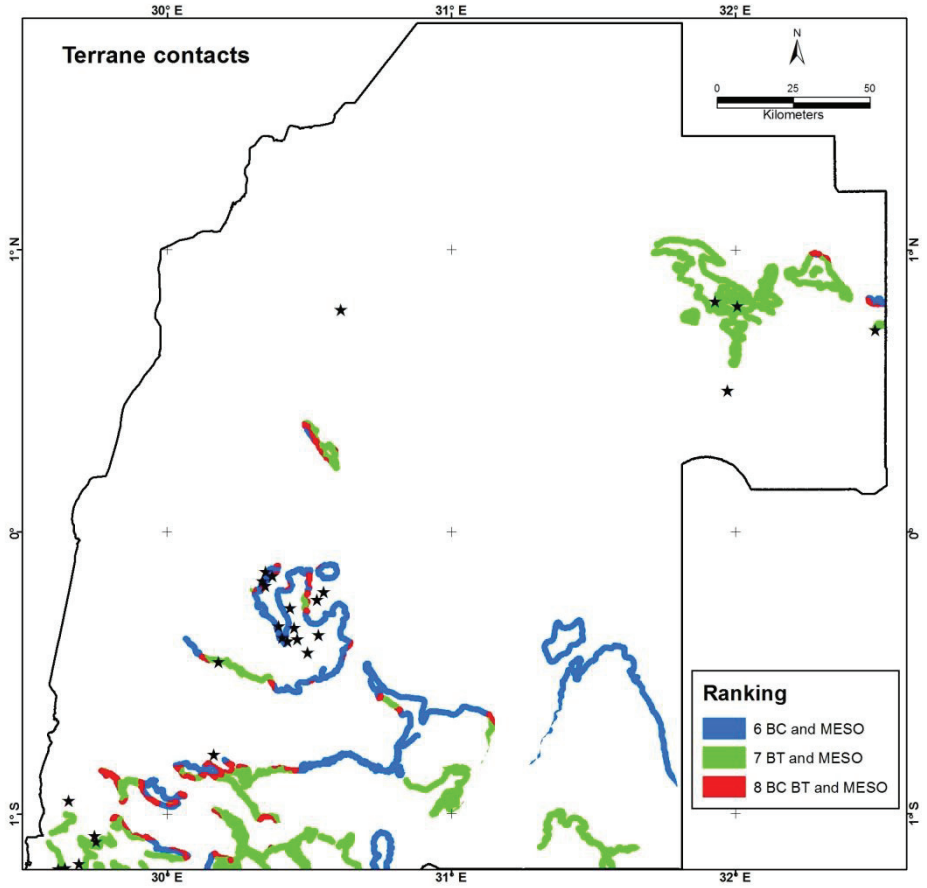

Figure 34: Extraction of terrane contacts as a predictor layer. Weighted according to field evidence (Palaeoproterozoic units are the source of gold which gets remobilised into the Mesoproterozoic sediments during the Lomamian Orogeny). Black stars indicate gold occurrences

4.6. Hydrothermal alteration extraction (Active Pathway)

Regions of enriched potassium (K), extracted from the gamma-ray spectrometric data are used to identify areas of 'hydrothermal alteration', specifically sericitisation. However the difficultly which arises is in separating elevated K values related to hydrothermal alteration from that of lithology and weathering. Three methods have been applied to try and alleviate this problem.

The first method originally proposed by *Saunders et al. (1987)* is based on the fact that thorium is less geochemically mobile than K and eU and was thus used as a lithological control to define ideal eU and K values. Normalisation of the data to thorium would therefore suppress the effects of the environment and lithology on the K and eU concentrations.

Extraction of the ideal K value (Ki) in relation to the thorium concentration is defined by:

Equation 1 **Ki = (K average/Th average)/Th map** *(de Quadros et al., 2003)*

Deviation from the ideal K values (Kd) are considered to be K anomalies obtained by the following equation.

Equation 2 **Kd= (K-Ki)/Ki** *(de Quadros, et al., 2003)*

The resultant value (Kd) represents K values due to hydrothermal processes.

The second method is a well known ratio using eTh/K which was analysed simultaneously with the Kd values. According to *Shives et al. (1997)*, low eTh/K ratios are good indicators for hydrothermally altered areas.

The third method uses the F parameter proposed by *Gnojek et al. (1985)* The F-parameter comprises two important relationships, the potassium abundance to the eTh/eU ratio and the uranium abundance to the eTh/K ratio and is expressed in the following equation:

Equation 3 **F = (K*eU)/eTh = K/(eTh/eU) = eU/(eTh/K)** *(de Quadros, et al., 2003)*

Integration of the three methods highlights anomalous hydrothermal areas related to sericitisation. This was achieved by visualisation in a ternary RGB map (Figure 35), where the anomalies related to the low eTh/K values were inverted and represented as high K/eTh for better correlation with the high Kd values and high F parameter.

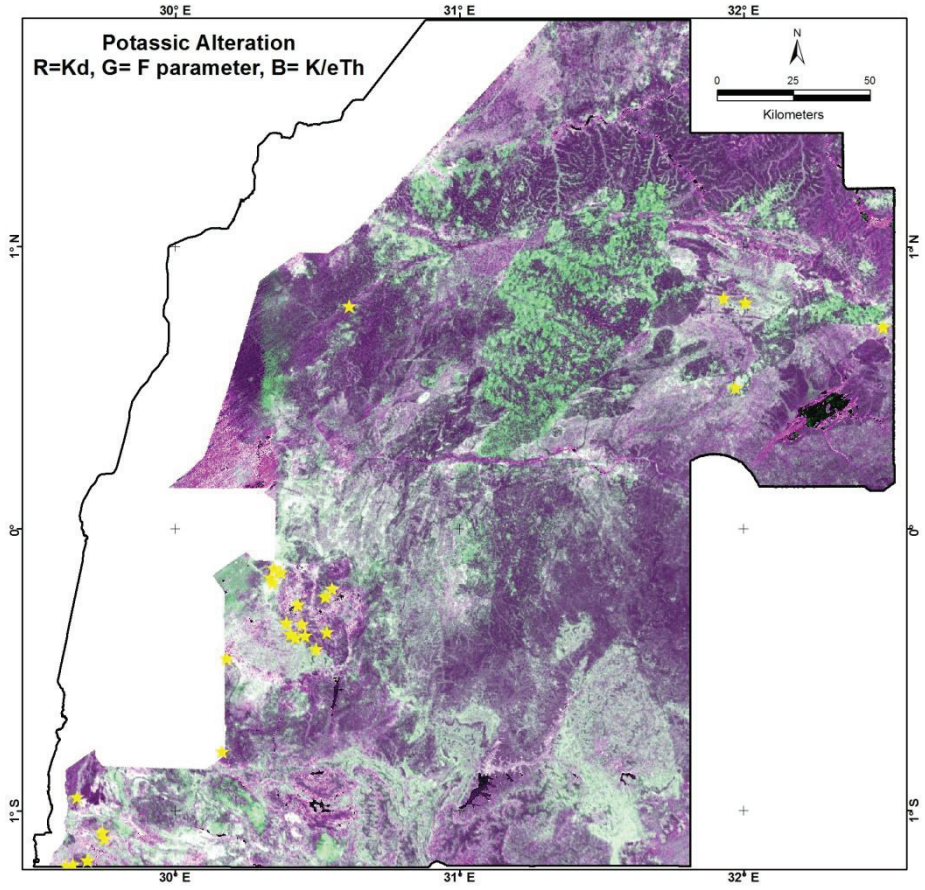

Figure 35: Ternary Image of Kd in red, eU/ (eTh/K) in green an K/eTh in blue. White areas indicate where all three are present and therefore represent hydrothermal alteration (sericitisation). Yellow stars indicate known gold occurrences.

The three maps were then combined in a principal component analysis, where the largest variation is recorded in the first PC image (PC1) as shown in Table 6.

Table 6: Eigenvector loadings of principal components for Kd, F parameter and K/eTh and their variances

Axis	Kd	F	K/eTh	%	Cumulative %
PC 1	0.9925	0.1164	0.0379	99.9073	99.90
PC 2	-0.1163	0.9932	-0.0044	0.0927	100.00
PC 3	-0.0382	-0.000	0.9993	0.0000	100.00

The first principal component score was then reclassified as weights for the prospectivity model and areas of alluvium mapped during phase 1 were then used to mask out accumulations K-alteration in the rivers. Figure 36 shows the results of the K-enrichment prediction layer.

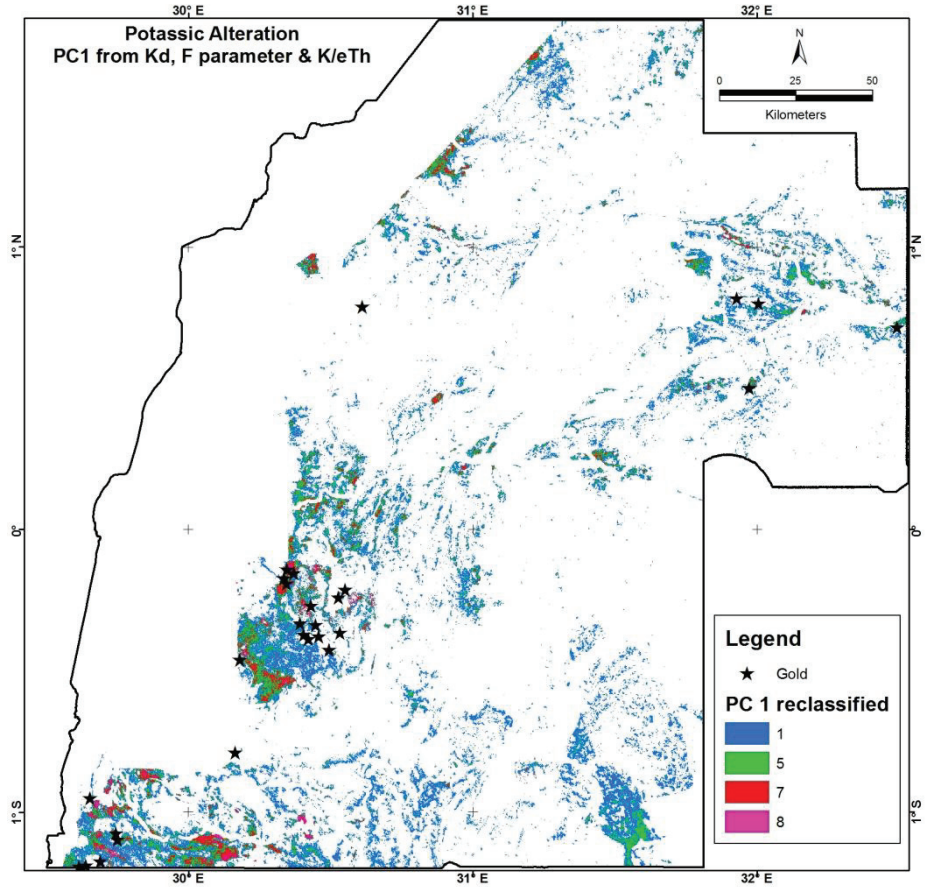

Figure 36: Hydrothermal alteration (K enrichment) extracted from gamma-ray spectrometric data, representing an indicator for the 'active pathway'. Black stars indicate gold occurrences

4.7. Geological complexity (Physical Throttle)

Fluid connectivity and hence deformation induced permeability can be understood in terms of geological complexity. Geological complexity is used to measure the abundance relationship between geological structures, lithological boundaries and gold mineralisation. This is a computer based technique quantified by fractal dimension analyses obtained by box-counting. This method minimises the human-bias often introduced in geological interpretations.

Since the gold occurrences in the study are not confined to one lithological unit, but appear to be structurally controlled, all structures involved in the orogenies (D1-D3) were extracted from the geological interpretation (Appendix 1) and analysed using shifting box-counting algorithm *(Ford et al., 2008)*. In this method a square box of length (r) is superimposed on a map and the number of boxes containing lines (structures) is represented as Nr. The size of the box is then halved and the process is repeated. Nr is the total number of boxes that contains lines for a given box size. A subset of the dataset and its methodology is shown in Figure 37.

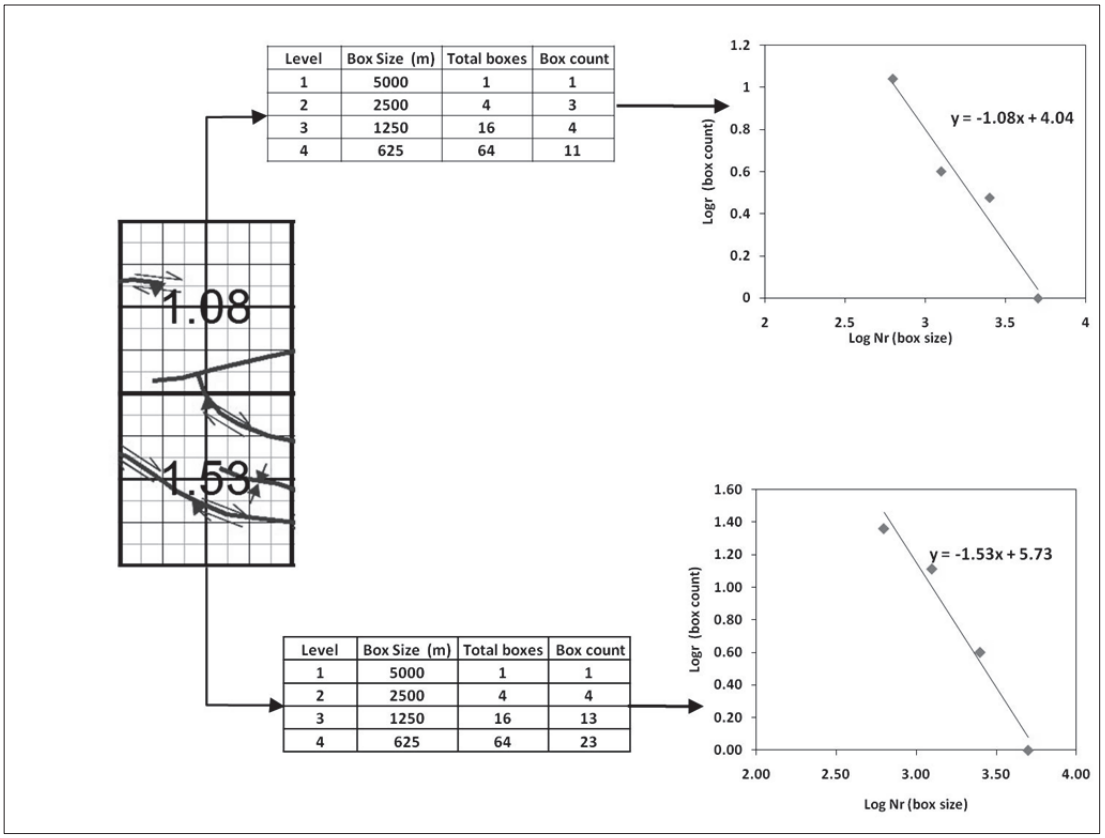

Figure 37: Calculation of the fractal dimension on the mineralised structure network

In order to assign an appropriate box size, the local scale fault control of mineralisation was assessed in a fractal analysis on the lode-gold deposits which occur to the south of the study area (*Msechu, 2011*). The inflection point in the plot logNr vs. logr (Figure 38) reveals an appropriate box size of 5 km (where logr =0.7).

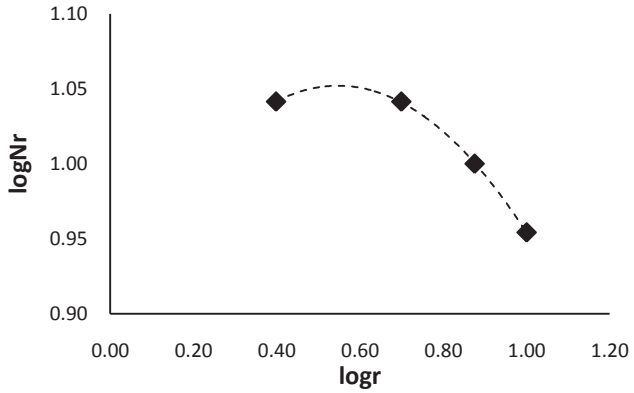

Figure 38: Estimation of a suitable box size for the calculation of the fractal dimension in the study area, where r is the box size and Nr is the number of boxes containing gold deposits

The structures were then divided into cells of measuring 5 km by 5 km and the fractal dimension was calculated, as the slope of the graph in a logr vs. log Nr plot, for every location in the study area using spatial resolutions of 5000, 2500, 1250, 650 m. The value of D was attributed to the centre of the 25 km^2 cell and interpolated using ordinary kriging spherical model and a search size of 7500 m. Figure 39 below shows the results of the fractal dimension calculation. The fractal dimension map was then reclassified (Figure 40) between 0-10 so as to be comparable to the other predictor layers.

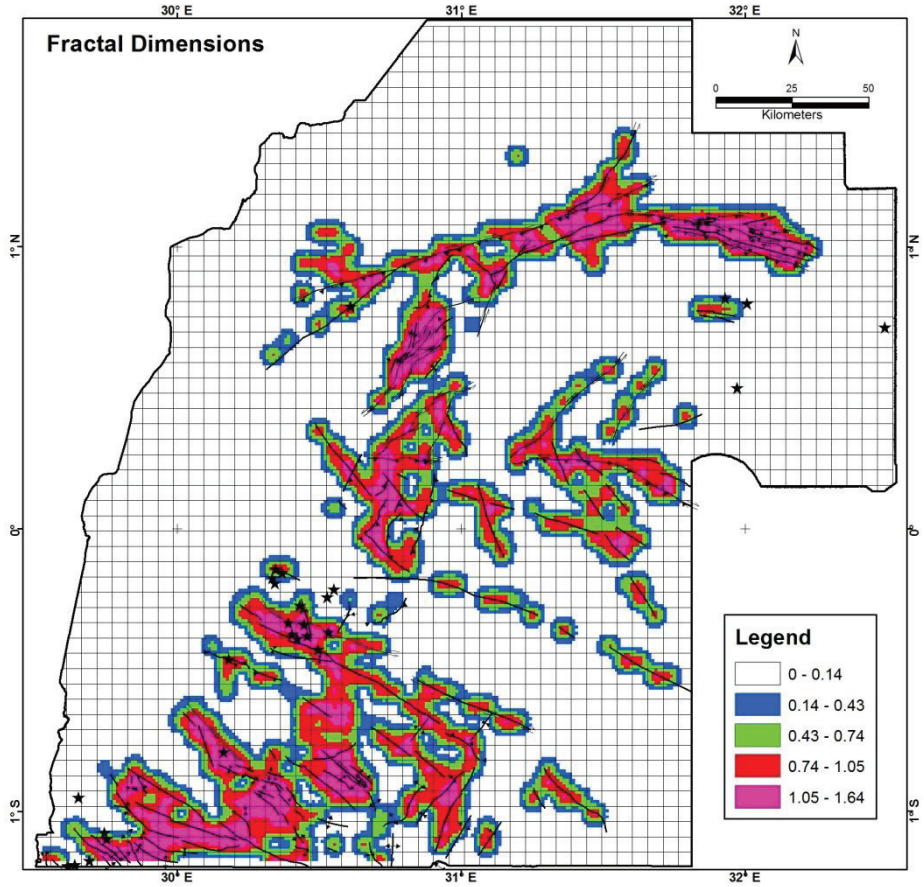

Figure 39: Interpolation of the fractal dimension values by ordinary kriging. Search radius = 7500m. Black lines = geological structures used in the fractal dimension calculation. Black stars indicate gold occurrences.

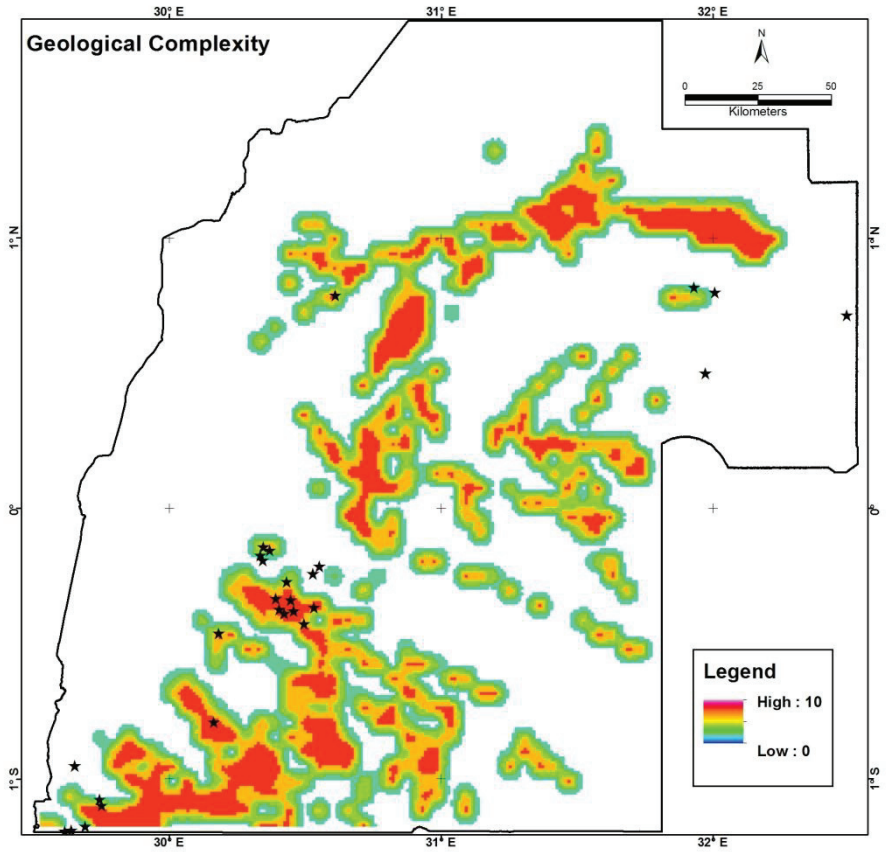

Figure 40: Geological complexity layer to map the physical throttle as a critical process. Black stars indicate gold occurrences

4.8. Rheological contrasts (Physical Throttle)

Although a unique lithology does not appear to exert much control on the location and distribution of gold occurrences in the study area, *Groves et al. (2000)* have demonstrated, using the Kalgoorie terrane as an example that lithological contacts which separate rocks of strongly contrasting rheologies are important. Numerical modelling of rock deformation is not an exact science due to the inability to simulate deformation with time, however relative differences in their interpreted geomechanical properties enables the rock types of the study area to be grouped according to relative competency as summarised in Table 7. Post tectonic intrusives and undeformed Neoproterozoic- Recent sediments not involved in the either of the Orogenies excluded and hence are not included in the classification.

Table 7: Relative rock competency

	VERY HIGH (VH)	HIGH (H)	MEDIUM (M)	LOW (L)
rock types	undifferentiated gneiss	basalt	sandstone	mudstone
	pre, syntectonic granite	quartzite	calc-silicate	pelite
	Pegmatites	conglomerate		phyllite
	quartz vein ridges	amphibolite		shale
				siltstone
				graphitic schist
				schist
				siltstone

The different rheological groups are buffered according to their relative sphere of influence as follows: VH -1000 m, H-750 m, M-500 m L-250 m and the contacts are extracted and weighted according to the concept that when subject to deformation, brittle fracturing will occur this increasing the rock permeability and the focus of fluid flow summarised in Table 8 and illustrated in Figure 41

.

Table 8: Weighting the geological contacts according to rheological contrasts

Contact	Weighting	Comment
VH-H	7	contrast across the contact is low, both units will fracture during deformation and hence increase permeability
VH-M	8	high rheological contrast across the contact and both units will fracture during deformation increasing permeability
VH-L	3	VH unit will act as a competent buttress and the L unit will behave in a plastic manner, thus decreasing permeability
H-M	6	Low rheological contrast across the contacts is unlikely to be able to focus fluids efficiently.
H-L	4	H unit will act as a competent buttress and the L unit will behave in a plastic manner, thus decreasing permeability
M-L	5	low rheological contrast across the contacts is unlikely to focus fluids

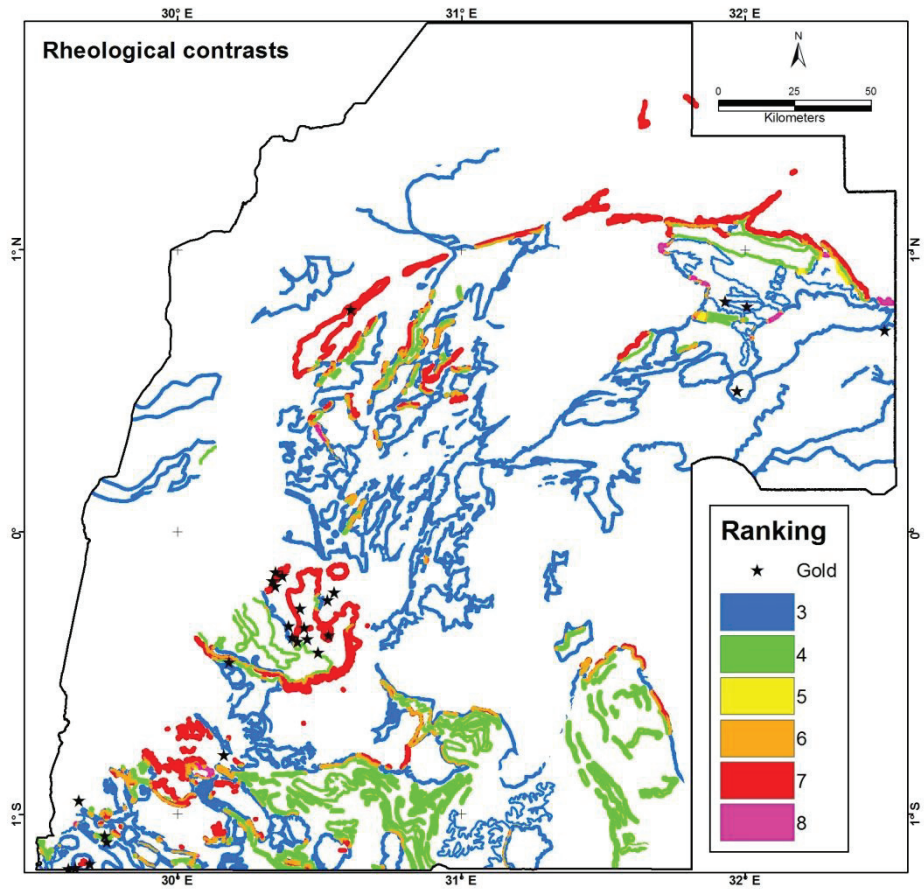

Figure 41: Rheological contrasts. Black stars indicate gold occurrences.

4.9. Integration of predictor maps

Knowledge-driven multi-class index overlay method is used to model the prospectivity. Each class of evidence (j) in a predictor map (i) is given a score S_{ij} (0-10) depending on its importance in mineral prospectivity and each predictor map is assigned a numerical weight (W_i) based on 'expert' judgement of its role in the critical processes of orogenic gold according to the following criteria, summarised in Table 9.

i. The relative importance of the critical process (i.e. source of gold) mapped by the proxies to mineralisation.
ii. The representativeness of a proxy (i.e. how well the mappable mineral proxy represents the process).
iii. The accuracy/extent of mapping the proxy.

Finally each of the predictor maps will be combined according to the equation from *Carranza (2009)* and displayed in Figure 42

$$\overline{S} = \frac{\sum_{i}^{n} S_{ij} W_i}{\sum_{i}^{n} W_i}$$

Where the output $\overline{S}$ for each location is the sum of the products of S_{ij} and W_i in each evidential map divided by W_i for each evidential map.

Table 9: Summary of the weighting criteria used to evaluate the importance of each critical process

	Critical Process	What is the relative importance of the critical process to mineralisation?		How well does proxy map the critical process?		What is the accuracy/extent of proxy?		SUM
PROXY		COMMENT	WEIGHT	COMMENT	WEIGHT	COMMENT	WEIGHT	
Tectono-stratigraphic domains	SOURCE OF GOLD	Certain terranes delineated by geological age are prospective *(Goldfarb, 2001).* This is an empirical relationship which can only be inferred from existing research.	6	Palaeoproterozoic and Mesoproterozoic rocks have been affected by the Ubendian and Lomamian orogenies respectively and are therefore more favourable for orogenic gold formation than the undeformed rift sediments.	8	Recent age dating (Mänttäri, 2011) does not cover all the extracted domains and in this case less accurate Rb-Sr age dating results (Cahen, 1982) and (Leggo, 1973) were used. Rb-Sr method is less accurate than the U-Pb as it can be reset by hydrothermal events.	3	17
Mantle tapping signatures		The mantle is more enriched in gold than the crust.	10	Amphibolites could be derived from other processes including metamorphism. The terrane boundaries are inferred to be tapping into the mantle.	3	Identification of all mantle derived products (lamprophyres and alkali magma series) is not totally possible at the scale and resolution of the datasets.	2	15
Gold occurrence		Gold has been introduced into the crust and depends on mantle fluids reaching the crust.	8	Some of the gold occurrences are not *in situ* and so reflect additional 'enrichment' processes unrelated to the source.	3	Existing gold occurrences can bias exploration endeavours away from geologically interesting unexplored areas simply because no work has been done there.	3	14
Structures	ACTIVE PATHWAY	Structures allow deep fluids access to the crust.	10	The co-existence of K enrichment anomalies at the intersection of structures and along thrusts implies the structures were active fluid pathways during mineralisation.	9	Recent rift related structures may have exploited pre-existing lines of weakness (Pan Africa age) and were not included in the analysis.	8	27
Terrane contacts		Remobilized gold from the Palaeoproterozoic schists deposited at the contact with the overlying Mesoproterozoic sediments. Dependant on structure therefore has a lower weighting.	9	Remobilised gold deposited at the contact between Mesoproterozoic and Palaeoproterozoic units is supported by field evidence *(Pekkala, 1994)* but it is not certain that all terrane contacts of this age are the sites of remobilised gold.	9	Limited to the Mesoproterozoic rocks, however gold may be remobilised from the Archaean basement into Palaeoproterozoic rocks.	6	24

Table 9 continued

	Critical Process	What is the relative importance of the critical process to mineralisation?		How well does proxy map the critical process?		What is the accuracy/extent of proxy?		SUM
PROXY		**COMMENT**	**WEIGHT**	**COMMENT**	**WEIGHT**	**COMMENT**	**WEIGHT**	
Hydrothermal alteration	**ACTIVE PATHWAY**	Gold is more soluble in high temperature fluids, thus hydrothermal alteration maps the path of gold -bearing hydrothermal fluids along major structures. Dependant on structures and terrane contacts therefore lower weighting.	**8**	The proxy only maps K enrichment (alkali metasomatism). Other signature alteration assemblages include: silica, carbonates (ankerite, dolomite and calcite), chlorite (in mafic host rocks).	**8**	Gamma-ray spectrometric dataset does not cover the west of the study area (Western Rift). Some areas of K enrichment may reflect fluvial and weathering processes.	**7**	**23**
Geological complexity	**PHYSICAL THROTTLE**	Large volumes of hydrothermal fluids are focussed into high-permeability zones near the location of gold deposits.	**10**	Areas with high fractal dimensions represent zones with higher connectivity and likelihood of increased permeability.	**8**	Lithological contacts also sites of higher permeability were not used in the fractal dimension analysis.	**5**	**23**
Rheological contrasts		Accumulation sites for mineralised fluids influenced the areas of high permeability .	**9**	Large rheological contrasts result in differential strain partitioning and have the potential to create compressional and dilational zones and hence sites of fluid accumulation.	**9**	The geological interpretation is not a solid bedrock interpretation and thus the lithological contacts represented on the map reflect the intersection of the bedrock geology and topography creating apparent trends in the GIS map. Uncertainty in the assigned relative geomechanical properties and relative ages could disqualify some lithological units.	**4**	**22**

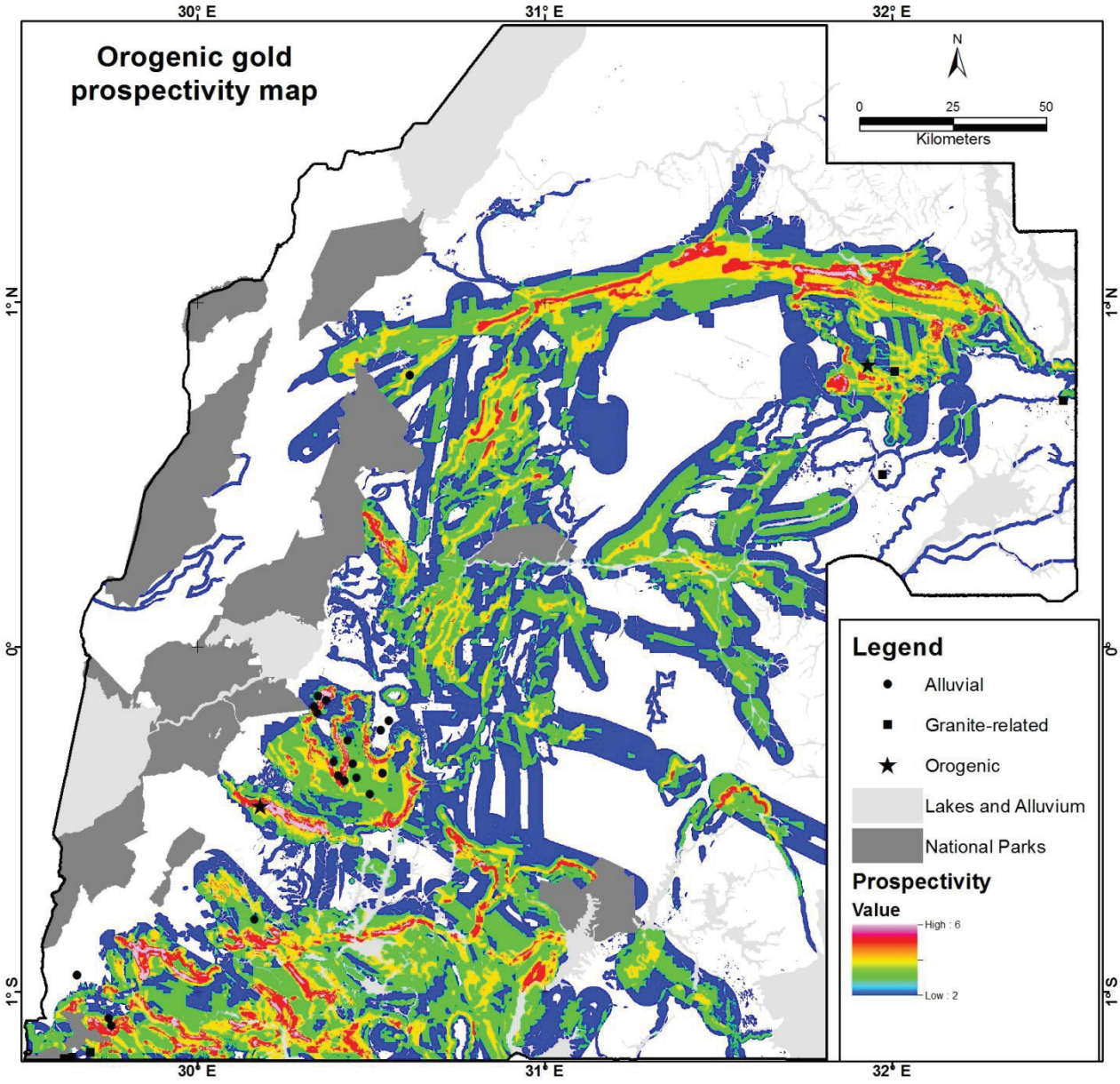

Figure 42: Final prospectivity map for orogenic gold in south-west Uganda

5. DISCUSSION

5.1. Geological Interpretation

The geological interpretation (Appendix 1) is the first to be produced covering the entire study area at 1:100 000 scale. Other published maps, involve subsets of the study area and the only other known publication is the country scale geological map produced at 1: 2 000 000. The main objective of phase 1 of the study is to produce a solid geological map of uniform geological detail from which to carry out a prospectivity analysis. This implies that any one area or polygon cannot have more than one geological attribute.

Recently (December, 2011) GTK have provided a non-finalised surface geological interpretation covering two separate areas (parts of the Kiboga area and from Buhweju to the south). These interpretations were created at 1:50 000 scale and although they do not cover the entire study area, are used to compare and contrast the results of the new geological interpretation (Appendix 1).

Differences between the geological interpretations, due to the differing mapping scale (1:100 000 vs, 1:50 0000) and the different objectives, (the GTK interpretation combined rocks of differing rheological properties into one unit) of the two studies as outlined below:
The GTK interpretations have differentiated between ten different types of gneisses: 'Kampala granitoids, orthogneiss', 'Hornblende gneiss', 'Mica gneiss', 'Kalangala granite, orthogneiss', 'Granitoid gneiss', '(Cordierite, sillimanite)-muscovite-biotite gneiss and schist', 'Muscovite bearing granite gneiss, porphyritic in part', 'Biotite bearing porphyritic granite gneiss', 'Variable granitic gneiss' and 'Quartzo-feldspathic gneiss. This differentiation, which is largely based on geochemical variation and field evidence, was not considered necessary for the purposes of the study and hence these units have been grouped together as undifferentiated gneisses.

The GTK interpretation also differentiated between three different classes of alluvium:
'Alluvium, swamp, lacustrine deposits', 'Alluvium; sand, silt, gravel' and 'Papyrus swamp, flood plain mud'. This study does not make the differentiation between different types of alluvium as it has no implications in the context of orogenic gold prospectivity.

The GTK interpretation has identified numerous occurrences of laterite, which is a surface reflection of prolonged chemical weathering, and in this study the underlying bedrock geology was interpreted beneath the laterite in (Appendix 1).

The variable topography and moderate-flat lithological contacts and geological structures particularly in the KAB (Appendix 1), reflect the surface expression however trends on the GIS map deviate from the true strike of the geological features.

The development of the western branch of the east African rift implies that the existing geometry of the geological terranes may not be similar to that at the time of mineralisation.

5.1.1. The geodynamic history

The oldest deformation event (D1) evident in the Palaeoproterozoic rocks is associated with S to SE dipping thrusts where the Palaeoproterozoic rocks and the Archaean gneisses were thrust northwards and stacked as shown in Figure 43.

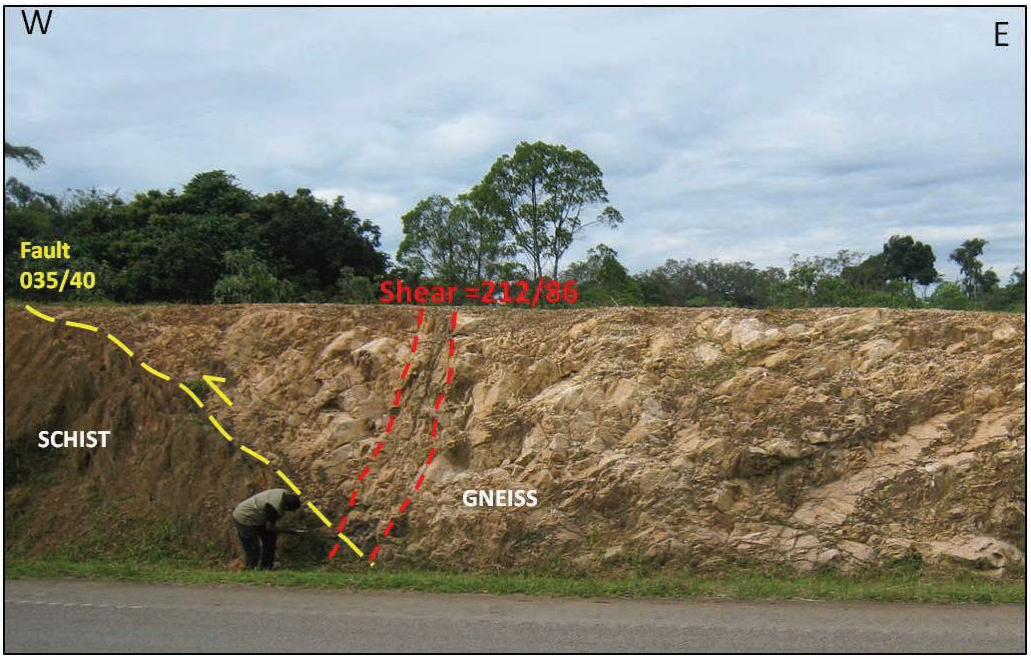

Figure 43: Photograph illustrating D1 event. Gneiss is thrust onto schist. NE trending shear post dates the thrusting event. (Observation point WP107 looking north).

The D1 event corresponds to NS compression of the Ubendian Orogeny (2100-1860 Ma) outlined by *Cahen (1982)*. Post peak deformation and related subsidence coincides with the intrusion of the Mubende granite at 1848 ± 6 Ma *(Mänttäri, 2011)* and the deposition of the Singo series at maximum sedimentation age of < 1970 Ma *(GTK and Westerhof, pers. comm.)*. NE trending thrusts and fold axes ('D2 structures', Appendix 1) west of the Mubende granite are considered to be part of the same D1 event and the difference in the orientation is due to the S-shaped ramp-flat basement as discussed below.

The Mubende granite measures 100 km by 50 km at the surface and separates a predominantly EW structural domain (east) from a predominantly NE oriented structural domain (west). The theory outlined below attempts to explain the current geometry and account for the space required by the Mubende granite. The Mubende granite intruded at 1848 ±6 Ma *(Mänttäri, 2011)* during post peak deformation of the Ubendian Orogeny as discussed in section 3.8. The Mubende granite is bounded on its eastern margin by a NE trending sinistral shear, the western margin appears to be offset by several dextral late (D5) faults and the current surface expression is a result of the intersection with topography. The NE oriented long axis and the eastern bounding shear indicate a strong structural control on the intrusion of the Mubende granite. A pull-apart basin in an extensional setting (possibly post-peak deformation during the onset of subsidence) coupled with roof uplift *(Grocott, 2002)* is suggested to account for the intrusion of the Mubende granite as shown in Figure 44. However more detailed field work is required to validate the dip direction on the pluton margins and the controlling structures are required to fully understand and validate the emplacement mechanism.

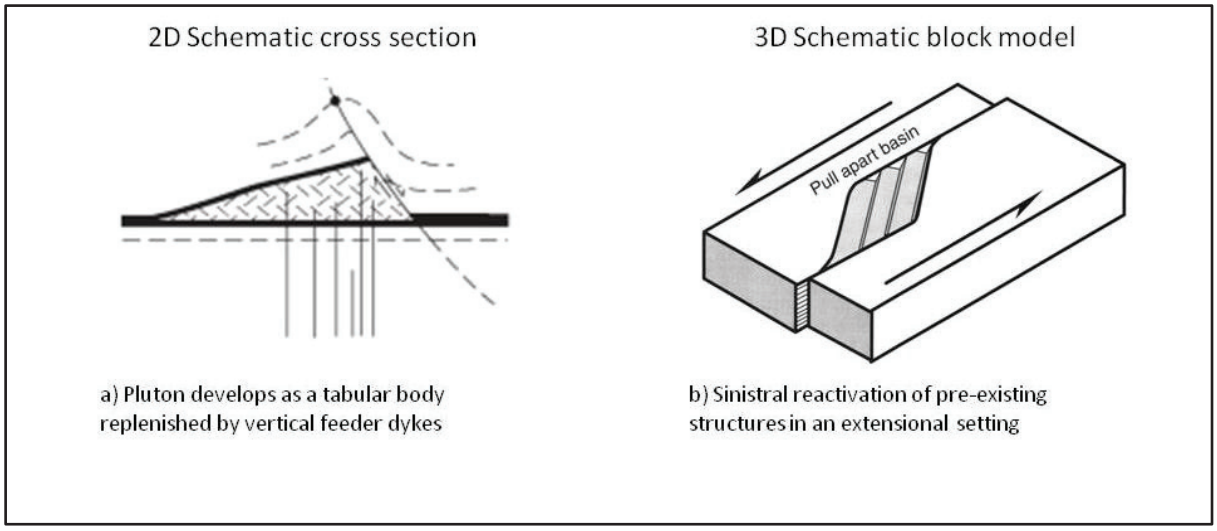

Figure 44: Model of Mubende granite emplacement by roof uplift and reactivation of pre-existing structures during extension. (Modified after *Grocott, 2002*).

In the west of the study area the trend of the structures in the Buganda Toro belt adopts a more ENE orientation coinciding with the Ruwenzori Mountains. The change in orientation is marked by a major NW trending fault believed to be part of the Lomamian Orogeny.

Later sinistral reactivation of the D1 and D2 structures occurred during the Lomamian Orogeny at 1000 Ma, *(De Waele, et al., 2008)* where NE-SW compression created the Karagwe Ankolean fold belt in the south of the study area. South-west verging folds mapped in the WD of the KAB indicate the dominant force came from the NE, whereas in the ED, early granitic intrusives appear to predate the main compressional event and cause strain partitioning. Fold axes in the ED thus trend NE trending and verge to the SE. Within the KAB the two domains (ED and WD) have therefore evolved differently.

Oblique collision between east and west Gondwana during the Pan African event (~650 Ma) resulted in the dextral reactivation of the EW trending D1 structures (reactivated D1 = RD1 see Appendix 1) and formation of NS sinistral shear zones.

5.2. Prospectivity modelling

The following sections evaluates the contribution of each of the predictor layers (Figure 5 and Chapter 4) to the final prospectivity map and overall contribution to orogenic gold mineral systems understanding in south-west Uganda. Since only 2 of the 27 gold occurrences (Mashonga and Kisita) in the study area can be considered 'orogenic', all gold occurrences are considered, irrespective of their genesis to compare and interpret the performance of the predictor maps in reflecting the respective critical processes.

5.2.1. Source of gold

Goldfarb, et al. (2001) have shown that certain terranes delineated by geological age, are prospective. This is an empirical relationship and thus it can only be inferred that all terranes within a certain age range are prospective.

In theory the mantle is more enriched in gold and thus the identification of mantle derived products (lamprophyres, kimberlites, alkali magma series) does reflect a source of gold. Field campaigns *(Tack, et al., 2010)* and *(Duchesne, 2004)* in neighbouring Burundi and in the area to the south of the current study have identified a such mantle derived products in the Mesoproterozoic Karagwe Ankolean Belt.

The prediction-rate curves (Figure 45) shows that at 30 % of the study area, 60% of the gold occurrences are predicted by the tectono-stratigraphic domains, whereas only 29 % are predicted by the mantle indicators at the same area. The tectono-stratigraphic domain predictor map out-performs the mantle indicator and is therefore considered to map the critical process "Source of gold" more accurately.

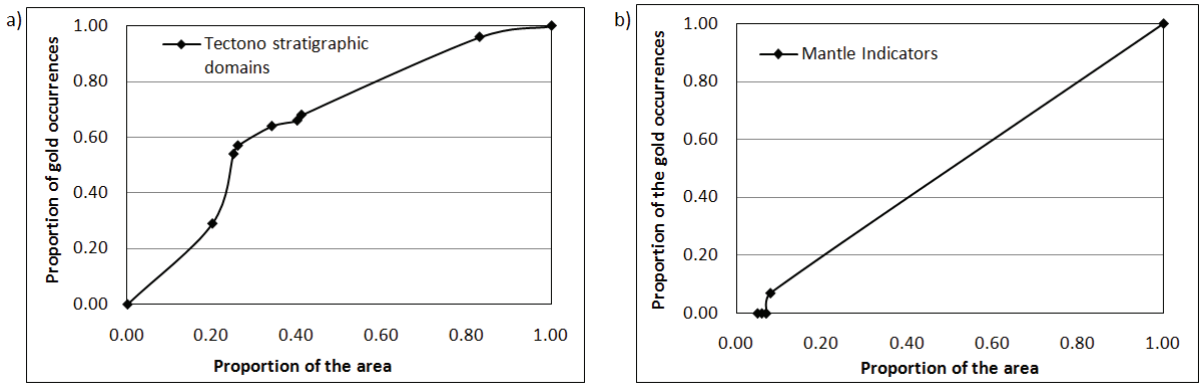

Figure 45: Prediction-rate curves representing a source of gold. a) Tectono-stratigraphic domain b) Mantle indicators

The low performance of the mantle indicators reflects the inaccuracy of the proxy, where identification of all mantle derived products (A-type magma series, lamprophyre) is not possible at the scale and resolution of the datasets. The extraction of proxies reflecting this process is therefore limited to amphibolites and terrane boundaries which are only inferred to be tapping into the mantle. In addition the dataset was insufficient for the identification of large crustal scale structures and craton boundaries. In this case, gravity data and magnetotelluric data would be more appropriate.

Gold occurrences as an indicator for orogenic gold is often a good place to start but can often bias exploration endeavours away from unexplored geologically interesting areas or areas with challenging cover material simply because no work has ever been done there. Table 4 summarises the gold occurrences into deposit classes based on the field evidence (current study) *(Barnes, 1961)* and *(Pekkala, 1994)* as well as metal associations given in the mineral database. In the study area, most exploration work has been centred around the alluvial workings in Buhweju district where stream sediment sampling *(Pekkala, 1994)* and geological mapping *(Bahiru, 2011)* have attempted to identify the source of the alluvial gold with little success. Although the metal association and deposit types do not always reflect on orogenic gold the mere existence of gold is used as the indicator. These alluvial gold workings are only considered to represent placer deposits (Figure 31) of a much larger hydrothermal system.

5.2.2. Active Pathway

Given the dominant structural control on all orogenic gold deposits, structure (all major faults, faults, shears, thrusts and fold axes old to be involved in either of the Ubendian, Lomamian or the Pan African orogenies) hydrothermal alteration and terrane contacts are indicators of an active pathway as a critical process. The performance of each of these predictor layers is shown in Figure 46 where structure (57%) out-performs both the terrane contacts (26%) and the hydrothermal alteration (52%) predictor layers at 30% of the study area.

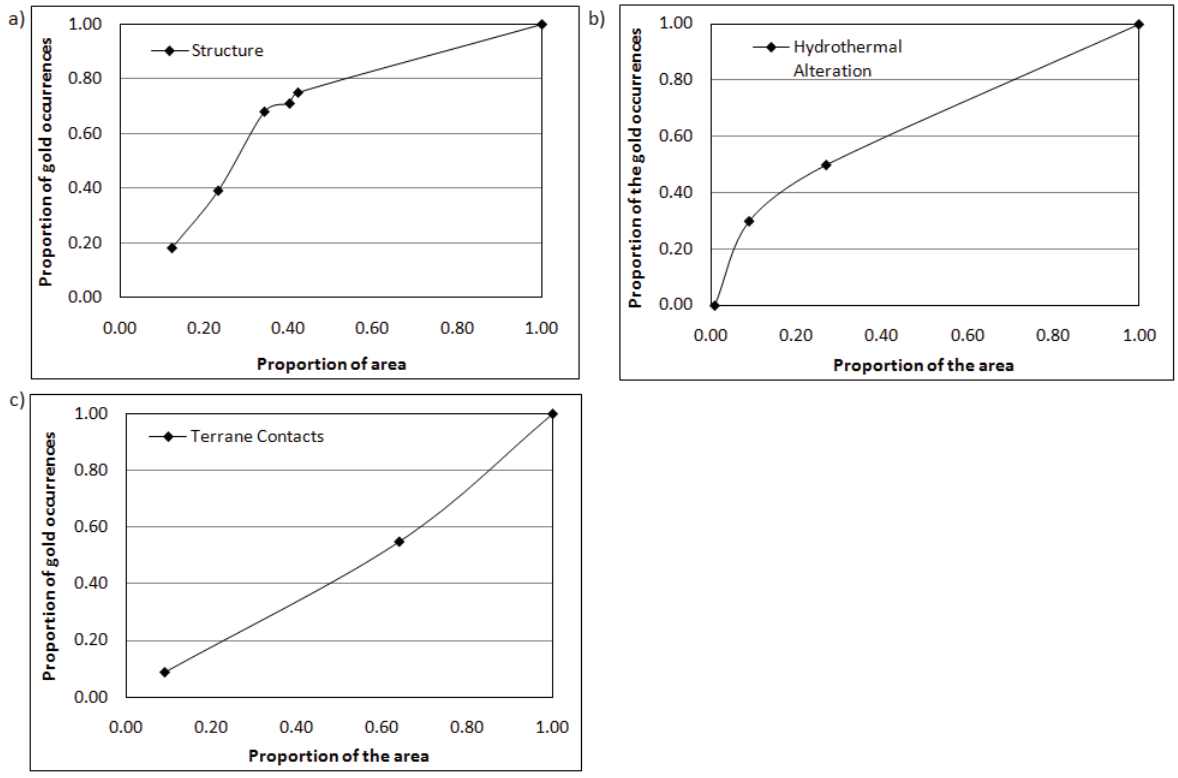

Figure 46: Prediction-rate curves representing active pathways as a critical process. a) Structure b) Hydrothermal Alteration c) Terrane contacts

Using gamma-ray spectrometric data to identify areas of enriched potassium provides a suitable first-pass regional overview of the potential hydrothermal alteration extent. However since this method can only detect 50 cm below the surface this is by no means complete. Encouragingly the methods applied in Chapter 4.6 did not highlight the felsic intrusives or weathering products and although there is still some 'K enrichment' along the river courses there is also a strong correlation between the mapped thrusts and the K enrichment, particularly at Kiboga, Mashonga and the area around Kamwenge where repeated stratigraphy involving schist and gneisses implies a stacked geometry. At the margins of the survey area, several strong K anomalies are thought to be related to epithermal alteration related to the adjacent rift valley, however this could be 'edge-effects' at the margin on the survey area. These additional dispersion processes are thought to falsely increase the performance of the hydrothermal alteration predictor layer.

The contact between Mesoproterozoic aged rocks and the underlying basement and Palaeoproterozoic rocks was targeted in the 'terrane contact layer' for the potential to host remobilised gold. The contacts coincide with the K-enrichment derived from gamma-ray spectrometric data further supporting the model of remobilisation and the active pathway as a critical process. The terrane contact between the Archaean gneisses and the Palaeoproterozoic belt was not extracted as there is no evidence to suggest gold remobilisation at this contact, however this may account for the low performance of the terrane contacts
The structures used to model the active pathway process were selected based on their type and relative age in the deformational history (only those related to orogenies), however recent rift-related structures (D5) may have exploited pre-existing structures which were not included in the model. In addition not all of these structures selected may be active fluid pathways and thus the co-existence of K-enrichment derived from gamma-ray spectrometric dataset and the interpreted structures supports the active fluid pathways process.

5.2.3. Physical Throttle

The geological complexity is a measure of the abundance relationship of the geological structures to gold mineralisation and thus areas of higher fractal dimensions represent zones of well connected fluid pathways, whereas the rheological contrasts allow differential failure behaviour and allows for brecciation in competent units and partitioning of strain *(Czarnota et al., 2010)*. Together these proxies represent a suitable trap to mineralisation.

Figure 47 shows that at 30 % of the study area, the geological complexity layer and the rheological contrasts map 58% and 44% of the gold occurrences respectively. The geological complexity layer out-performs the rheological contrast layer as a proxy for "Physical Throttle" since hydrothermal fluids are focussed (geological complexity) into of areas higher permeability (rheological contrasts).

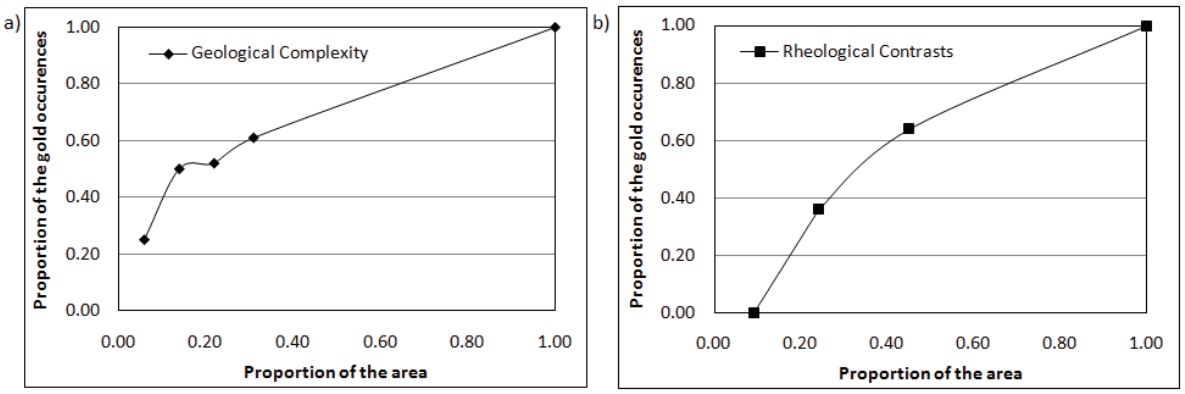

Figure 47: Prediction-rate curves representing physical throttle as a critical process. a) Geological complexity b) Rheological contrasts

The relatively low performance of the rheological contrast layer compared to that of the geological complexity is due to the fact that the lithological contacts were extracted from a surface geological map where the trends on the map reflect the intersection with topography and thus deviate from the true strike of the geological features.

5.2.4. Prospectivity map

The prospectivity map is evaluated as to whether the gold occurrences which are well-predicted are of orogenic-type and those poorly-predicted are of other types using a binary map. The binary map (Figure 49) was created by thresholding the prospectivity map (Figure 42). A threshold value of 4 was chosen to correspond to the area at which 83% of the deposits are predicted as illustrated in the prediction-rate curve (Figure 48).

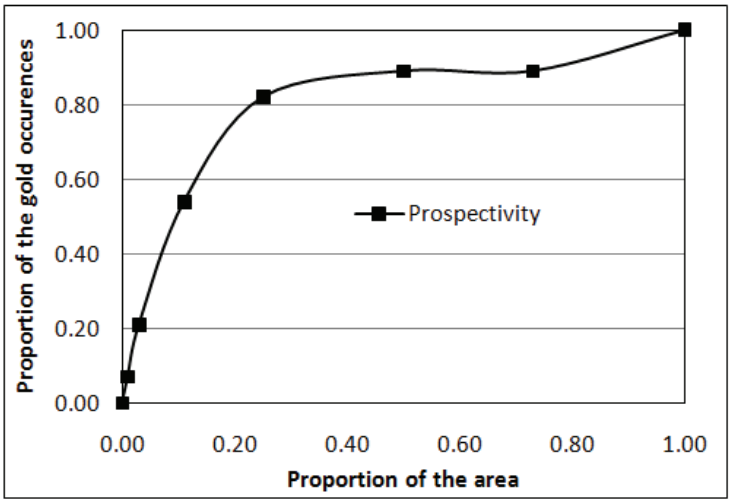

Figure 48: Prediction-rate curve for the final prospectivity map in south-west Uganda.

The areas of high prospectivity show that both Mashonga and Kisita (orogenic gold occurrences) are well predicted by the model. Of the 18 alluvial gold occurrences 10 are within areas of high prospectivity. These alluvial gold occurrences are considered to be proximal to the source since gold recovered from panning the rivers is coarse and angular (Figure 31). Of the six non-orogenic, granite-related gold occurrences all are correctly not predicted, although two lie close to high prospectivity.

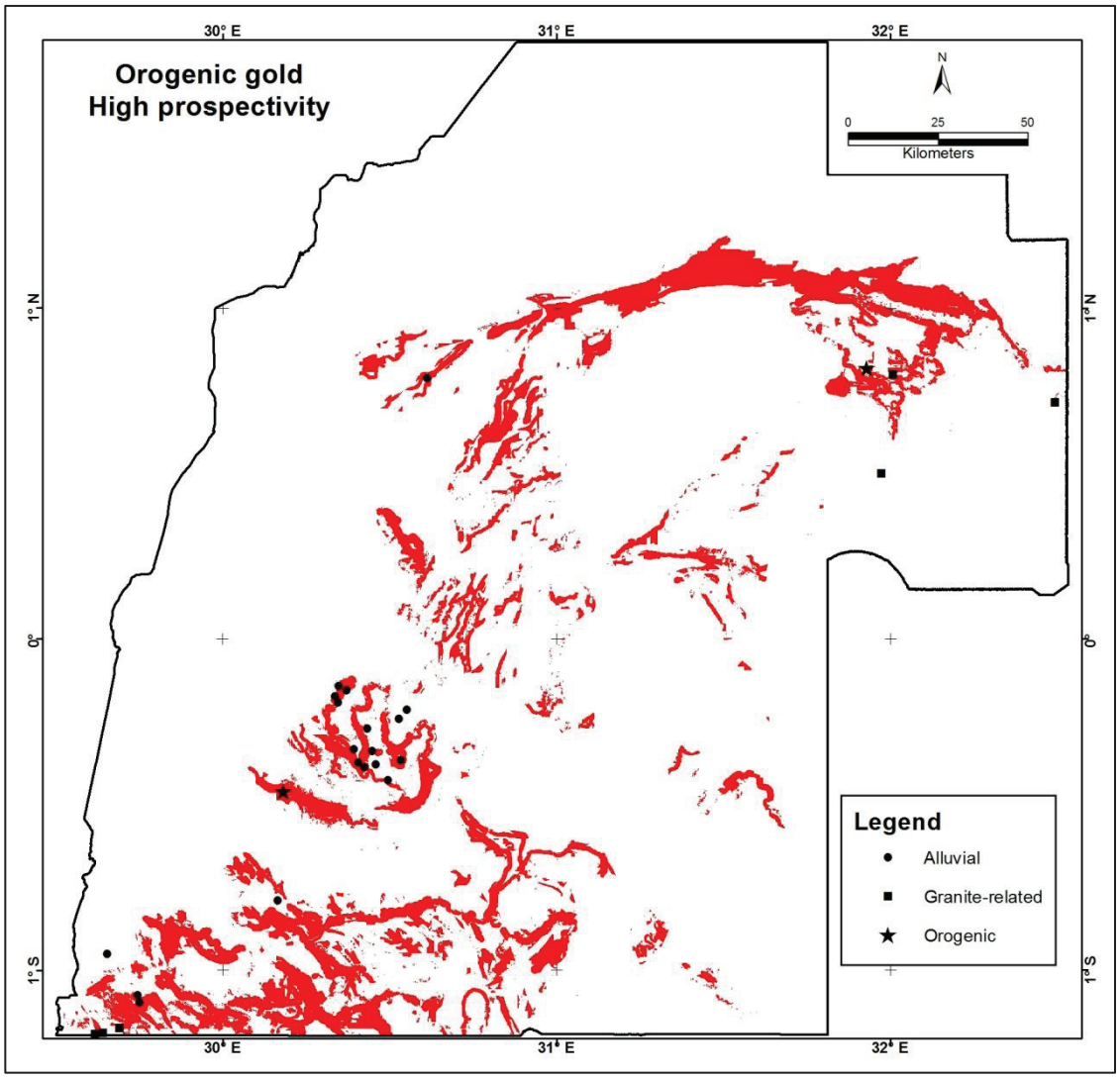

Figure 49: Areas of high prospectivity (red) and gold occurrences

6. CONCLUSION AND RECOMMENDATIONS

The following chapter attempts to provide plausible answers to the research questions formulated in Chapter 1.4. Since the geodynamic history of a mineral system, governs its architecture, they will be addressed in that order.

What is the geodynamic history of the system?

The first deformation event (D1 and D2) is characterised by north-directed thrusting marking the collision of the Congo and Tanzania cratons at ~ 2.1Ga *(Cahen, 1982)*. This event is responsible for the WNW-ESE trending fold and thrust belt in the Kiboga area and oblique sinistral reverse movement along the NE trending segments of the S-shaped Buganda Toro Belt (D2 in Appendix 1). Clockwise rotation of the principal stress direction causes sinistral reactivation of the D1 and D2 fabric and the creation of a pull-apart basin accommodating the intrusion of the Mubende Granite at 1848 ± 6 Ma *(Mänttäri, 2011)*.

Worldwide the geodynamics of the Mesoproterozoic era is characterised by tensional tectonics, this coincides the intracratonic extensional setting proposed for the KAB by *Tack (2010)* at 1375 Ma and the initiation of basin formation *(Pohl, 1994)*. This was followed by the next major compressional event (D3) at 1.0 Ga *(De Waele, et al., 2008)* characterised by NW trending tight upright SW verging folds and intruded by S-type granites (G3) and the "Tin granites" (G4).

The Pan African Orogeny (D4) between 725- 500 Ma is defined by the oblique collision between east and west Gondwana *(Westerhof, pers. comm.)*. During this event NS shear zones are thought to be responsible for the reactivation and remobilisation of mineralised structures from the previous orogenies. The earlier ESE trending D1 thrusts are reactivated by dextral strike-slip movement; while the NE structures reactivated by predominantly reverse movement in the D4 event.

The architecture of a mineral system is intrinsically linked to the geodynamic history and is concerned with the distribution of dilation sites and the long-lived features which define high permeability regions in the crust.

What is the architecture of the system?

The south-west region of Uganda hosts a number of district-scale features considered to be a critical ingredient in the architectural development of a large mineral system, however many of these features are still poorly understood.

The data indicate a complex history of crustal recycling throughout the Proterozoic and that the area is made up of a collection of different domains. One of these major boundaries separates the Archaean Basement rocks from the Palaeoproterozoic Buganda Toro Belt. The Buganda Toro Belt possibly delineates a long lived accretionary margin in a subduction setting marking the collision between the Congo and Tanzania Cratons - (D1). Although no known mineralisation is associated with this boundary, alluvial gold (Butiti) is coincident with a splay off this major terrane boundary in a compressional imbricate fan.

The structures west of the Mubende granites have left-stepping geometries (similar to the overall shape of the Buganda Toro Belt indicating a sinistral transtensional tectonic environment for the given D1 - D3 stress field and later reactivated by sinistral NS Pan African (D4) shears. Although no known gold has been found in this region, Figure 42 and Figure 49 show this region to be highly prospective.

Regional magnetic data shows that the region is traversed by a swarm of dolerite dykes ~1680 Ma *(Mänttäri, 2011)* aligned parallel to the interpreted extensional direction during deformation (D1) of the Buganda Toro Belt and the intrusion of the Mubende Granite at ~1848 ± 6 Ma *(Mänttäri, 2011)*. Although these dykes are younger than mineralisation they may be recording a pre-existing weakness later reactivated as steep pathways for mineralisation at Kisita.

South-east of Kamwenge, repetition of the stratigraphy in a sinistral reverse compressional setting is coincident with high prospectivity (Figure 42 and Figure 49) suggesting that thrust maybe active fluid pathways and brittle fracturing associated with this event increased the permeability of the rocks.

Gold mineralisation in the Buhweju area is mostly alluvial, derived from palaeoplacers (Figure 31). Cross bedding and ripple marks, commonly observed in this area imply that they have suffered little deformation and metamorphism, precluding these rocks from being host to mineralisation. However juxtaposition of the older Palaeoproterozoic rocks at thrusted contacts (Mashonga) indicates that gold has been remobilised along the contact in a compressional environment.

The intra-cratonic extensional setting proposed for the evolution of the KAB by *Tack et al.(2010)* implies that mantle derived fluids have gained access into the crust. This is confirmed by fluid inclusion studies on hydrothermal quartz veins *(Pohl, et al., 1991)*. Areas of high prospectivity (Figure 49) show that these fluids were possibly remobilised into D3 fold hinges in a transtensional setting (D3) and later reactivated by NS sinistral shears and brittle faulting during the Pan African Orogeny (D4).

6.1. Recommendations

The mineral systems approach to district-scale targeting, has resulted in the generation of a new target map for orogenic gold in south-west Uganda. The map (Figure 42) and the prediction-rate curves (Chapter 5.2) summarises the critical processes of orogenic gold formation where evidence for a favourable source of gold and an active pathway is critical to orogenic gold mineralisation. Evidence for a favourable physical throttle, although considered important, is less critical at the district-scale. This is largely indicative of the level of detail in the geological mapping and the resolution of the regional geo-datasets.

In addition to the well predicted orogenic gold deposits, the map shows a number of areas, not previously known for hosting gold deposits but with favourable geological ingredients representing new opportunities. Of the prospective areas, eight have been selected for future exploration as summarised in Table 10 and illustrated in Appendix 3.

One of the most significant outcomes of this research shows how a process-based understanding of the orogenic gold mineral system derived from the consideration of the geodynamic history and architecture of a mineral system can be developed into a targeting model at the district-scale using limited regional data.

The successful application of prospectivity mapping to geology-focussed exploration for orogenic gold deposits in Uganda should result in a more cost effective line of investigation and increase the chances of discovery. Quantification of the geological parameters and the computer-based nature of these methodologies are ideal for the production of an integrated deposit target map.

Table 10: Targets selected for future exploration

New Targets	Area (km^2)	Comment
MUGARAMA	700	• Hosted in volcano-sedimentary Buganda Toro Supergroup • Associated with splays off the major terrane boundary separating the Basement gneisses and the Palaeoproterozoic Buganda Toro Supergroup. • In contact with the Mubende granite where important rheological contrasts occur. • Enriched K coincident with mapped structures indicating fluid pathways.
NYAIBANDA	360	• Hosted in volcano-sedimentary Buganda Toro Supergroup • Sheared out fold hinges • NE shears (D2) reactivated by NS sinistral Pan African shears
RUBONA	450	• Pre-tectonic intrusives - rheological contrasts • Hosted in volcano-sedimentary Buganda Toro Supergroup • Enriched K coincident with mapped structures indicating fluid pathways • Sheared out fold hinges
BIHANGA	220	• NE trending thrusts (D2) reactivated by NS Pan African shears • Enriched K coincident with intersecting structures indicating fluid pathways • Buganda Toro sequence
MASHONGA	53	• Thrust separating Mesoproterozoic and Palaeoproterozoic rock remobilisation. • Thrust coincident with high K enrichment • Conglomerate and quartzite potential host rocks • Artisanal gold workings in the area • Granite intrusive
BUGANGARI	250	• Host Buganda Toro Supergroup • Remobilisation during Lomamian and Pan African Orogenies • High K enrichment in fold hinges • Artisanal gold workings in the area
NAKADULA	160	• Fold and thrust belt in Kiboga area • thrusts coincident with high K enrichment • Basalt host in Buganda Toro Supergroup
BUTITI	200	• Splay off major terrane boundary • Quartzite host rock • Artisanal gold working in area
KISITA	150	• NS-NE structural intersection • Folded sandstone, shale and magnetite

6.2. Limitations

Although this study has addressed the geodynamic history and architecture of the district-scale orogenic gold mineral system in Uganda, more detailed fieldwork is required to validate the significance of these claims to target structurally controlled hydrothermal mineralisation into sites of low mean stress. In addition much remains to be understood about the metamorphic pressure and temperature of the system.

Hydrothermal alteration in the region could only be detected by gamma-ray spectrometric data due to the absence of regional geochemical data and the dense vegetation which inhibits the spectral determination of rocks and mineral assemblages.

Most of the gold occurrences in the region are alluvial and extracted by artisanal miners with scarce information on the source or the production statistics. Only two validated *in situ* gold occurrences (Mashonga and Kisita) is insufficient to accurately validate the prospectivity map.

LIST OF REFERENCES

Aanyu, K., & Koehn, D. (2011). Influence of pre-existing fabrics on fault kinematics and rift geometry of interacting segments: Analogue models based on the Albertine Rift (Uganda), Western Branch-East African Rift System. *Journal of African Earth Sciences, 59*(2-3), 168-184.

Bahiru, E. A. (2011). *Inter - relationship between lithology and structure and its control on gold mineralization in Buhweju area, SW of Uganda.* Unpublished MSc Thesis, University of Twente ITC, Enschede.

Barnes, J. W. (1961). *The Mineral Resources of Uganda.* Bull.4

Bauer, F. U., Glasmacher, U.A and Ring, U. (2010). Thermal and exhumation history of the central Ruwenzori Mountains, Western Rift of the East African Rift System, Uganda. *International Journal of Earth Sciences, 99*, 1575-1597.

Begg, G. C., Griffin, W. L., Natapov, L. M., O'Reilly, S. Y., Grand, S. P., O'Neill, C. J., Hronsky, J. M. A., Djomani, Y. P., Swain, C. J., Deen, T., & Bowden, P. (2009). The lithospheric architecture of Africa: Seismic tomography, mantle petrology, and tectonic evolution. *Geosphere, 5*(1), 23-50.

Bierlein, F. P., Groves, D. I., & Cawood, P. A. (2009). Metallogeny of accretionary orogens -- The connection between lithospheric processes and metal endowment. *Ore Geology Reviews, 36*(4), 282-292.

Brinckmann, J., Lehmann, B., & Timm, F. (1994). Proterozoic gold mineralization in NW burundi. *Ore Geology Reviews, 9*(2), 85-103.

Buchwaldt, R., Toulkeridis, T., Todt, W., & Ucakuwun, E. K. (2008). Crustal age domains in the Kibaran belt of SW-Uganda: Combined zircon geochronology and Sm-Nd isotopic investigation. *Journal of African Earth Sciences, 51*(1), 4-20.

Cahen, L. (1982). Geochronological correlation of the late Precambrian sequences on and around the stable zones of equatorial Africa. *Precambrian Research, 18*(1-2), 73-86.

Carranza, E. J. M. (2010). Improved Wildcat Modelling of Mineral Prospectivity. *Resource Geology, 60*(2), 129-149.

Carranza, E. J. M. (Ed.). (2009). *Geochemical anomaly and mineral prospectivity mapping in GIS*: Elsevier.

Chavez, P. S., Stuart, J. R., Sides, C., & Jeffrey, A. A. (1991). Comparison of three different methods to merge multi-resolution and multi-spectral data: Landsat TM and Spot Panchromatic. *Photogrammetric Engineering and Remote Sensing, 57*(3), 295-303.

Czarnota, K., Blewett, R. S., & Goscombe, B. (2010). Predictive mineral discovery in the eastern Yilgarn Craton, Western Australia: An example of district scale targeting of an orogenic gold mineral system. *Precambrian Research, 183*(2), 356-377.

de Quadros, T. F. P., Koppe, J. C., Strieder, A. J., & Costa, J. F. C. L. (2003). Gamma-ray data processing and integration for lode-Au deposits exploration. *Natural Resources Research, 12*(1), 57-65.

De Waele, B., Johnson, S. P., & Pisarevsky, S. A. (2008). Palaeoproterozoic to Neoproterozoic growth and evolution of the eastern Congo Craton: Its role in the Rodinia puzzle. *Precambrian Research, 160*(1-2), 127-141.

Dewaele, S., Henjes-Kunst, F., Melcher, F., Sitnikova, M., Burgess, R., Gerdes, A., Fernandez, M. A., Clercq, F. D., Muchez, P., & Lehmann, B. (2011). Late Neoproterozoic overprinting of the cassiterite and columbite-tantalite bearing pegmatites of the Gatumba area, Rwanda (Central Africa). *Journal of African Earth Sciences, 61*(1), 10-26.

Duchesne, J. C., Liegeois, J. P., Deblond, A. and Tack, L. (2004). Petrogenesis of the Kabanga–Musongati layered mafic–ultramafic intrusions in Burundi (Kibaran Belt): geochemical, Sr–Nd isotopic constraints and Cr–Ni behaviour. *Journal of African Earth Sciences, 39*, 133 - 145.

Ford, A., & Blenkinsop, T. G. (2008). Evaluating geological complexity and complexity gradients as controls on copper mineralisation, Mt Isa Inlier. *Australian Journal of Earth Sciences, 55*(1), 13-23.

Gabert, G. (1990). Lithostratigraphic and tectonic setting of gold mineralization in the Archean cratons of Tanzania and Uganda, East Africa. *Precambrian Research, 46*(1-2), 59-69.

Gnojek, I., & Prichystal, A. (1985). A new zinc mineralization detected by airborne gamma-ray spectrometry in northern Moravia (Czechoslovakia). *Geoexploration, 23*, 491-502.

Goldfarb, R. J., Groves, D. I., & Gardoll, S. (2001). Orogenic gold and geologic time: a global synthesis. *Ore Geology Reviews, 18*(1-2), 1-75.

Griffis, W. (2010). American Paramount Gold commences due diligence process on the Kisita Gold Mine. Retrieved 28 February 2011, from Business Wire:

Grocott, J., Taylor, G.K. (2002). Magmatic arc fault systems, deformation partitioning and emplacement of granitic complexes in the Coastal Cordillera, north Chilean Andes. *Journal of the Geological Society, London, 159*, 425-442.

Groves, D. I., & Bierlein, F. P. (2007). Geodynamic settings of mineral deposit systems. *Journal of the Geological Society, 164*, 19-30.

Groves, D. I., Goldfarb, R. J., Gebre-Mariam, M., Hagemann, S. G., & Robert, F. (1998). Orogenic gold deposits: A proposed classification in the context of their crustal distribution and relationship to other gold deposit types. *Ore Geology Reviews, 13*(1-5), 7-27.

Groves, D. I., Goldfarb, R. J., Knox-Robinson, C., Ojala, J., Gardoll, S. J., Yun, G. Y., & Holyland, P. (2000). Late-kinematic timing of orogenic gold deposits and significance for computer-based exploration techniques with emphasis on the Yilgarn Block, Western Australia. *Ore Geology Reviews, 17*(1-2), 1-38.

Hepworth, J. V., & Macdonald, R. (1966). Orogenic belts of the northern Uganda Basement. *Nature, 210*(5037), 726-727.

Johnson, R. J., & Williams, C. E. F. (1960). *Explanation of the Geology of Sheet 59 (Kiboga)*: Geological Survey of Uganda.

Kerrich, R. (1993). Perspectives on genetic models for lode gold deposits. *Mineralium Deposita, 28*(6), 362-365.

Klerkx, J. (1987). Crustal evolution of the northern Kibaran belt, eastern and central Africa. *In Kroner, A., (Ed), Proterozoic Lithospheric Evolution. American Geophysical Union and the Geological Society of America*, 217-233.

Leggo, P. J. (1973). Geochronology of Uganda basement, East-Africa. *Transactions-American Geophysical Union, 54*(4), 496-497.

Lenoir, J. L., Liégeois, J. P., Theunissen, K., & Klerkx, J. (1994). The Palaeoproterozoic Ubendian shear belt in Tanzania: geochronology and structure. *Journal of African Earth Sciences, 19*(3), 169-184.

Link, K., Koehn, D., Barth, M. G., Tiberindwa, J. V., Barifaijo, E., Aanyu, K., & Foley, S. F. (2010). Continuous cratonic crust between the Congo and Tanzania blocks in western Uganda. *International Journal of Earth Sciences, 99*(7), 1559-1573.

Magoon, L. B., & Dow, W. G. (1991). The petroleum system. In: Magoon, L.B., Dow, W.G. The Petroleum System–From Source to Trap. *AAPG Memoir, 60*, 3-24.

Mänttäri, I. (2011). *Radiometric ages for rock samples from Uganda*: GTK Consortium.

McCuaig, T. C., Beresford, S., & Hronsky, J. (2010). Translating the mineral systems approach into an effective exploration targeting system. *Ore Geology Reviews, 38*(3), 128-138.

Msechu, M. E. (2011). Modeling of prospectivity for lode - au mineralization in the Kibaran of Uganda. University of Twente

Pekkala, Y., Baguma, Z., Byamugisha, S., Turyasingura, P. (1994). Geochemical exploration programme on gold and base metals, Buhweju, SW- Uganda. Department of Geological Survey and Mines (DGSM).

Pohl, W. (1987). Metallogeny of the northeastern Kibaran Belt, Central Africa. *Geological Journal, 22*, 103-119.

Pohl, W. (1994). Metallogeny of the northeastern Kibara belt, Central Africa--Recent perspectives. *Ore Geology Reviews, 9*(2), 105-130.

Pohl, W., & Gunther, M. A. (1991). The origin of the Kibaran (late midproterozoic) tin, tungsten and gold quartz vein deposits in central Africa - A fluid inclusions study. [Article]. *Mineralium Deposita, 26*(1), 51-59.

Robb, L. J. (2005). *Introduction to ore-forming processes*. Malden, USA: Blackwell Publishing.

Rumvegeri, B. T. (1991). Tectonic significance of Kibaran structures in Central and Eastern Africa. *Journal of African Earth Sciences (and the Middle East), 13*(2), 267-276.

Saunders, D. F., Terry, S.A. & Thompson, C.K. (1987). Test of national uranium resource evaluation gamma-ray spectral data in petroleum reconnaissance. *Geophysics, 52*(11), 1547-1556.

Schenk, V., Appel, P., Jons, N., Loose, D., Schumann, A., & Wegner, H. (2007). Metamorphic reworking of the Congo craton in Uganda. *Geochimica Et Cosmochimica Acta, 71*(15), A887-A887.

Shives, R. B. K., Charbonneau, B.K., Ford, K.L. (1997). *The detection of potassic alteration by gamma-ray spectrometry recognition of alteration related to mineralisation*. Paper presented at the Exploration 97, Fourth Decennial International Conference. Mineral Exploration.

Sibson, R. H., Robert, F., Poulsen, K.H. (1988). High angle reverse faults, fluid-pressure cycling, and mesothermal gold–quartz deposits. *Geology, 16*, 551-555.

Tack, L., Liégeois, J. P., Deblond, A., & Duchesne, J. C. (1994). Kibaran A-type granitoids and mafic rocks generated by two mantle sources in a late orogenic setting (Burundi). *Precambrian Research, 68*(3-4), 323-356.

Tack, L., Wingate, M. T. D., De Waele, B., Meert, J., Belousova, E., Griffin, B., Tahon, A., & Fernandez-Alonso, M. (2010). The 1375 Ma "Kibaran event" in Central Africa: Prominent emplacement of bimodal magmatism under extensional regime. *Precambrian Research, 180*(1-2), 63-84.

Theunissen, K. (1989). On the Rusizian basement rise in the Kibaran belt of Northeastern Lake Tanganyika. Collision belt geometry or restraining bend emplaced in the Late Kibaran strike-slip environment. *IGCP, 2*(225), 85-92.

Trauth, M. H., & Schlüter, T. (2008). *Geological atlas of Africa: with notes on stratigraphy, tectonics, economic geology, geohazards and geosites of each country*. DE: Springer Verlag.

Walshe, J. L., Cooke, D. R., & Neumayr, P. (2005). *Five questions for fun and profit: A mineral systems perspective on metallogenic epochs, provinces and magmatic hydrothermal Cu and Au deposits.* . Paper presented at the Mineral Deposit Research: Meeting the Global Challenge. Proceedings of the 8th Biennial SGA Meeting.

Williams, P. J., Barton, M.D., Johnson, D. A., Fontboté, L., De Haller, Antoine, M. Geordie, O., Nicholas H.S., and Marschik, R. (2005). Iron oxide copper-gold deposits: geology, space-time distribution, and possible modes of origin. *Economic Geology, 100th Anniversary Volume*(100th Anniversary Volume), 371-405.

Wyborn, L. A. I., Heinrich, C. A., & Jaques, A. L. (1994). *Australian Proterozoic Mineral Systems: Essential ingredients and mappable criteria.* Paper presented at the AusIMMM Annual Conference.

WP	LATITUDE	LONGITUDE	DATE	ALTITUDE	ROCK UNIT	STRUCTURE CODE	DIP DIR	DIP	MOVE-MENT	PHOTO	COMMENT
001	-0.39149	31.45926	20111003	1244	schist & sandy layer	SZ	077	00	DEX	4131;4132 (N); 4135-4136 (stereophoto) 1m scale	sheared boudin & sheared through the fold axis. All photos looking N. Im scale.
001	-0.39149	31.45926	20111003	1244	schist & sandy layer	S0	357	25		4131;4132 (N); 4135-4136 (stereophoto) 1m scale	fold limb. isoclinal folding. Fold axes plunge to NE.
001	-0.39149	31.45926	20111003	1244	schist & sandy layer	S0	247	38		4131;4132 (N); 4135-4136 (stereophoto) 1m scale	fold limb. isoclinal folding. Fold axes plunge to NE.
002	-0.39151	31.45926	20111003	1246	granitic gneiss	SZ	052	84	SIN	4137 (N) Hammer L & R of fault zones	C-C' fabric in albitized granite with ser & chl.
002	-0.39151	31.45926	20111003	1246	granitic gneiss	QV	041	80		4137 (N) Hammer L & R of fault zones	Faults subparallel to quarts veins?
003	-0.40312	31.36148	20111003	1281	quartzite & mudstone	S0	018	37		4138 (NE) 4m scale of photo- pencil on S0	anticlinal closure to the E. Less deformed not sheared . probably younger than WP001
003	-0.40312	31.36148	20111003	1281	quartzite & mudstone	S1	001	62		4138 (NE) 4m scale of photo - hammer on S1	well bedded unit
004	-0.38137	31.30512	20111003	1271	siltstone	S0	105	05		4139 (NW) pencil on S0	wavy undulating bedding. BT fm
004	-0.38137	31.30512	20111003	1271	siltstone	S1	227	58		4139 (NW)	wavy undulating bedding. BT fm
004	-0.38137	31.30512	20111003	1271	siltstone	S2	329	74		4139 (NW) hammer on S2	wavy undulating bedding. BT fm
005	-0.37675	31.27881	20111003	1350	siltstone	S0	021	08		no photo	closure between WP004 & WP005
005	-0.37675	31.27881	20111003	1350	siltstone	S1	003	88		no photo	closure between WP004 & WP005
006	-0.37805	31.24686	20111003	1272	granite						boulders in stream. WP taken from car
007	-0.38078	31.23661	20111003	1299	Malongo						Malongo
008	-0.39049	31.18637	20111003	1263	granite						granite
009	-0.40821	31.14824	20111003	1260	granite						dome N of road
010	-0.44916	31.06162	20111003	1310	clay soils					4140-4142	sparsely vegetated undulating landscape. Looking W. Dark clay soil

WP	LATITUDE	LONGITUDE	DATE	ALTITUDE	ROCK UNIT	STRUCTURE CODE	DIP DIR	DIP	MOVE-MENT	PHOTO	COMMENT
011	-0.51147	30.90683	20111004	1309	granitic gneiss	S1	320	48			close to sch contact
012	-0.57107	30.91914	20111004	1295	graphitic schist	S0	219	50			hills of highly foliated graphitic sch.
012	-0.57107	30.91914	20111004	1295	graphitic schist	S1	317	76			hills of highly foliated graphitic sch.
012	-0.57107	30.91914	20111004	1295	graphitic schist	Li1	227	60			hills of highly foliated graphitic sch.
013	-0.57165	30.91962	20111004	1290	graphitic schist	S0	279	50		4143	4143 - red pen S1 blue pen is Li1
013	-0.57165	30.91962	20111004	1290	graphitic schist	S1	219	88		4143	4143 - red pen S1 blue pen is Li1
013	-0.57165	30.91962	20111004	1290	graphitic schist	S2	255	73		4143	4143 - red pen S1 blue pen is Li1
013	-0.57165	30.91962	20111004	1290	graphitic schist	Li2	267	52			intersection of S1 & S2
014	-0.5707	30.92001	20111004	1298	graphitic schist	S0	157	80		4146 (060 red= S0) 4147 -(overall pic NE)	exposure on cliff isoclinal folding & crenulated
014	-0.5707	30.92001	20111004	1298	graphitic schist	S1	195	74		4146 (060 blue = S1) 4147 -(overall pic NE)	exposure on cliff isoclinal folding & crenulated
014	-0.5707	30.92001	20111004	1298	graphitic schist	S0	158	80		4145 (060 red = S0) 4147 -(overall pic NE)	exposure on floor isoclinal folding & crenulated. Closure of S1 deformation.
014	-0.5707	30.92001	20111004	1298	graphitic schist	S1	211	78		4145 (060 blue = S1) 4147 -(overall pic NE)	exposure on floor isoclinal folding & crenulated. Closure of S1 deformation.
015	-0.57174	30.91915	20111004	1294	graphitic schist	S0	312	76			
015	-0.57174	30.91915	20111004	1294	graphitic schist	S1	272	70			
016	-0.5991	30.93062	20111004	1262	Lake Mburo National Park						370 km2; 7000USh/car & USD30 per person
017	-0.57865	31.00988	20111004	1281	granitic gneiss	SZ	033	88	DEX	4151 vertically down. Pencil along C fabric	v.coarse grained. Localized QV DEX shear
018	-0.58515	30.92432	20111004	1318	schist	S0	257	56		4161 NW.red top= S2 red pen = S1 blue = F1; 4164 (NW red pen=S0)	more pelitic sch. Minor graphitic units. forms higher hills than graphitic unit- competent unit.

WP	LATITUDE	LONGITUDE	DATE	ALTITUDE	ROCK UNIT	STRUCTURE CODE	DIP DIR	DIP	MOVE-MENT	PHOTO	COMMENT
018	-0.58515	30.92432	20111004	1318	schist	S1	312	78		4161 NW.red top= S2 red pen = S1 blue = F1; 4164 (NW red pen=S0)	more pelitic sch. Minor graphitic units. forms higher hills than graphitic unit- competent unit.
018	-0.58515	30.92432	20111004	1318	schist	S2	241	58		4161 NW.red top= S2 red pen = S1 blue = F1; 4164 (NW red pen=S0)	more pelitic sch. Minor graphitic units. forms higher hills than graphitic unit- competent unit.
018	-0.58515	30.92432	20111004	1318	schist	Li1	162	70		4161 NW.red top= S2 red pen = S1 blue = F1; 4164 (NW red pen=S0)	more pelitic sch. Minor graphitic units. forms higher hills than graphitic unit- competent unit.
018	-0.58515	30.92432	20111004	1318	schist	F1	042	22		4161 NW.red top= S2 red pen = S1 blue = F1; 4164 (NW red pen=S0)	more pelitic sch. Minor graphitic units. forms higher hills than graphitic unit- competent unit.
019	-0.5023	30.89118	20111004	1290	gneissic schist	S1	220	72		4165-4171 N (EW section)	highly fissile. Alternation sch & qtz bands. Cross cut by mafic dykes & acidic dykes
019	-0.5023	30.89118	20111004	1290	gneissic schist	S1	241	70		4165-4171 N (EW section)	highly fissile. Alternation sch & qtz bands. Cross cut by mafic dykes & acidic dykes
019	-0.5023	30.89118	20111004	1290	gneissic schist	S2	181	86		4165-4171 N (EW section)	highly fissile. Alternation sch & qtz bands. Cross cut by mafic dykes & acidic dykes
019	-0.5023	30.89118	20111004	1290	gneissic schist	S1	175	60		4165-4171 N (EW section)	highly fissile. Alternation sch & qtz bands. Cross cut by mafic dykes & acidic dykes
019	-0.5023	30.89118	20111004	1290	gneissic schist	S2	239	44		4165-4171 N (EW section)	highly fissile. Alternation sch & qtz bands. Cross cut by mafic dykes & acidic dykes
020	-0.49937	30.84961	20111004	1309	biotite gneiss					photo 4172;4173;4175;4176	acidic dyke with amph+ms+bt+chl cross cutting bt gneiss. Migmatic in places.
021	-0.82064	30.81846	20111005	1387	sandstone					4178	well sorted ss. subrounded grains. Clast supported. Sugary texture. Forms smooth competent caps on ridges // drainage

WP	LATITUDE	LONGITUDE	DATE	ALTITUDE	ROCK UNIT	STRUCTURE CODE	DIP DIR	DIP	MOVE-MENT	PHOTO	COMMENT
022	-0.82064	30.81846	20111005	1387	schist	S1	135	48			strongly foliated pelitic sch
023	-0.8204	30.81853	20111005	1384	sandstone	S0	033	40			asymetrical folding. Anticline to S syncline to N
024	-0.81849	30.81745	20111005	1350	sandstone	S0	357	50			
025	-0.81813	30.81762	20111005	1357	micaceous sandstone	S0	023	33			lies in between sch below & sandstone above. Med-coarse grained. Parallel alignment of flakey minerals
025	-0.81813	30.81762	20111005	1357	micaceous sandstone	S1	281	76			lies in between sch below & sandstone above. Med-coarse grained. Parallel alignment of flakey minerals
025	-0.81813	30.81762	20111005	1357	micaceous sandstone	S2	159	62			lies in between sch below & sandstone above. Med-coarse grained. Parallel alignment of flakey minerals
026	-0.81304	30.81698	20111005	1259	schist	S1	137	86			
027	-0.7809	30.78627	20111005	1356	quartzite						fine grained grey qtz with purple MnOx. bad S0 readings
028	-0.77782	30.78215	20111005	1387	tuff/pelite	S0	284	13			dark grey volcanic material with acicular shards of ? Aphanitic ground mass. bedding= ashfall layers.
029	-0.77207	30.77748	20111005	1421	tuff/pelite	S0	159	35			dark grey volcanic material with acicular shards of ? Aphanitic ground mass. bedding= ashfall layers.
029	-0.77207	30.77748	20111005	1421	tuff/pelite	Li1	097	22			
029	-0.77207	30.77748	20111005	1421	tuff/pelite	FT	137	58		98 (TW)	
030	-0.75495	30.76415	20111005	1336	quartzo-feldspathic schist	S1	167	85		99-101 (TW)	subrounded quartz eyes in micaceous unit. Strongly lateritized- dodgy reading.
031	-0.68487	30.56472	20111006	1452	mica schist	S0	220	86			
031	-0.68487	30.56472	20111006	1452	mica schist	S1	042	75	DEX	4181 (book= S0 & pencil S1)	dex rotation of andalusite ? porphyroblast

WP	LATITUDE	LONGITUDE	DATE	ALTITUDE	ROCK UNIT	STRUCTURE CODE	DIP DIR	DIP	MOVE-MENT	PHOTO	COMMENT
032	-0.71299	30.56366	20111006	1498	quartzite	S0	014	68			slightly weathered sugary texture. Forms prominent ridges.
032	-0.71299	30.56366	20111006	1498	quartzite	S1	054	42			slightly weathered sugary texture. Forms prominent ridges.
033	-0.72054	30.52685	20111006	1646	alluvium					4188; 4189 SW	in valley looks folded unit - just morphology of the area & river.
034	-0.74434	30.54468	20111006	1719	slate	S0	060	60			
034	-0.74434	30.54468	20111006	1719	pelite	S1	068	78			slatey
034	-0.74434	30.54468	20111006	1719	pelite	S0	082	60			slatey
034	-0.74434	30.54468	20111006	1719	pelite	S1	030	68			slatey
035	-0.74786	30.5304	20111006	1484	quartzite						
036	-0.96292	30.48268	20111006	1359	biotite granite						v.cg. Qtz= 80%. 12%- Bt. Kfs & msc. WNW-ESE fabric on imagery not in rock - probably joints
037	-0.97684	30.30278	20111006	1419	quartzite						grey well bedded. Haematite & tourmaline in veinlets. Sn granites nearby.
038	-0.93106	30.29921	20111006	1448	mica schist	SZ	286	38			strongly sheared associated with smokey QV. Boxworks of py
038	-0.93106	30.29921	20111006	1448	mica schist	Ls	226	25		4192; 4193; 4194 SW	
038	-0.93106	30.29921	20111006	1448	mica schist	F1	220	05			
039	-0.89212	30.29054	20111006	1407	granite					103 (TW)	no bt. WNW-ESE joints seen on imagery
040	-0.88007	30.23551	20111007	1469	amphibolite schist	SZ	282	86	DEX REV	4195 E. Pencil oriented // to shear	
040	-0.88007	30.23551	20111007	1469	amphibolite schist	Ls	228	56	DEX REV	4195 E. Pencil oriented // to shear	dark black in colour. Possibly a xenolith within the granite body or magmatic differention
041	-0.87909	30.23757	20111007	1466	granite	SZ	098	80		4196; 4197 ;4198	sheared granite tongue. Forms kopjes/ large Kfs phenocryst with cleavage perpendicular to shear

WP	LATITUDE	LONGITUDE	DATE	ALTITUDE	ROCK UNIT	STRUCTURE CODE	DIP DIR	DIP	MOVE-MENT	PHOTO	COMMENT
042	-0.88025	30.23061	20111007	1466	granite	QV	270	30			
042	-0.88025	30.23061	20111007	1466	granite	sL	210	48			
042	-0.88025	30.23061	20111007	1466	granite	SZ	240	78	DEX NORM		
043	-0.8177	30.15817	20111007	1613	quartzite	S0	292	48			v.close to granite contact. Interbedded with minor schose material
043	-0.8177	30.15817	20111007	1613	quartzite	S1	048	70			
044	-0.83152	30.11505	20111007	1543	gneiss schist intercalated	S0	008	72		panoramic 4202-4204m (S)	see notebook. W verging folds. Dom stress from E.
045	-0.90912	30.01555	20111007	1397	quartz vein ridges					4208 N	with micaceous sch along the contacts & mafic dykes. EW ridges fits imagery. Hbl randomly oriented post tect.
046	-0.9365	30.04038	20111007	1548	quartz vein ridges	JT	060	88		4209-4210	108 orientation. Crackled appearance
047	-0.95213	30.04128	20111007	1545	phyllite	S0	026	42			grey powdery texture crenulated bedding
047	-0.95213	30.04128	20111007	1545	phyllite	S1	170	66			grey powdery texture crenulated bedding
048	-0.99763	29.94206	20111007	1692	mica schist	S0	228	58			purple grey micaceous sch. S1 relationship S0 anticline to SE.
048	-0.99763	29.94206	20111007	1692	mica schist	S1	002	85			
049	-0.94157	29.87369	20111007	1993	schist					photo 4218	porphyroblast in sch grab sample
050	-0.91451	29.85025	20111007	1760	granite						coarse grained. Light in ternary image. Strongly weathered no mineral banding.
051	-0.89099	29.79428	20111007	1513	granite					4219 & 4220	granite host to artisinal workings?
052	-0.85237	29.72665	20111007	1480	mica schist	S1	172	52			
053	-0.7179	29.69342	20111007	1091	Savanna Lodge						
054	-0.75651	29.71087	20111008	1160	conglomerate					4222; 4223 (NW)	not cemented. Clast supported dominantly qtz pebbles

WP	LATITUDE	LONGITUDE	DATE	ALTITUDE	ROCK UNIT	STRUCTURE CODE	DIP DIR	DIP	MOVE-MENT	PHOTO	COMMENT
055	-0.76613	29.7237	20111008	1153	sandstone & conglomerate recent rift sediments					4224 E; 4225 NW	cross bedding indicating flow to the N
056	-0.82069	29.78228	20111008	1431	schist	S0	322	56		4228; 4229 S0 hammer & S1= pencil	bt msc sch. Qv with tml & msc
056	-0.82069	29.78228	20111008	1431	schist	S1	292	60			
057	-0.82621	29.78878	20111008	1483	quartzite						maybe rxtlzd gneiss. but field evidence suggests qtz
058	-0.78841	29.80397	20111008	1450	gneiss	S0	340	65			dominantly gneiss minor schose bands
058	-0.78841	29.80397	20111008	1450	gneiss	S1	172	84			
059	-0.76844	29.82007	20111008	1215	Nyengo River					4230 E	
060	-0.7923	29.82472	20111008	1216	gneiss						WP taken from moving car. Pink bands
061	-0.79557	29.82547	20111008	1261	schist						
062	-0.84848	29.98311	20111008	1609	gneiss	S0	108	20		4236 SW	downthrown block see sketch in notebook
062	-0.84848	29.98311	20111008	1609	gneiss	S1	108	12		4237 SW	downthrown block see sketch in notebook
062	-0.84848	29.98311	20111008	1609	gneiss	S2	106	83		4238 SW	downthrown block see sketch in notebook
062	-0.84848	29.98311	20111008	1609	gneiss	S0	114	85		4234; 4235 SW	upthrown block alternating bands of sch & gneiss variable thicknesses. NW directed thrusting force from SE
062	-0.84848	29.98311	20111008	1609	gneiss	S1	140	75			upthrown block
062	-0.84848	29.98311	20111008	1609	gneiss	S2	106	83			upthrown block
062	-0.84848	29.98311	20111008	1609	gneiss	FT	296	75			
062	-0.84848	29.98311	20111008	1609	gneiss	F2	156	26			
063	-0.72656	30.16793	20111008	1484	graphitic schist	S0	278	26			bedding is questionable. Marker layer
063	-0.72656	30.16793	20111008	1484	graphitic schist	S1	165	73			

WP	LATITUDE	LONGITUDE	DATE	ALTITUDE	ROCK UNIT	STRUCTURE CODE	DIP DIR	DIP	MOVE-MENT	PHOTO	COMMENT
063	-0.72656	30.16793	20111008	1484	graphitic schist	S2	352	53			
064	-0.6797	30.158	20111008	1501	mica schist	S1	330	22			
064	-0.6797	30.158	20111008	1501	mica schist	S2	245	30			
065	-0.68005	30.16076	20111008	1489	hotsprings in gneiss	S0	215	70		4238-4242	second hotspring on 340 trend. About 20 km from rift along NW-SE oriented transform fault?
065	-0.68005	30.16076	20111008	1489	hotsprings in gneiss	S1	052	26			
066	-0.38495	30.15178	20111009	1443	Mashonga alluvial mines						in a valley bowl surrounded by tea estates. qtz & cgt to N gneiss & sch to S.
067	-0.38461	30.1515	20111009	1440	schist	S0	232	20		4252 - trench photo.113-115 (TW)	Reddish purple in colour.
067	-0.38461	30.1515	20111009	1440	schist	S1	318	65			
067	-0.38461	30.1515	20111009	1440	schist	S2	100	65			
068	-0.38616	30.15188	20111009	1420	granite						coarse grained porphyritic large Kfs laths
069	-0.36592	30.10627	20111009	1565	conglomerate						poorly sorted well rounded dominantly qtz pebbles up to 15cm diameter. Clayey matrix with finer grained qtz. Sheared bxa with chl. ser alb alteration-EW structure
070	-0.36568	30.10653	20111009	1578	conglomerate						qtz cgt contact. fining upward sequence. Cgt- qtz- slts/phyl
071	-0.3552	30.09678	20111009	1632	quartzite & phyllite	S0	274	78			
071	-0.3552	30.09678	20111009	1632	quartzite & phyllite	S1	254	88			phyl above & qtz below
072	-0.3548	30.09606	20111009	1601	quartzite & phyllite	S0	050	36		4270; 4271	
072	-0.3548	30.09606	20111009	1601	quartzite & phyllite	S1	333	86		131-134 TW	

WP	LATITUDE	LONGITUDE	DATE	ALTITUDE	ROCK UNIT	STRUCTURE CODE	DIP DIR	DIP	MOVE-MENT	PHOTO	COMMENT
073	-0.35446	30.09562	20111009	1589	quartzite & phyllite	S0	008	31			
073	-0.35446	30.09562	20111009	1589	quartzite & phyllite	S1	160	72			
074	-0.11189	30.30293	20111009	1412	mica schist	S1	120	60			
075	-0.11486	30.30523	20111009	1463	quartzite						
076	-0.12405	30.319	20111009	1307	Chitaka Camp						
077	-0.10291	30.34419	20111009	1610	gabbro						
078	-0.19356	30.4086	20111010	1507	mica schist	S0	005	38			
078	-0.19356	30.4086	20111010	1507	mica schist	S1	163	70			
078	-0.19356	30.4086	20111010	1507	mica schist	S0	140	42		149 TW	SW verging asymetrical folds. Dominant pressure from NE
078	-0.19356	30.4086	20111010	1507	mica schist	S1	163	70			
079	-0.18242	30.40552	20111010	1620	conglomerate						matrix supported quartz dominated pebbles up to 15cm diameter poorly sorted. No fabric
080	-0.1824	30.40557	20111010	1617	quartzite	S0	266	56			
080	-0.1824	30.40557	20111010	1617	quartzite	S1	292	76			weak shear. NE block moved up.
081	-0.18136	30.40461	20111010	1637	quartzite	S0	030	15			
081	-0.18136	30.40461	20111010	1637	quartzite	S1	068	88			
081	-0.18136	30.40461	20111010	1637	quartzite	S2	124	80			
082	-0.18088	30.40081	20111010	1691	quartzite					153-155	wellbedded = cross bedding
083	-0.28321	30.38866	20111010	1805	alluvial workings						targeting the pebble layer. Adit below pebble layer.
084	-0.28877	30.39342	20111010	1847	alluvial workings						large artisinal workings. Oriented 340. targeting base of pebble layer to the impermeable clay layer
085	-0.28986	30.38973	20111010	1908	MUTI REEF						lateritized pebble layer. Older river course of same river. Under road. Forbidden to dig.

WP	LATITUDE	LONGITUDE	DATE	ALTITUDE	ROCK UNIT	STRUCTURE CODE	DIP DIR	DIP	MOVE-MENT	PHOTO	COMMENT
086	-0.29204	30.38985	20111010	1955	quartzite						massive red qtz with ca-si veins
087	-0.37712	30.44686	20111010	1663	mudstone	S0	325	17			red coloured mudstone. Finely laminated.
087	-0.37712	30.44686	20111010	1663	mudstone	S1	180	70			
087	-0.37712	30.44686	20111010	1663	mudstone	S2	200	88			
087	-0.37712	30.44686	20111010	1663	mudstone	SZ	215	64			
087	-0.37712	30.44686	20111010	1663	mudstone	Ls	180	52			
088	-0.32542	30.47003	20111010	1664	mudstone	S0	196	66			
088	-0.32542	30.47003	20111010	1664	mudstone	S1	264	75			
089	-0.32542	30.47003	20111010	1664	gossanous vein	QV	280	88			
089	-0.32542	30.47003	20111010	1664	siltstone	S0	196	30			
090	-0.29023	30.43623	20111010	1674	granite						
091	-0.27006	30.4267	20111010	1484	granite						
092	-0.25001	30.43187	20111010	1465	granite						
093	-0.24269	30.43499	20111010	1523	granite						
094	0.05209	30.49477	20111011	1625	granite	SZ	278	86	DEX REV	4339-4341	coarse grained. weakly sheared. Qtz. Kfs. bt. msc
094	0.05209	30.49477	20111011	1625	granite	Ls	012	12			
095	0.1769	30.44993	20111011	1534	schist granite contact	S0	206	22			
095	0.1769	30.44993	20111011	1534	schist	S0	210	35			
096	0.1769	30.44993	20111011	1270	gneiss						with QV
097	0.25332	30.44482	20111011	1274	quartzite						ridge
097	0.25332	30.44482	20111011	1274	quartzite	S0	050	84			
097	0.25332	30.44482	20111011	1274	quartzite	S1	276	58			angular unconformity with sch. Anastomosing qtz
097	0.25332	30.44482	20111011	1274	schist?	S0	261	40			angular unconformity with sch. Anastomosing qtz
097	0.25332	30.44482	20111011	1274	schist?	S1	252	48		4345	angular unconformity with sch. Anastomosing qtz
097	0.25332	30.44482	20111011	1274	schist?	S2	238	76			angular unconformity with sch. Anastomosing qtz

WP	LATITUDE	LONGITUDE	DATE	ALTITUDE	ROCK UNIT	STRUCTURE CODE	DIP DIR	DIP	MOVE-MENT	PHOTO	COMMENT
098	0.30446	30.45263	20111011	1249	gneiss						not insitu v.fin mineral banding
099	0.28847	30.60062	20111011	1328	quartzite						
100	0.33393	30.64931	20111011	1338	gneiss	SZ	128	55			qv parallel to shear cut by NNW fault (340)- 10 cm displacement.
101	0.37853	30.71253	20111011	1290	biotite granite						deep red on ternary only evidence is bt rich granite.
102	0.46731	30.69457	20111011	1310	siltstone	SZ	330	38	SIN		boudin of smokey QV
102	0.46731	30.69457	20111011	1310	siltstone	S1	064	84			
103	0.5399	30.66008	20111011	1407	quartzite						ridges blocks not in place
104	0.65056	30.56795	20111011	1342	quartzite	S0	110	40			well bedded & heavily jointed
104	0.65056	30.56795	20111011	1342	quartzite	S1	308	58			
105	0.65875	30.52318	20111011	1463	mudstone	SZ	316	81			oxidized. purple in colour. v.fine grained well laminated
106	0.60184	30.68228	20111012	1280	gneiss	SZ	278	79			strongly sheared dominantly felsic with minor chl. bt. minor cross cutting gabbroic dykes
106	0.60184	30.68228	20111012	1280	gneiss	S1	175	25			
107	0.60677	30.70666	20111012	1263	gneiss siltstone contact	FT	122	86		4350-4351	strongly sheared purple-red-green in colour
107	0.60677	30.70666	20111012	1263	quartzite schist contact	FT	255	40		see notebook	
107	0.60677	30.70666	20111012	1263	quartzite	S0	232	78			steep shear same orientation as seen in slts
107	0.60677	30.70666	20111012	1263	tuff quartzite contact (faulted contact)	FT	252	72			tuff v.fine grained dominantly purple in colour. with yellow spots of oxidized fragments
108	0.59684	30.71147	20111012	1318	schist gneiss intercalated	S0	318	83			road cut over 20m see notebook
108	0.59684	30.71147	20111012	1318	schist gneiss intercalated	S1	181	06			
108	0.59684	30.71147	20111012	1318	schist gneiss intercalated	S2	063	75			
108	0.59684	30.71147	20111012	1318	schist gneiss intercalated	SZ	130	85			

WP	LATITUDE	LONGITUDE	DATE	ALTITUDE	ROCK UNIT	STRUCTURE CODE	DIP DIR	DIP	MOVE-MENT	PHOTO	COMMENT
109	0.53241	30.45394	20111012	1265	gneiss schist quartzite intercalated	S0	253	71		4353-4355	faulted sequence of gneiss rxtlzd QV & qtz. See note book.indicates antlicline plunging SE
109	0.53241	30.45394	20111012	1265	gneiss schist quartzite intercalated	S1	161	64			
109	0.53241	30.45394	20111012	1265	gneiss schist quartzite intercalated	S2	198	85			
109	0.53241	30.45394	20111012	1265	gneiss schist quartzite intercalated	SZ	318	88			
110	0.53241	30.93344	20111012	1309	Mubende Granite						coarse grained aphanitic blueish tint. Sharp contact on imagery
111	0.48002	31.1094	20111012	1318	Mubende Granite					4356-4358	bt altered to chl or epi
112	0.51335	31.31994	20111012	1294	Mubende Granite	SZ	150	85		4364	sheared E contact of granite. Pegmatitic boudins indicating sinistral movement
112	0.51335	31.31994	20111012	1294	Mubende Granite	S1	070	80			
113	0.64026	31.54768	20111013	1258	carbonaceous shale	S1	173	70			finely laminated. slatey cleavage. Dark in colour. Anticline to SW. qtz ridge to W
113	0.64026	31.54768	20111013	1258	carbonaceous shale	S2	210	63			finely laminated. slatey cleavage. Dark in colour. Anticline to SW. qtz ridge to W
114	0.63979	31.58243	20111013	1322	quartzite						
115	0.6389	31.59008	20111013	1338	sandstone						
116	0.63851	31.59533	20111013	1337	conglomerate					196 (TW)	millimetric sica veins. Subangular clasts of quartz. Poorly sorted 0.2-4cm & matriz supported, sandy matrix.

WP	LATITUDE	LONGITUDE	DATE	ALTITUDE	ROCK UNIT	STRUCTURE CODE	DIP DIR	DIP	MOVE-MENT	PHOTO	COMMENT
117	0.63981	31.61207	20111013	1340	sandstone						v.gritty
118	0.65734	31.61033	20111013	1365	sandstone	S0	185	38			v.gritty, subr grains of quartz minor kfs & lithic fragments. Feruginous quartz vein not in place. Dense feoxides
118	0.65734	31.61033	20111013	1365	sandstone	S1	196	62			v.gritty, subr grains of quartz minor kfs & lithic fragments. Feruginous quartz vein not in place. Dense feoxides
119	0.67014	31.60981	20111013	1358	carbonaceous shale	S1	155	53			dark grey in colour slatey cleavage
119	0.67014	31.60981	20111013	1358	carbonaceous shale	S2	130	48			dark grey in colour slatey cleavage
120	0.67269	31.60038	20111013	1355	Kisita Mine	S0	130	80			sh-ss contact (NE) minlzd QV (NS) boxed geometry of veins. Weak ser/chl alteration in host v.discreet
120	0.67269	31.60038	20111013	1355	Kisita Mine	S1	008	58			sh-ss contact (NE) minlzd QV (NS) boxed geometry of veins. Weak ser/chl alteration in host v.discreet
120	0.67269	31.60038	20111013	1355	Kisita Mine	S2	258	75			sh-ss contact (NE) minlzd QV (NS) boxed geometry of veins. Weak ser/chl alteration in host v.discreet
120	0.67269	31.60038	20111013	1355	Kisita Mine	QV	086	52		4369; 4370;4371	Strong gossanous oxides. Dense v.heavy. Runs at 8g/t makes 200g gold/week. Boxed geometry of subsidiary veins.
121	0.67301	31.60073	20111013	1367	Kisita Mine					4372	looking N.Z assymetry confirming WP120 which suggests & anticlinal closure to the NE
122	0.62031	31.83629	20111014	1241	Singo Granite					4378	pinkish in colour. Porphyritic. Plag, kfs, qtz msc bt. No fabric

WP	LATITUDE	LONGITUDE	DATE	ALTITUDE	ROCK UNIT	STRUCTURE CODE	DIP DIR	DIP	MOVE-MENT	PHOTO	COMMENT
123	0.75488	31.79188	20111014	1149	mudstone & shale	S0	308	73		4379 -marker	v.fine grained red-purple in colour. Strongly weathered.
123	0.75488	31.79188	20111014	1149	mudstone & shale	S1	261	46		4379-red magnet	v.fine grained red-purple in colour. Strongly weathered.
123	0.75488	31.79188	20111014	1149	mudstone & shale	S2	136	88		4379-blue pencil	v.fine grained red-purple in colour. Strongly weathered.
124	0.77881	31.78808	20111014	1135	mudstone & shale	S0	036	83			v.fine grained red-purple in colour. Strongly weathered.
124	0.77881	31.78808	20111014	1135	mudstone & shale	S1	146	88			v.fine grained red-purple in colour. Strongly weathered.
124	0.77881	31.78808	20111014	1135	mudstone & shale	S2	176	83			v.fine grained red-purple in colour. Strongly weathered.
125	0.78367	31.78699	20111014	1136	mudstone & shale	S0	013	73		4380	v.tight anticline plunging E
125	0.78367	31.78699	20111014	1136	mudstone & shale	S1	000	60		4380	v.tight anticline plunging E
125	0.78367	31.78699	20111014	1136	mudstone & shale	S0	228	88		4380	v.tight anticline plunging E
126	0.82307	31.788	20111014	1200	tuff					204 (TW)	v.fine grained yellow saprolite of volcanic tuff?
127	0.84128	31.77688	20111014	1175	mudstone & shale	S0	205	87			
128	0.86751	31.77344	20111014	1236	quartzite						
129	0.90825	31.7795	20111014	1197	gabbro/ dolerite						in Kiboga Town